2008

The Apollo Nuclease Binds To TRF2 and Protects

Megan van Overbeek

THE APOLLO NUCLEASE BINDS TO TRF2 AND PROTECTS TELOMERES IN S PHASE

A Thesis Presented to the Faculty of

The Rockefeller University

In Partial Fulfillment of the Requirements for

the degree of Doctor of Philosophy

by

Megan van Overbeek

June 2008

THE APOLLO NUCLEASE BINDS TO TRF2 AND PROTECTS TELOMERES IN S PHASE

Megan van Overbeek, Ph.D.

The Rockefeller University 2008

Members of the β-CASP family of proteins are involved in DNA repair and RNA processing. We identified a member of this family of enzymes, hSNM1B/Apollo, in complex with the telomere binding proteins TRF2/Rap1. Due to its low abundance at telomeres, we consider Apollo to be a telomere accessory factor, and not part of the core telomere protein complex, shelterin. Apollo localizes to telomeres by interacting directly with the TRFH domain of TRF2. Structural analysis of this interaction revealed an interface in the TRFH domain of TRF2 that is predicted to be shared by numerous accessory factors recruited to the telomere by TRF2, in addition to Apollo.

Disruption of the Apollo-TRF2 interaction by expressing an allele of Apollo that cannot bind to TRF2 (ApolloΔTRF2) or reducing the amount of endogenous Apollo in cells by RNAi resulted in deprotection of telomeres in S-phase, as evidenced by the presence of Telomere-dysfunction Induced Foci (TIFs). Additionally, Apollo-deficient telomeres have an aberrant signal seen by FISH that is more frequent after treatment with the DNA

replication inhibitor, Aphidicolin. Together, the data are consistent with a role for Apollo during of after telomere replication.

Isolation of the Apollo protein complex revealed that soluble Apollo is complexed in 1:1 stoichiometry with TRF2/Rap1, suggesting that Apollo might function primarily at telomeres. Additional components include DBC-1, which interacts directly with Apollo and localizes to Cajal bodies, the translesion synthesis polymerase polη, and the homolgous recombination factor Rad51. The association of these proteins with Apollo suggests potential roles for Apollo in telomerase recruitment and formation of the protective t-loop structure at chromosome ends.

This thesis is dedicated to my daughter

Helena Aleksandra Rudensky

ACKNOWLEDGEMENTS

First and foremost I would like to thank my advisor, Titia de Lange, for her limitless energy. Her clear thinking and creativity inspired me when my research was most challenging. I would also like to thank past and present members of my thesis committee: Mike Rout, Fred Cross, and Hiro Funabiki for the expert advice and perspective they have provided over the years. They always challenged and encouraged me at our yearly committee meetings. I would also like to express my appreciation to Virginia Zakian, for serving as the external examiner on my thesis committee.

To the past and present members of the de Lange lab, I would like to express my appreciation for making the lab an intellectually stimulating and constructive work environment. I would particularly like to thank Jeffrey Ye for watching over me in my first year. Hiro Takai, Diego Loayza, Sara Buonomo, Eros Lazzerini-Denchi, and Agnel Sfeir were also exceedingly generous with their scientific knowledge, advice, and reagents. I would like to thank the former and current graduate students of the de Lange lab, Josh Silverman, Rich Wang, Nadya Dimitrova, Jill Donigian, Kristina Hoke, Jan-Peter Daniels, Dirk Hockemeyer, Wilhelm Palm and Peng Wu for their camaraderie and generosity with scientific advice and reagents.

I would also like to thank Stew Barnes, Stephanie Blackwood, Sarah Hooper, Rita Rodney, Kaori Takai, Eliana Forero, Diana Argibay and Devon White for organizing the lab and making it a productive place to do research. I am also indebted to Lola MacRae for her help with formatting and proofreading my thesis. Additionally, the Rockefeller University Dean's Office has been extremely helpful during the dissertation process.

Zhulun Wang and Valerie Doye were the first individuals to give me an opportunity to pursue bench science. I would like to thank them for their openness, encouragement, and support. I am beholden to my family, old and new. To the van Overbeeks, Deborah, Thomas and Johannes, thank you for motivating me, and for your consistent love and patience. To Eugene Rudensky, for your continued support throughout this endeavor. Many thanks to Sasha Rudensky Sr. for advice, perspective, and humor. Thanks to Oakland for raising me.

TABLE OF CONTENTS

LIST OF FIGURES

LIST OF ABBREVIATIONS

ALT	Alternative Lengthening of Telomeres
APB	ALT associated PML Body
AT	Ataxia-Telangiectasia
ATLD	Ataxia-Telangiectasia Like Disorder
ATM	Ataxia-Telangiectasia Mutated
ATR	ATM and Rad3-Related
BrdU	Bromo-deoxyuridine
ChIP	Chromatin Immunoprecipitation
CO-FISH	Chromosome Orientation FISH
DAPI	4,6-diamidino-2-phenylindole
DKC	Dyskeratosis Congenita
DNA-PKcs	catalytic subunit of DNA-dependent Protein Kinase
DSB	Double Stranded Break
dsDNA	Double-stranded DNA
FACS	Fluorescence Activated Cell Sorting
FISH	Fluorescence *In Situ* Hybridization
HR	Homologous Recombination
hTERT	Human Telomerase Reverse Transcriptase
hTR	Human Telomerase Reverse RNA
HU	Hydroxyurea
ICL	Interstrand Cross Link
IF	Immunofluorescence
IP	Immunoprecipitation
IR	Ionizing radiation
KO	Knock-Out
MEF	Mouse Embryonic Fibroblast
MMC	Mitomycin C
NBS	Nijmegen Breakage Syndrome
NER	Nucleotide Excision Repair
NHEJ	Non-Homologous End Joining
NLS	Nuclear Localization Signal
NMD	Nonsense-mediated RNA Decay
OB	Oligonucleotide/Oligosaccharide Binding
PCNA	Proliferating Cell Nuclear Antigen
PD	Population Doubling
PFGE	Pulsed Field Gel Electrophoresis

PIKK	Phosphatidyl Inositol 3-Kinase-like Kinase
PNA	Peptide Nucleic Acid
RS-SCID	Radio-Sensitive Severe Combined Immunodeficiency
SA β-gal	Senescence Associated β-galactosidase
SCE	Sister Chromatid Exchange
ssDNA	Single-stranded DNA
TIF	Telomere Dysfunction Induced Foci
TRD	Telomere Rapid Deletion
TRF1	TTAGGG repeat binding factor 1
TRF2	TTAGGG repeat binding factor 2
T-SCE	Telomere Sister Chromatid Exchange
UV	Ultraviolet

CHAPTER 1: INTRODUCTION

Telomere Structure

With the advent of linear chromosomes came the ability to exchange genetic information in meiosis. However, a new problem arose, that of maintaining chromosome ends, or telomeres. One challenge of replicating linear chromosomes is referred to as the "end replication problem" and was first described by Watson in 1972 [1]. Short RNA primers are used by DNA-replication machineries to initiate DNA synthesis. Removal of the terminal primer at the end of lagging strand synthesis leaves a small gap that cannot be filled in. Loss of terminal sequences with each round of DNA replication will occur if this gap is not compensated for. A second challenge of maintaining linear chromosomes is that cells must be able to distinguish between double and single stranded DNA at natural chromosome ends and sites of DNA damage. Telomeres of diverse organisms have managed to solve these problems.

Repeats

Telomeres of most eukaryotic organisms are consist of tandem G-rich repeats. The first telomeres to be sequenced were those of linear rDNA from *Tetrahymena thermophila,* which revealed 20-70 repeats of the sequence TTGGGG [2]. The telomeres of other organisms contain a variation of this sequence. One version of telomeric repeat, TTAGGG, is found in such dissimilar organisms as acellular slime molds, Trypanosomes, and vertebrates. The similarity of chromosome end sequences across a diverse set of organisms suggests a common mechanism for preserving chromosome

ends. Telomere sequences have a defined orientation in that the G-rich strand always runs 3' to 5' from the end towards the centromere.

The number of simple telomere repeats at chromosome ends varies dramatically across organisms. The *Oxytricha* micronucleus can contain as little as 20 bp of repetitive DNA . Human telomeres have 5-15 kb of TTAGGG repeats [3 4 5], laboratory mouse telomeres are 50-150 kb in length [6], and chicken telomeres are 10 kb-1 Mb in length [7]. Within a cell, the amount of telomeric DNA varies from telomere to telomere, resulting in a smear when terminal restriction fragment analysis (TRF) is performed.

3' overhang

A 3' overhang on the G-rich strand is a common feature of telomeres. The predicted products of DNA replication of a linear chromosome would be a molecule with one blunt end (the product of leading strand synthesis) and an end with a short 5' overhang (the product of lagging strand synthesis). The presence of a 3' overhang on both ends of a chromosome indicates that telomeres are processed by a nuclease after DNA replication. This processing event might be required to create a substrate for telomere extension by telomerase or to generate a substrate for proteins to bind to protect the ends of chromosomes. The gap left by removal of the last RNA primer in lagging strand synthesis is predicted to be 8-12 nucleotides long. Human telomeres lose 50-150 bp/end/cell division, suggesting active degradation of chromosome ends. The mechanism and the nucleases involved in the attrition of human telomeres are not known.

The sequence of the 5' end of human chromosomes is precisely defined where the majority of human chromosome ends terminate with CCAATC-5' [8]. The 5' end sequence in ciliates is also extremely specific; the C-rich strand

in Euplotes always ends in AACCCC-5' and in Tetrahymena the end sequence is either CAACCC-5' or CCAACC-5'. The 3' G-rich strand end sequence is more precise in ciliates than in human cells [9 10].

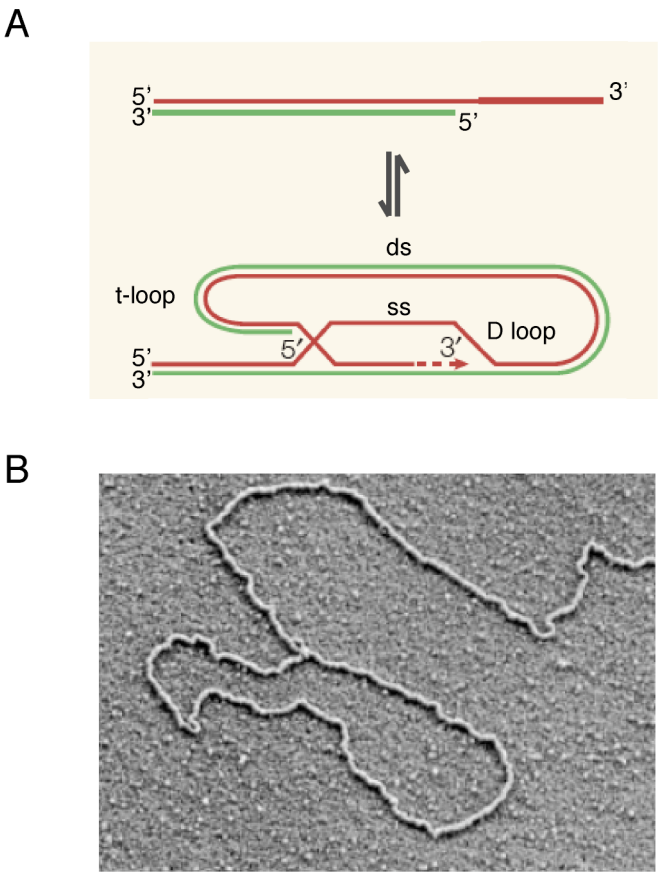

Figure 1-1: Chromosome ends form t-loops.

(A) Schematic identifying different aspects of a t-loop. (B) Electron micrograph depicting a t-loop isolated from mouse liver{Griffith et al., 1999, Cell, 97, 503-14.}.

T-loops

The 3' overhang in many organisms is concealed by the formation of a telomeric loop structure, or t-loop, at chromosome ends (Fig. 1-1). T-loops were first observed by electron-microscope analysis of purified, naked telomeric DNA from mouse and human cells [11]. T-loops are formed through

strand invasion of the 3' G-rich overhang into the double-stranded part of the telomere. This creates a displacement loop (D loop) of about 150 nt as discerned from coating with *E. coli* single strand binding protein (SSB); 150 nt is consistent with the average length of the 3' overhang in human cells. T-loops appear to be a solution that many organisms have adopted as they can be detected in Oxytricha, trypanosomes, and plants [12 13 14]. Most recently, t-loops have been isolated in their native chromatin context from chicken erythrocyte and mouse lymphocyte nuclei [15]. The steps required to form a t-loop parallel the initial steps of homologous recombination. Recruitment of the homologous recombination machinery to telomeres has been proposed to shape the t-loop structure [16]. However, this process would have to be tightly controlled to prevent inappropriate resolution of the t-loop.

Telomere maintenance by telomerase

An activity that could extend GT rich primers was isolated from Tetrahymena extracts. This activity was termed telomerase and was characterized as a ribonucleoprotein complex whose RNA and protein components were both required for activity[17 18]. Most organisms use telomerase to maintain the ends of their chromosomes.

Generally, telomerase consists of a reverse transcriptase, an RNA template and accessory factors that are not required for catalytic activity of the enzyme and instead potentially regulate recruitment to telomeres. The single stranded G-rich overhang provides a primer for telomere repeat addition to chromosome ends by active telomerase. After elongation of the G-rich strand, C-strand synthesis is presumed to occur to generate double stranded DNA. DNA polymerases α and δ, along with primase, are required

for telomere elongation by telomerase in budding yeast {Diede and Gottschling, 1999, Cell, 99, 723-33}. This data indicates that telomerase needs to interact with lagging strand DNA synthesis machinery to be active and that these two processes, elongation by telomerase and C-strand synthesis, might be coordinated. Telomerase needs to be active in unicellular eukaryotes to permit further generations. Telomerase is active in human germline tissues and in a high percentage of tumors[20]. However, in the human soma, telomerase is repressed by limiting hTERT transcription, as hTERC is ubiquitous [21] [20].

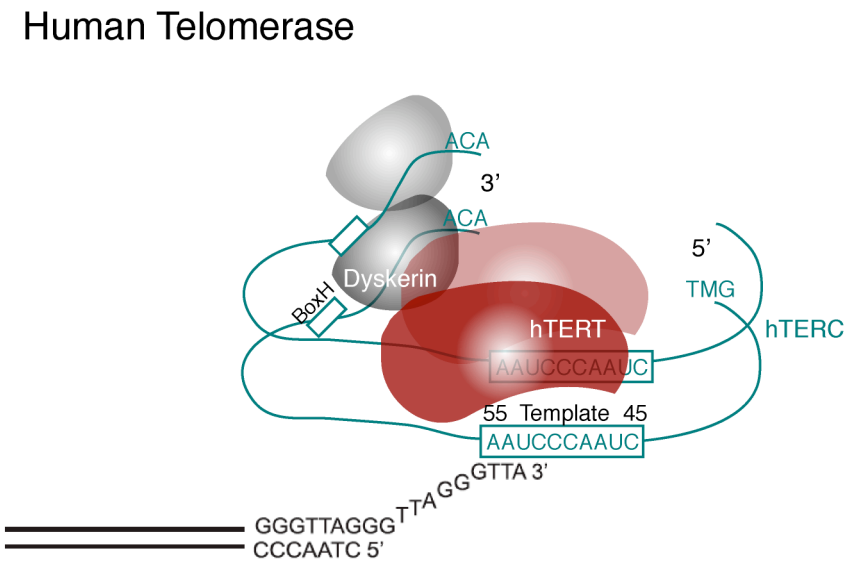

Figure 1-2. Human telomerase.

Human telomerase is depicted as a dimer with two components of each hTERT, hTERC, and dyskerin.

Purified catalytically active human telomerase was found to have two copies of each hTERT, hTERC, and Dyskerin [22] (Fig. 1-2). A mutation in the RNA binding protein Dyskerin is associated with a rare X-linked disease, dyskeratosis congenita (DKC) [23]. Dyskerin is predicted to be

important for the stability of hTERC as patients with mutated dyskerin have 5-fold less hTERC than unaffected siblings [23]. Additionally, autosomal dominant forms of DKC exist that are due to mutations in hTERC or hTERT. These genetic observations are consistent with a role for dyskerin in telomerase function [24]. The phenotypes of this disease include defects in highly regenerative tissues such as skin and blood and most patients die of bone marrow failure. Furthermore, DKC patients have shorter telomeres and exhibit chromosome instability [23 25].

Other strategies to maintain telomere integrity

Most telomerase negative human tumors maintain their telomeres by a mechanism termed Alternative Lengthening of Telomeres (ALT) [26 27]. This process relies on telomere-telomere recombination events leading to telomeres of extremely heterogeneous lengths compared with related non-ALT cells [27 28 29]. ALT-associated PML bodies (APBs) are present in cells that maintain their telomeres by an ALT mechanism [27]. APBs contain proteins involved in recombination as well as the telomere binding proteins TRF1 and TRF2 [30]. Budding yeast telomeres can also be maintained by recombination-based pathways in the absence of telomerase, termed survivor pathways [31]. Survivor pathway Type I relies on Rad51p whereas the Type II survivor pathway is Rad50p dependent [32 33]. Recombination-based telomere length maintenance cannot occur in the absence of both of these proteins [33].

Senescence

Replicative senescence was first reported by Hayflick and Moorhead in 1961[34]. In their experiments, normal diploid fibroblasts stopped dividing

in spite of growth in optimal conditions indicating that normal cells have a finite capacity to replicate. Olovnikov hypothesized that shortening of chromosome ends with each round of replication might explain Hayflick's observation[35]. The sequencing of telomeres permitted TRF analysis and the comparison of telomere length. It was observed that telomeres shorten as cultured human fibroblasts divide [5 36 37 38]. Definitive proof for the relationship between telomere shortening and cellular senescence came when the ectopic expression of telomerase prevented the onset of replicative senescence in human primary fibroblasts [39].

Human telomere binding proteins – Shelterin

Shelterin is a specialized six-member protein complex found at human telomeres. The individual components that make up shelterin are TRF1, TRF2, Pot1, Tin2, TPP1 and Rap1 (Fig. 1-3). Shelterin is required for the protection of telomeres from the DNA damage response and for telomere length regulation[40]. TRF1 and TRF2 bind directly to double stranded TTAGGG repeats as homodimers, engaging DNA with two Myb domains [41 42 43 44 45]. Pot1 binds to single stranded DNA with OB-folds [46 47]. Tin2 makes contact with and stabilizes TRF1, TRF2, and TPP1. TPP1 acts as a bridge between Tin2 and Pot1. Rap1 binds to TRF2 [48 49 50 51 52]. Shelterin can exist as a single complex or in subcomplexes containing TRF1 or TRF2 and their direct binding partners [48 53].

A

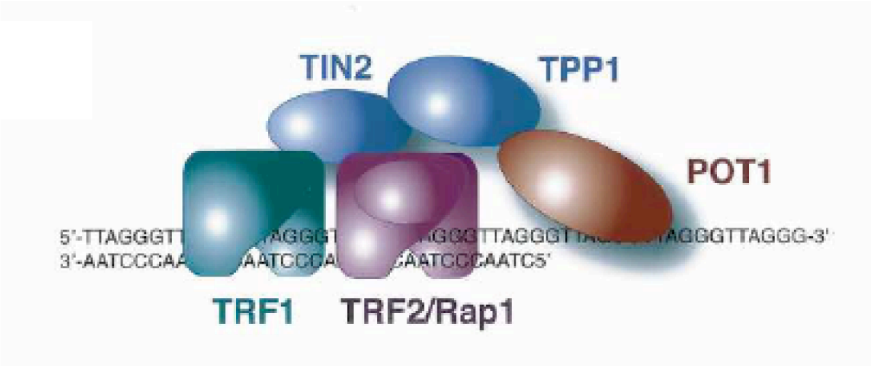

B

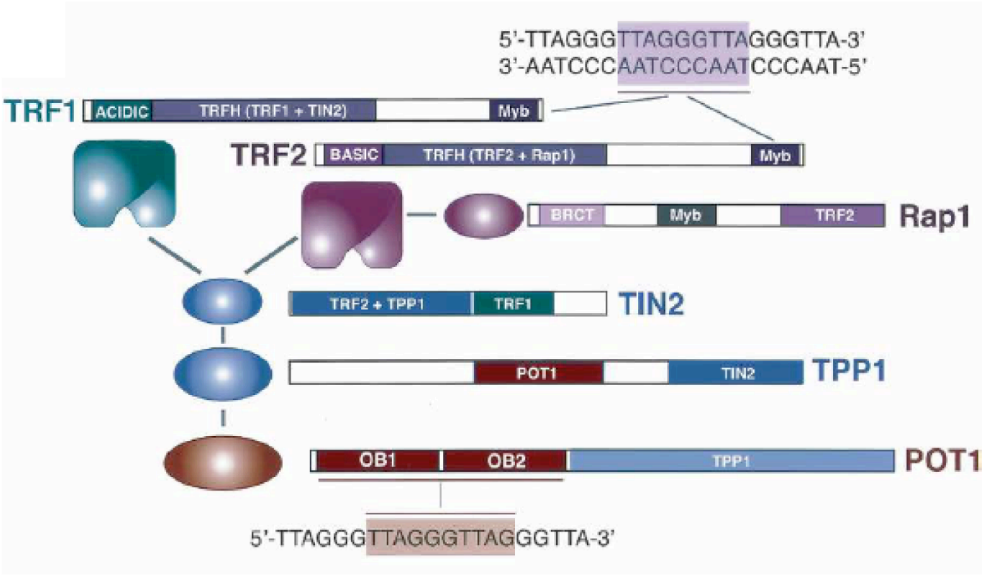

Figure 1-3. Shelterin binds to mammalian telomeres.

(A) Schematic of shelterin on telomeric DNA. For simplicity, POT1 is only shown as binding the site closest to the duplex telomeric DNA although it can also bind to the 3' end. (B) The six known subunits of shelterin, their domain structure, protein interactions, and DNA-binding sites.

TRF1

The first shelterin component to be identified was TRF1 based on its ability to bind to TTAGGG repeats [42].

TRF1 has an N-terminal acidic domain, a homodimerization domain (TRFH), a hinge domain, and a C-terminal DNA binding Myb domain. TRF1 binds to double stranded telomeric DNA as a homodimer. Each Myb domain binds one 5'YTAGGGTTR3' half site. The length of DNA between bound Myb domains from a single TRF1 homodimer can vary indicating flexibility in the hinge domain [43 54]. TRF1 is a negative regulator of telomere length. Overexpression of TRF1 in a clone of the human tumor cell line HT1080 results in telomere shortening. Removal of TRF1 from telomeres by the expression of a dominant-negative allele results in the lengthening of telomere tracts [55 56 57]. It was concluded that TRF1 affects the telomerase pathway as overexpression of TRF1 in telomerase negative cells did not affect the shortening rate [58]. Mouse knockout experiments showed that TRF1 is an essential gene suggesting a role beyond telomere length regulation [59].

TRF2

TRF2 was discovered by searching the human gene database for TRF-like proteins [41 44]. TRF2 and TRF1 have the same domain layout with one major difference: TRF2 has an N terminal basic domain whereas the N-terminus of TRF1 is acidic. Like TRF1, TRF2 binds to double stranded DNA as a homodimer [41]. In spite of the near identical three-dimensional structure of the homodimerization domains (TRFH) of TRF2 and TRF1, they cannot form heterodimers due to steric constraints [60]. In contrast to vertebrates, fission yeast contain only one TRF factor, Taz1 [61]. Like TRF1, TRF2 has a role in telomere length regulation. The telomeres of human primary fibroblasts that overexpress TRF2 shorten faster than telomeres from cells expressing TRF1. There is no change in the length of the G-rich 3' overhang in TRF2 overexpressing cells, eliminating the possibility of

increased shortening due to enhanced 5' resection. TRF2 binding to telomeres is indispensable for telomere protection. The details of this role are discussed below.

Rap1

Human Rap1 was discovered in a two-hybrid screen for TRF2-interacting proteins. The C-terminus of Rap1 binds to the TRFH and hinge domains of TRF2 [62]. In a pulldown experiment with endogenous TRF2, Rap1 was found in 1:1 stoichiometry with TRF2 [16]. Heterodimerization with TRF2 is essential for Rap1 protein stability, as evidenced by decreased Rap1 protein levels in TRF2 deleted cells [63]. In contrast to budding yeast ScRap1p, hRap1 does not directly bind to telomeric DNA [62]. ScRap1 engages DNA with two Myb domains, whereas the single Myb domain of hRap1 is predicted to mediate protein-protein interactions [64 65]. The fission yeast Rap1 ortholog also cannot bind telomeric DNA directly and is dependent on the TRF-like factor, Taz1 for localization to telomeres [66]. The function of Rap1 has not been fully established. Rap1 is an essential gene in mice, suggesting a role in telomere protection (van Overbeek and de Lange unpublished results). Rap1 also contributes to telomere length regulation since the expression of an allele lacking the N-terminal BRCT domain of Rap1 leads to a reduction in telomere length heterogeneity [67].

Pot1/TPP1

The first telomere-specific binding proteins to be discovered, Telomere End Binding Protein (TEBP) α/β, were isolated from *Oxyticha nova* macronuclear DNA [68]. To bind effectively to telomeres TEBP α/β require both the 3' G-rich overhang and the adjacent duplex DNA. The

crystal structure of TEBP α/β in complex with telomeric DNA revealed that these proteins use three oligosaccharide/oligonucleotide-binding (OB) folds to bind to single stranded DNA and a fourth to interact with each other [69].

Schizosaccharomyces pombe Pot1 (protection of telomeres) was identified by homology to the OB-fold containing N-terminus of TEBP α [46]. Deletion of SpPot1 results in rapid telomere degradation and senescence. The surviving *S. pombe* cells have circular chromosomes. Further searches for OB-fold containing proteins using the N-terminus of SpPot1 in human databases identified human Pot1 [46].

hPot1 binds specifically to single-stranded telomeric DNA [70 71]. The overexpression of hPot1 lacking its N-terminal OB-fold results in rapid telomere elongation, suggesting that hPot1 can act as a negative regulator of telomere length [47]. IF and ChIP analysis revealed that Pot1ΔOB still localizes to telomeres presumably through a protein interaction within shelterin {Loayza and de Lange, 2003, Nature, 424, 1013-8}. This interaction is mediated by TPP1 {Ye et al., 2004, Genes Dev, 18, 1649-54} {Hockemeyer et al., 2007, Nat Struct Mol Biol, 14, 754-61}.

TPP1 was discovered in biochemical experiments that searched for Tin2 and Pot1 interacting factors [50 72 51]. TPP1 serves as a bridge between Tin2 and Pot1 and is required for Pot1 localization to telomeres [50 51 72]. Recent structural and functional studies have shown that Pot1 and TPP1 are equivalent to the TEBP α/β complex in *O. nova* [73 74].

Tin2

Tin2 was identified in a yeast two-hybrid screen using TRF1 as bait. In this study, the C-terminus of Tin2 was shown to bind to the TRFH

domain in TRF1 [75]. Further studies have demonstrated that Tin2 can bind TRF1 and TRF2 simultaneously [48 49]. Disruption of Tin2 results in destabilization of TRF1 and TRF2 at the telomere and a DNA damage response at telomeres [48 49]. Structural analysis of the interaction of the C-terminus of Tin2 with TRF1-TRFH identify the interaction interface as Tin2$_{256-276}$ and a loop between alpha helix 3 and 4 in TRF1-TRFH [76]. TRF2-TRFH does not mediate a stable interaction with Tin2. Instead, the N terminus of Tin2 binds to a short motif in the hinge domain of TRF2 [76]. Tin2 is also required for the localization of TPP1 to telomeres [72 51 50] and through TPP1 the localization of Pot1 to the telomere. Through its multiple interactions, Tin2 is able to stabilize shelterin on telomeres.

Telomere Protection Mediated by TRF2

TRF2 prevents NHEJ at the telomere

Removal of TRF2 from the telomere, either by expression of a dominant negative allele or by genetic ablation in the mouse, leads to a DNA damage response at telomeres and fusion of telomere ends to each other [77 45 63]. Preceding the fusion event, the G-rich 3' overhang is removed by the XPF/ERCC1 nuclease [78]. Fusion events can not occur in the absence of Ligase 4 and Ku70, implicating NHEJ in the reaction [79 63 80]. In cells with defective NHEJ, deprotected telomeres can still recruit DNA damage factors in discrete foci that co-localize with telomeres. These foci are called Telomere-dysfunction Induced Foci (TIFs). TIFs contain phosphorylated histone H2AX (γ-H2AX), 53BP1, phosphorylated Rad17, ATM phosphorylated on S-1981, Mre11, Nbs1 and MDC1 [77 81]. The formation of TIFs after removal of TRF2 is dependent on ATM [77 82].

Depending on the cell type, TRF2 deficiency either results in senescence or apoptosis [83] [45]. The senescence induced by TRF2 removal is similar to cells that enter into replicative senescence. In TRF2 deficient cells, p53 levels are stabilized, p21 and p16 levels are induced, and cells stain positive for SA-β-galactosidase [45] [77]. Cells that overexpress TRF2 senesce with shorter telomeres than cells with wildtype levels of TRF2 [58]. These experiments suggest that senescence is induced by the inability of short telomeres to load a sufficient amount of TRF2 rather than by chromosome ends that lack telomeric DNA. What is the minimum length of a human telomere that can still be protected by TRF2? Senescence can be bypassed in cells by the expression of human papilloma virus (HPV) oncoproteins E6 and E7 which abrogates the function of p53 and Rb, respectively [84]. Experiments using single telomere length analysis (STELA) on DNA from MRC5 cells driven into crisis by the expression E6 and E7 suggest that a minimum of 12.8 TTAGGG duplex repeats are required to prevent telomere-telomere fusions [85]. Considering that the TRF1 DNA binding half site is 5'YTAGGGTTR 3', one TRF homodimer needs three repeats to bind to telomeres[54]. This suggests that a minimum of four TRF homodimers bound to the telomere is required to prevent telomere fusion.

TRF2 prevents inappropriate homologous recombination at the telomere

An allele of TRF2 lacking its N-terminal basic domain (TRF2ΔB) causes senescence and TIFs when overexpressed [86]. This allele retains the ability to bind to telomeres and prevents telomere-telomere fusions. Further investigation revealed that telomere tracts are rapidly lost in cells expressing TRF2ΔB as a result of homologous recombination of the t-loop structure. Consistent with this model, telomere loss and presumably the formation of

telomeric circles is dependent on the Rad51 paralog XRCC3, which has been implicated in Holliday Junction resolution [87] [86]. The basic domain of TRF2 may be preventing branch migration of the 5' end into the t-loop structure possibly by recruiting a nuclease. If branch migration is not prevented, the resulting double Holliday Junction will be a target for resolvases producing short telomeres and telomere circles.

Other models have been proposed to describe the function of the basic domain of TRF2. Griffith and colleagues have shown that the basic domain of TRF2 can bind directly to DNA junctions and in this capacity might stabilize t-loops {Fouche et al., 2006, J Biol Chem, 281, 37486-95}. Consistent with this finding, work from the Gilson lab has shown that the basic domain of TRF2 makes direct contact with DNA in a structure and not a sequence specific manner and is expected to be important for making the appropriate contacts that would stabilize t-loops {Amiard et al., 2007, Nat Struct Mol Biol, 14, 147-154}.

Processes similar to t-loop HR have been identified in other organisms. T-loop resolution by homologous recombination is suppressed by Ku in *Arabadopsis thaliana* [88]. A deletion process termed Telomere Rapid Deletion (TRD) in yeast occurs where up to several kilobases of telomeric DNA is lost in a single step[89] [90]. The mechanisms behind TRD and t-loop HR might be similar.

The formation of the protective t-loop structure parallels the first steps of interchromatid homologous recombination. HR machinery might be required at telomeres to initiate t-loop formation. However, it must be tightly controlled by shelterin to prevent recombination of the telomere and subsequent shortening of telomeres. Consistent with a positive role of HR at

telomeres, Rad54 and the Rad51 paralog, Rad51D, have a role in telomere length maintenance and telomere capping [91] [92]. Also, the MRN complex in addition to its roles in HR is thought to act in conjunction with telomerase in telomere length maintenance [93].

How does TRF2 prevent telomeres from being recognized as sites of DNA damage?

TRF2 could prevent telomeres from being recognized as sites of DNA damage in several ways. TRF2 was shown *in vitro* to stimulate t-loop formation [11] [94]. Secondly, the protection offered by TRF2 could be mediated through its binding partners. TRF2 recruits the shelterin factor Rap1 and many proteins involved in DNA repair to the telomere including the NER nuclease XPF/ERCC1 and the Mre11 complex [62] [16] [78]. The importance of Rap1 and TRF2 accessory proteins in mediating the role of TRF2 at the telomere is not fully understood. Lastly, TRF2 has been shown to bind to ATM, a kinase upstream in signaling the DNA damage response, and to inhibit its activation [95]. TRF2 might bind to ATM locally at telomeres and suppress its activity.

Telomere length regulation

Based on the isolation of catalytically active human telomerase from HEK-293 cells it has been estimated that there are only 20-50 molecules of telomerase per cell [22]. Work in yeast has shown that telomerase does not elongate every telomere each cell cycle. Instead, telomerase has a preference for telomeres as they become shorter implying that telomeres exist in extendible and non-extendible states [96]. In an extendible state telomeres must be able to recruit telomerase to their ends. In budding yeast, the single

stranded binding protein Cdc13p interacts directly with Est1p of yeast telomerase [97]. A direct interaction between hTERT and the shelterin component TPP1 has been reported [74]. Additionally, *in vitro* work has demonstrated that telomerase is more processive when TPP1 is bound to Pot1 on single stranded DNA compared with Pot1 alone suggesting that TPP1 can stabilize telomerase [73].

The access of telomerase to telomeres is regulated through a negative feedback loop in *cis* by telomere binding proteins. The evidence for this mechanism in human cells comes from experiments with TRF1. The number of TRF1 molecules/telomere is proportional to telomere length. Furthermore, the overexpression of TRF1 leads to shortening of telomeres in telomerase positive cells without affecting the intrinsic activity of telomerase [55]. More recent studies have shown that Pot1 mediates TRF1 negative regulation of telomerase at the 3' end of telomeres [47]. The C-terminus of ScRap1p was shown to function in a similar manner to TRF1 in *S. cerevisiae* by targeting experiments[98]. This role is also consistent for Taz1 at telomeres in *S. pombe* [61]. Human Rap1, which cannot bind directly to telomeres, negatively affects telomere length [62]. It is not known whether Rap1 functions in the same pathway as TRF1 or in a parallel pathway.

Replication of telomeres

In contrast to the late replication timing of budding yeast telomeres, experiments using BrdU labeling show that the telomeres of humans and the barking deer (*Muntiacus muntjac)* replicate throughout S-phase [99 100 101 102]. The repetitive and G-rich nature of telomeres are predicted to complicate replication. G-quadruplex secondary structures have been observed *in vitro*

using double stranded DNA oligos of telomere repeat sequences [103] [104] [105]. These structures might form *in vivo* and act as a barrier to replication. Helicases are likely to be required to unwind G-quadruplexes and telomere binding proteins might act to prevent the formation of G-quartet structures once those strands are unwound. Consistent with this hypothesis, the WRN helicase is required for the efficient replication of G-rich telomeric DNA [106]. Furthermore, TRF2 interacts directly with WRN and has been proposed to regulate its telomere specific role [107]. Also consistent with the hypothesis stated above, Pot1 has been shown to *in vitro* to disrupt G-quadruplex formation [108]. Nucleases have also been implicated in the resolution of G-quadruplex structures in yeast and humans [109] [110] [111].

Taz1 is required for telomere replication in *S. pombe*. [112] In cells without Taz1 replication forks stall at telomere sequences whether they are placed internally or at natural chromosome ends. This demonstrates that the phenotype is due to characteristics of the telomere sequence and not position within a chromosome. Taz1 is predicted to act by either altering the telomere complex to allow for replication fork passage or by recruiting helicases to manage telomere specific secondary structures.

CHAPTER 2: IDENTIFICATION OF SNM1B/APOLLO AS A SHELTERIN ASSOCIATED FACTOR

This chapter describes the identification of a new shelterin associated factor, the SNM1B nuclease part of the β-CASP family of nucleases. Shelterin associates with several accessory factors that are distinguished from the shelterin core components (TRF1, TRF2, Rap1, TIN2, TPP1, and Pot1) based on their lower abundance at telomeres and/or their transient association with chromosome ends (Fig. 2-1) [40]. Most shelterin associated factors have additional non-telomeric functions, contributing to the DNA damage response or other chromosomal transactions. The telomeric position of these factors creates a paradox, since it is generally assumed that shelterin protects telomeres from detrimental reactions mediated by these type of proteins.

Pulldown experiments of endogenous TRF2 from HeLa nuclear extracts have revealed the association of the Mre11/Rad50/Nbs1 complex and XPF/ERCC1 with telomeres [16 78]. The Mre11/Rad50/Nbs1 complex is involved globally in double strand break (DSB) signalling and the repair of DSBs through homologous recombination [113 114]. Mre11 and Rad50 are localized to telomeres in all cell cycle stages whereas Nbs1 is localized to telomeres specifically in S-phase. The role of the Mre11 complex at telomeres has not been elucidated. In contrast, MEFs deficient for the nucleotide excision repair (NER) nuclease, XPF/ERCC1, exhibit telomeric DNA containing double-minute chromosomes, which have been proposed to be the product of 3' overhang invasion into interstitial telomere related sequences. At dysfunctional telomeres, XPF/ERCC1 is required to clip the 3' overhang to enable fusion by NHEJ of telomere ends.

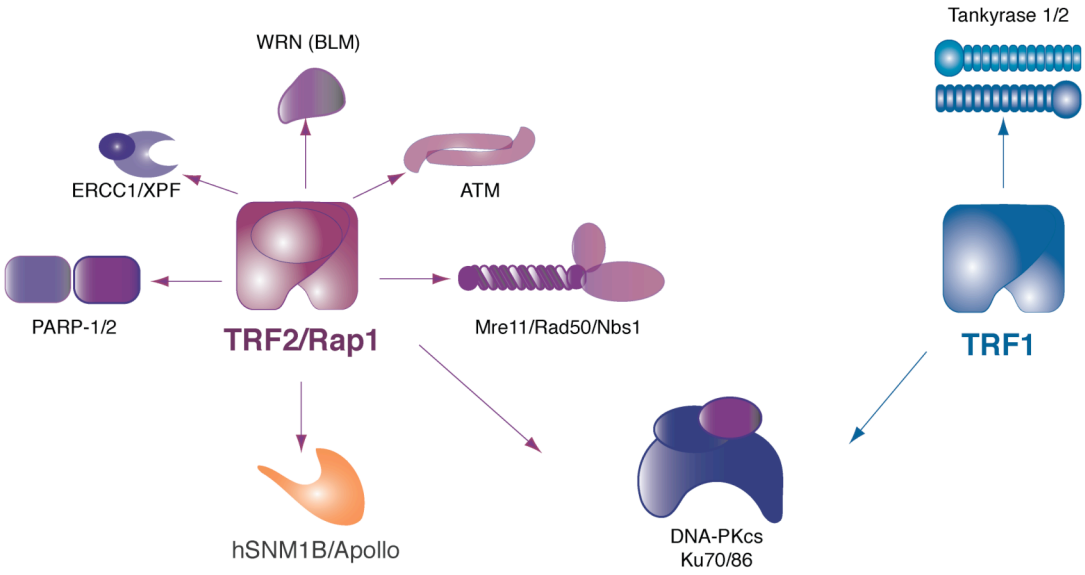

Figure 2-1. Shelterin associated factors.

Cartoon representation of shelterin associated factors recruited to telomeres via interactions with TRF1 and/or TRF2.

Other DNA repair factors localized to telomeres include DNA-PKcs and the Ku70/86 heterodimer. Both are part of the NHEJ machinery, which is normally repressed at telomeres by TRF2 [115 116 117]. TRF2-/- Ku70-/- MEFs exhibit telomere sister chromosome exchanges (T-SCEs), implying that Ku can inhibit homologous recombination at telomeres in the absence of TRF2 [80]. This activity might be important to prevent cells from adopting an ALT mechanism to maintain their telomeres. For instance, when telomeres become shortened as a consequence of replicative attrition, they may contain insufficient TRF2 to repress HR. In this setting Ku could be critical to repress HR.

The WRN RecQ helicase is another example of a factor that binds to telomeres and may have positive and negative effects. Individuals with mutated WRN display cellular defects associated with telomere maintenance such as premature aging and genomic instability. WRN binds to TRF2 and is required for efficient lagging strand replication of telomeres. WRN is predicted to act by unwinding G-quadruplex structures at TTAGGG repeats that might otherwise impede the replication fork. [107] [106]. However, WRN can also resolve t-loops in vitro using its helicase and 3'-5' exonuclease activities by degrading and releasing the 3' overhang [118]. If unregulated, WRN might cause unscheduled opening of the t-loop.

TRF2 interacts with the ATM kinase (based on co-IP experiments) and overexpression of TRF2 inhibits autophosphorylation and activation of ATM [95]. In this capacity, TRF2 might protect telomeres from inappropriate processing events by prohibiting the local activation of the ATM pathway at telomeres.

Several PARPs (Poly(ADP-ribose) polymerases), including PARP-1, PARP-2, Tankyrase-1, and Tankyrase-2 associate with telomeres [119]. PARP-1, which interacts with TRF2, binds to DNA breaks and poly(ADP)-ribosylates proteins involved in DNA repair and chromatin structure. PARP-1 has been shown to localize to eroded telomeres by FISH and colocalizes with TRF2 at damaged telomeres [120]. PARP-2 also interacts with TRF2 and has been proposed to regulate the binding of TRF2 to telomeres by poly(ADP-ribosylation) [121]. Tankyrase-1 and Tankyrase-2 both bind to and poly(ADP)-ribosylate TRF1 and regulate telomere length by affecting the ability of TRF1 to bind to telomeres [122] [123] [124] [125] [126] [127]. Tankyrase-1 also

affects sister-telomere cohesion. Cells that lack Tankyrase-1 cannot progress through anaphase due to the continued association of their telomeres [128].

β-CASP family of nucleases

The metallo-β-lactamase superfamily is characterized by a highly conserved HxHxDH motif that is required for Zn ion coordination and necessary for catalytic activity of the enzymes. Enzymes of this family act on substrates that have ester linkages and negative charge [129]. Members of this family include cAMP phosphodiesterases, aryl sulfatases, and nucleases. The β-CASP (metallo-β-lactamase-associated CPSF Artemis SNM1/PSO2) class of enzymes within the metallo-β-lactamase superfamily act on nucleic acid substrates and are involved in DNA repair and RNA processing [130].

CPSF-73 (cleavage-polyadenylation specificity factor 73) is an RNA endonuclease that cleaves the 3' end of pre-mRNAs to allow for the synthesis of a poly(A) tail [131 132]. There are three human orthologs of the *S. cerevisiae* inter-strand crosslink (ICL) repair protein SNM1/PSO2 (Sensitive to nitrogen mustard 1/Psoralen-UVA sensitive 2), SNM1A, SNM1B, and SNM1C (Artemis). Artemis is the most characterized of the β-CASP class of enzymes that uses DNA as a substrate. Mutations in human Artemis were discovered in patients with RS-SCID (radiosensitive severe combined immunodeficiency)[133]. Artemis is involved in V(D)J recombination [133 134 135] and is also implicated in non-homologous end joining (NHEJ) of IR-induced DNA breaks [136]. Artemis-deficient mouse cells are radiosensitive, showing an increased level of IR-induced genome instability [137]. Although their functions have not been fully worked out, both SNM1A and SNM1B have been implicated in ICL repair [138 139]. SNM1A has been reported to colocalize

with Mre11 and 53BP1 at IR-induced breaks, and to physically interact with 53BP1 [140].

Results

Biochemistry and isolation of the Rap1/TRF2 protein complex

To search for TRF2 and Rap1-interacting partners, FLAG-HA2-Rap1 was expressed in HeLa S3 cells, and clonal cell lines were isolated (Fig.2-2A). Rap1 binds to TRF2 with a 1:1 stoichiometry and heterodimerization with TRF2 is essential for Rap1 stability [16 63]. Two cell lines that expressed tagged Rap1 at roughly the same level as endogenous Rap1 (N-terminally tagged Rap1-N8 and C-terminally tagged Rap1-C12) and tested for the ability of tagged Rap1 to efficiently IP TRF2 were used for affinity purification experiments (Fig. 2-2A). Clones N8, C12, and the vector expressing cell lines were grown to 10 liters in suspension in high density medium [1.5-1.8 x 10^6 cells/ml] to yield 1.5-1.8 x 10^{10} cells/experiment. Nuclei were isolated from these cells through douncing and soluble nuclear proteins were extracted in 420 mM KCl following the method of Dignam et al. [141]. The Rap1/TRF2 complex was isolated by tandem affinity purification using FLAG and HA epitopes, and the isolated proteins were analyzed by SDS-PAGE in combination with Coomassie or silver staining. (Fig. 2-2B,D).

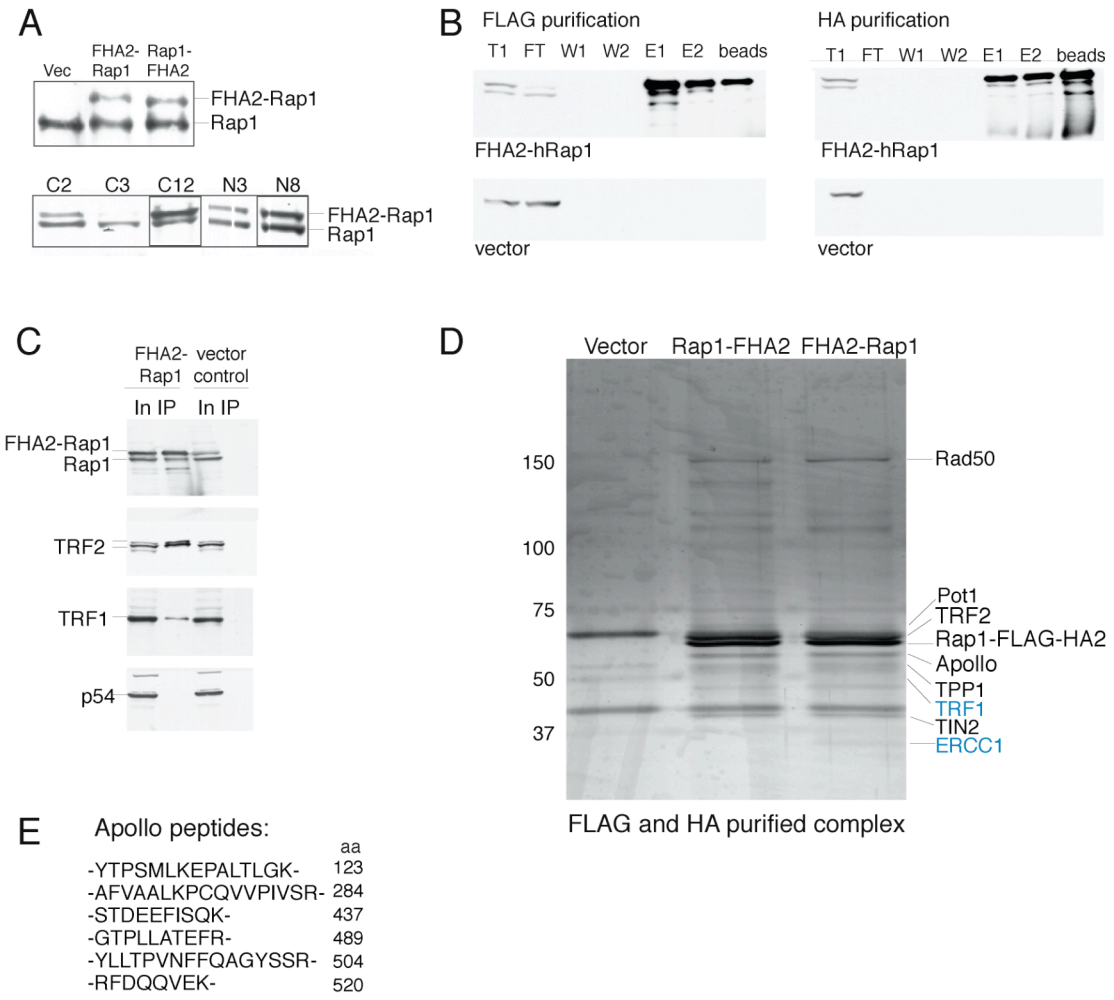

Figure 2-2. Apollo interacts with the TRF2/Rap1 complex.

(A) HeLa S3 parental cell lines (above) and examples of clones (below). Clonal cell lines used to isolate the TRF2/Rap1 complex are shown in gray boxes (C-terminally tagged clone 12, N-terminally tagged clone 8). (B) Tandem purification using tagged Rap1 FLAG and HA epitopes. Total (T1), Flow through (FT), Washes (W1-W2), Elutions (E1-2). Immunoblots were probed with anti-Rap1 #765. (C) Immunoblotting analysis of the purified TRF2/Rap1 complex. The affinity-purified TRF2/Rap1 complex from HeLaS3 cells expressing N terminally tagged hRap1 or vector control cells analyzed for the presence of hRap1 (765), TRF1 (371), TRF2 (647), or a control nuclear protein (anti-p54) is shown. Input (I) lanes contained 0.1% of input lysate, elution (E) lanes contained 2% of the eluate. (D) Proteins present in purified TRF2/Rap1 complex. Shown is a silver-stained gel of the indicated affinity-purified TRF2/Rap1complexes derived from HeLaS3 cells expressing FHA2-tagged hRap1 (N- or C-terminally tagged as indicated) and material derived from vector control cells processed in parallel. Relevant interacting proteins that were identified by mass spectrometry and immunoblotting are indicated in black and blue, respectively, next to the lanes. (E) Peptide sequences identifying SNM1B/Apollo.

The isolated TRF2/Rap1 complex from both N- and C-terminally tagged Rap1 contained specific bands that were not present in the vector control, indicating that the position of the affinity tag did not interfere with our ability to pulldown Rap1 interacting partners (Fig. 2-2D). The polypeptides in the FHA_2-Rap1 preparations were subjected to mass spectrometry analysis using two methods. In collaboration with the Chait lab at Rockefeller, the entire lane was sliced into 2 mm pieces, or individual bands were cut out and analyzed using the mass spectrometry facility at Rockefeller. All bands were trypsin digested and analyzed by MS/MS. We found the presence of previously identified TRF2-associated components RAD50 and ERCC1 by both methods (Fig. 2-2D).

Prior to this study, it was assumed that TRF1 and TRF2 formed independent complexes at telomeres where TRF1 and its interacting factors were responsible for telomere length regulation and the TRF2 complex was responsible for protecting telomeres from the DNA damage response. However, in both methods to isolate the TRF2/Rap1 complex, polypeptides were recovered from all six shelterin components: TRF1, Pot1, TRF2, Rap1, Tin2, and TPP1 (Fig. 2-2C-D). The TRF1/Tin2 complex isolated in a similar manner also revealed the presence of all six shelterin components and further experiments showed that Tin2 is the lynchpin of these two complexes [48].

The putative nuclease hSNM1B (Apollo) identified as part of the TRF2/Rap1 complex

In the course of these experiments, a protein migrating slightly faster than tagged Rap1 was reproducibly observed. The identity of this Rap1 associated protein remained elusive using the Chait lab technique involving

slicing the entire gel lane. Therefore, we repeated the isolation of the Rap1 complex to excise the 60 kDa band for mass spectrometry (Fig. 2-2D). Mass spectrometry of the 60 kDa Rap1-associated protein identified six peptides from SNM1B (Fig. 2-2E).

Figure 2-3. SNM1A, SNM1B/Apollo, and SNM1C/Artemis nuclease domains.

A

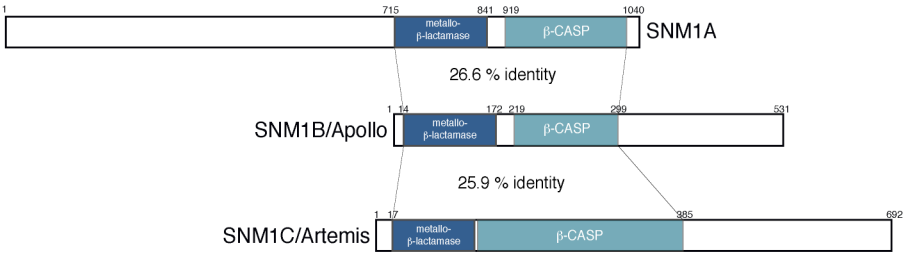

B

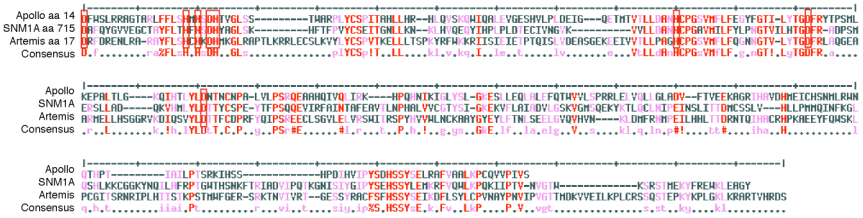

C

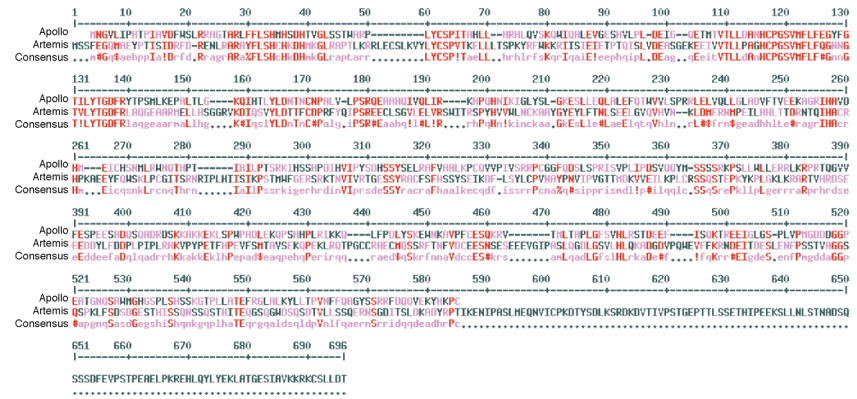

Figure 2-3. SNM1A, SNM1B/Apollo, and SNM1C/Artemis nuclease domains.

(A) Alignment showing the relative position of metallo-β-lactamase and β-CASP domains in SNM1A-C. Numbers correspond to amino acids. The % identity of SNM1A and SNM1C relative to SNM1B in nuclease domain indicated. (B) Alignment of the metallo-β-lactamase and β-CASP regions of SNM1A, SNM1B/Apollo, and SNM1C/Artemis. Residues required for Zn ion coordination and endonuclease activity of Aretmis are shown in red boxes. Specific amino acids used for the alignment are shown in (A). (C) Alignment of full length Apollo and full length Artemis. Alignments were generated using MultAlin (http://bioinfo.genopole-toulouse.prd.fr/multalin/multalin.html).

The nuclease domains of SNM1A, SNM1B, and SNM1C demonstrate a great deal of conservation. The metallo-β-lactamase and β-CASP domains of SNM1B and SNM1A share 26.6% identity (Fig. 2-3A-B). Artemis and SNM1A share 22.5% identity in this conserved region (Fig. 2-3A-B). Alignment of the metallo-β-lactamase and β-CASP domains in these three proteins reveals a total conservation in Apollo and SNM1A of the residues shown to be required for Aretmis endonuclease activity, and are predicted to be involved in Zn ion coordination in the metallo-β-lactamase super family (Fig. 2-3B shown in red boxes) [142] [130]. Artemis has roughly the same relatedness to SNM1B as it has to SNM1A in its metallo-β-lactamase and β-CASP domains (25.9% and 22.5% identity, respectively) (Fig. 2-3B). Yet, Artemis and SNM1B share a structural similarity in the N-terminal position of their nuclease domains, whereas the nuclease domain of SNM1A is C-terminally positioned (Fig. 2-3A). To emphasize the structural relatedness of SNM1B and Artemis, we refer to this protein as Apollo, the twin brother of Artemis in Greek mythology.

The C-terminus of Artemis is rich in SQ sites, the predicted phosphorylation motif for the phosphoinositide-3-OH-kinase-related kinases (PIKKs) ATM, ATR, and DNA-PKcs [143] [144]. Artemis has been shown to be phosphorylated by DNA-PKcs on these sites and this phosphorylation confers endonuclease activity on Artemis [145]. Artemis has also been reported to be a phosphorylation target of ATM and ATR [146]. These sites are not conserved in Apollo (Fig. 2-3C). Human Apollo has four different S/TQ sites at residues 349, 364, 418, and 444 (Fig. 2-3C, Fig. 2-4B-C). Only T349 is conserved in the mouse (Fig. 2-4B-C). An Apollo peptide containing phosphorylated SQ344 was isolated from human cells in a screen for

proteins phosphorylated by ATM or ATR in response to DNA damage [147]. This site is conserved only in chimpanzees and not other primates or mammals examined and might reflect a unique method of modulating human Apollo that is not found outside the great apes (Fig. 2-4C).

Figure 2-4. Structure, detection, and phosphorylation of SNM1B/Apollo.

A

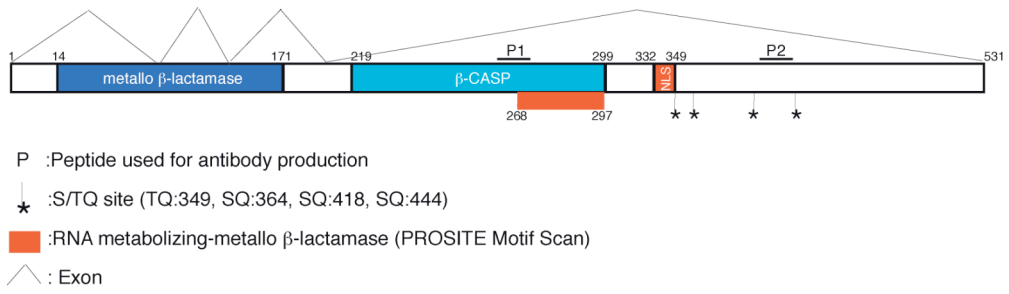

B

C

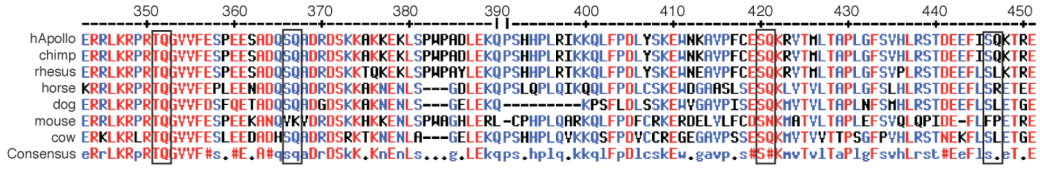

Figure 2-4. Structure, detection, and phosphorylation of SNM1B/Apollo.

(A) Schematic of human Apollo indicating peptides used for making antibodies, putative PIKK phosphorylation sites, nuclease domains, NLS, and exon structure. (B) Alignment of human, mouse, and chicken Apollo showing divergence in C-terminus and lack of conservation of S/TQ sites. Nuclease domains and NLS are boxed in red. Phosphorylation sites in human Apollo are indicated with (*). (C) Alignment of putative PIKK phosphorylation sites in mammalianApollo homologs. Putative phosphorylation sites are in black boxes. Numbers above represent amino acid position.

The C-terminal part of the β-CASP motif in Apollo contains an RNA metabolizing motif that is also found in SNM1A but not Artemis (Prosite motif Scan) (Fig. 2-4A). The genomic structure of Apollo has four exons (Fig. 2-4A). Human and mouse Apollo have two splice variants, one containing all four exons and one lacking exon 2. The latter mRNA has a frameshift into an alternative reading frame in exon 3 that ends with a stop codon at amino acid 72. This form of Apollo is predicted to be 8.2 kDa and to only contain a portion of the metallo-β-lactamase domain and no NLS.

Apollo interacts with TRF2

The association of Apollo with shelterin was verified based on recovery of endogenous shelterin components in immunoprecipitates (IPs) of transiently transfected Myc-tagged Apollo in 293T cells. Myc-Apollo brought down TRF2 and Rap1 but not TIN2 or TRF1 (Fig. 2-5A). IPs of Apollo co-transfected with individual shelterin components showed an association of Apollo with TRF2 and Rap1, whereas the recovery of Apollo in association with TRF1, TIN2, and POT1 was minimal (Fig. 2-5B). In order to determine whether Apollo could associate with TRF2 and to what extent Rap1 contributed to the interactions, we co-transfected Apollo with several TRF2 truncation alleles. These experiments indicated that Apollo can associate with the TRFH (TRF homology) [41 60] region of TRF2, which is a protein-protein interaction domain that mediates homodimerization of TRF2 (Fig. 2-5C,E). Since the TRFH domain is not sufficient for the interaction of TRF2 with Rap1 [62], these results imply that the Apollo-TRF2 interaction is likely to be Rap1 independent. The co-IP of Apollo and Rap1 (Fig. 2-5A-B) is probably due to the efficient association of Rap1 with endogenous TRF2. In

the course of these experiments, we also found that Apollo had the ability to interact with itself, resulting in co-immunoprecipitation of Myc-tagged and HA-tagged Apollo (Fig. 2-5D). These results suggest that Apollo associates with shelterin through an interaction with TRF2.

Figure 2-5. Apollo interacts with the TRFH domain of TRF2.

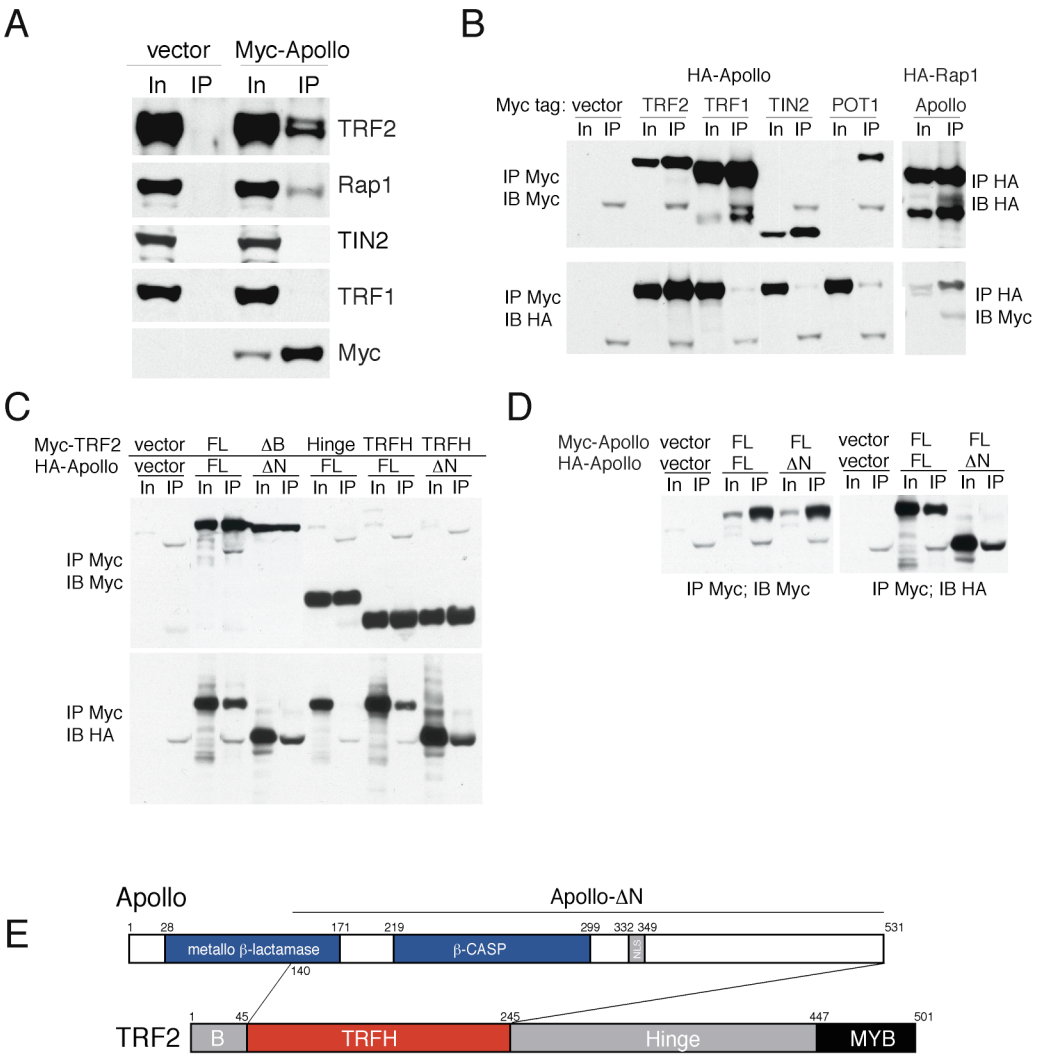

Figure 2-5. Apollo interacts with the TRFH domain of TRF2.

(A) Interaction of Apollo with endogenous TRF2 and Rap1, but not TIN2 or TRF1. 293T cells were transiently transfected with pLPC-Myc-Apollo and immunoprecipitations (IP) were performed with the Myc antibody 9E10. IPs were analyzed by immunoblotting for the proteins indicated at the right, using the following Abs (top to bottom): 647, 765, 864, 371, and 9E10. For panels A-D lanes marked In represent 2.5% of in the input lysate used for the IPs.(B) Co-IP of Apollo with co-transfected TRF2 and Rap1. 293T cells were transiently transfected with the indicated pLPC constructs and IPs were performed with the 9E10 Myc antibody (left) or an HA antibody (HA.11) (right). IPs were analyzed by immunoblotting (IB) for protein expression (top), and for interaction with Apollo (bottom) using the indicated antibodies.(C) Apollo interacts with the TRFH domain of TRF2. Myc IPs of extracts from 293T cells transfected with the indicated constructs were immunoblotted with the Myc antibody to detect TRF2 alleles and the HA antibody to detect Apollo. The TRF2 domains referred to above the lanes (FL: full length) and the ΔN version of Apollo are shown in panel E. (D) Apollo interacts with itself. 293T co-transfection experiments were as in panels B and C with the indicated constructs. Antibodies used for IP and IB are indicated. (E) Schematic of the interaction between Apollo and TRF2. B, basic domain. TRFH, TRF homology domain. MYB, Myb-type DNA binding domain. NLS, putative nuclear localization signal.

Structural analysis of the Apollo-TRF2 interaction

The extreme C-terminus of Apollo (aa 496-532) is required for interaction with the TRFH domain of TRF2 [148]. The Lei lab (University of Michigan) tested the binding strength of this interaction using isothermal titration calorimetry (ITC). Apollo$_{aa\ 496\text{-}532}$, refered to as Apollo$_{TBM}$, binds to the TRFH domain of TRF2 with a Kd of 0.12 μM, whereas no binding enthalpy was observed under the same conditions between Apollo and the TRFH domain of TRF1 (Fig. 2-6A). The structures of the TRFH domains in TRF1 and TRF2 are almost identical [60]. To understand how Apollo interacts specifically with TRF2 and not TRF1, the TRFH domain of TRF2 was co crystallized with Apollo$_{aa498\text{-}509}$ (Fig. 2-6B-C). Residues L500 and Y504 in Apollo make key interactions with TRF2-TRFH, whereas these residues are occluded from interacting with TRF1-TRFH (Fig. 2-6D, Fig. 2-7A). Tin2 can bind to the same molecular surface on TRF2-TRFH as Apollo. However, Tin2 binds weakly to TRF2-TRFH (Kd of 6.5 μM) and strongly to TRF1-TRFH (Kd of 0.31 μM). Comparison of these structures revealed that Tin2F258 lacks the ability to make electrostatic interactions that ApolloY504 makes with TRF2-TRFH in the equivalent position (Fig. 2-6E, Fig. 2-7A). From this comparison arose the putative TRF1-TRFH and TRF2-TRFH binding motifs, FxLxP and YxLxP, respectively (Fig. 2-7E).

A

TRFH	TRFH-binding peptide	K_d(μM)
$TRF2_{TRFH}$	$Apollo_{TBM}$	0.12
$TRF2_{TRFH}$	$Apollo_{TBM}$Y504A	> 1,000
$TRF2_{TRFH}$	$Apollo_{TBM}$L506A	> 1,000
$TRF2_{TRFH}$	$Apollo_{TBM}$L506E	nd
$TRF2_{TRFH}$	$Apollo_{TBM}$P508A	> 350
$TRF2_{TRFH}$F120A	$Apollo_{TBM}$	nd
$TRF1_{TRFH}$	$Apollo_{TBM}$	nd

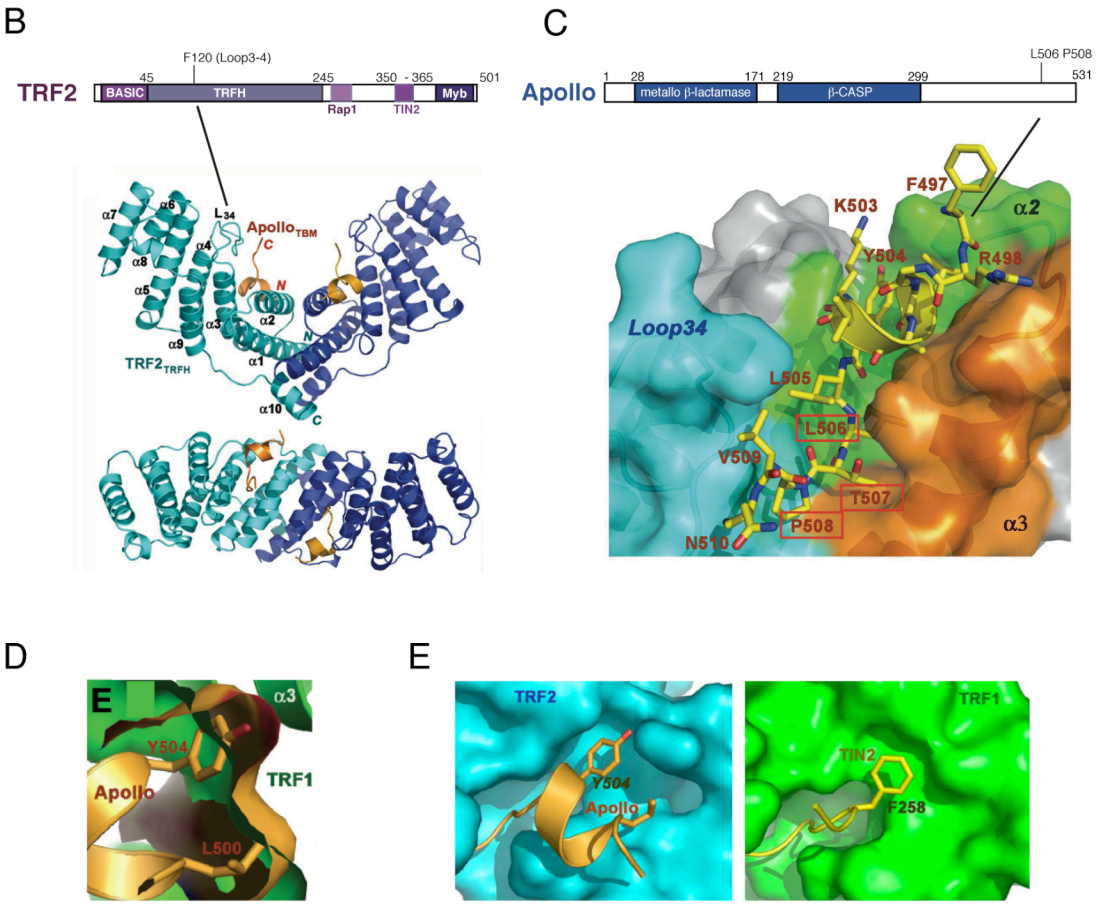

Figure 2-6. Structural analysis of the Apollo-TRF2 interaction.

(A) In vitro ITC measurements of the interactions of TRF2-TRFH and TRF1-TRFH with wild type and mutant Apolloaa496-532 peptides. (B) Overall structure of the dimeric TRF2-TRFH/Apolloaa496-532 complex. TRF2-TRFH and Apolloaa496-532 are colored in blue and orange, respectively. Schematic of TRF2 above indicating position of F120 in the context of the full length protein. (C) TRF2-TRFH/Apolloaa496-532 interface. Residues mutated in Apollo for co-IP experiments are boxed. Above, schematic of Apollo indicating positions of L506 and P508 in the context of the full length protein. (D) Overlay of TRF1-TRFH structure with Apollo peptide showing the occlusion of Apollo residues L500 and Y504. (E) Hydrophobic and electrostatic interactions of Apollo Y504 in context of the TRF2-TRFH domain (left). Hydrophobic pocket showing Tin2 F258 interaction in the context of the TRF1-TRFH domain. Above experiments were performed by Yong Chen and Ming Lei, University of Michigan {Chen et al., 2008, Science, 319, 1092-6}.

Based on this structure, mutation of F120 in the TRF2-TRFH domain in a loop between alpha helix 3 and 4 was predicted to abolish interaction with Apollo. Apollo residue L506 fits into a hydrophobic cleft in TRF2 and P508 stacks with F120 in the TRFH domain of TRF2 (Fig. 2-7A). Mutation of these residues in Apollo is expected to abrogate interaction with TRF2. I mutated Apollo at the residues predicted to be required for Apollo binding to the TRFH of TRF2 and tested the ability of this point mutant to co-IP with TRF2. As shown in previous co-IP experiments, Apollo robustly interacts with TRF2 and TRF2ΔB (Fig. 2-7B). In agreement with the structure predictions, TRF2ΔB-F120A did not co-IP with Apollo and Apollo-L506EP508A (from here on referred to as ApolloΔTRF2) did not co-IP with TRF2 (Fig. 2-7B).

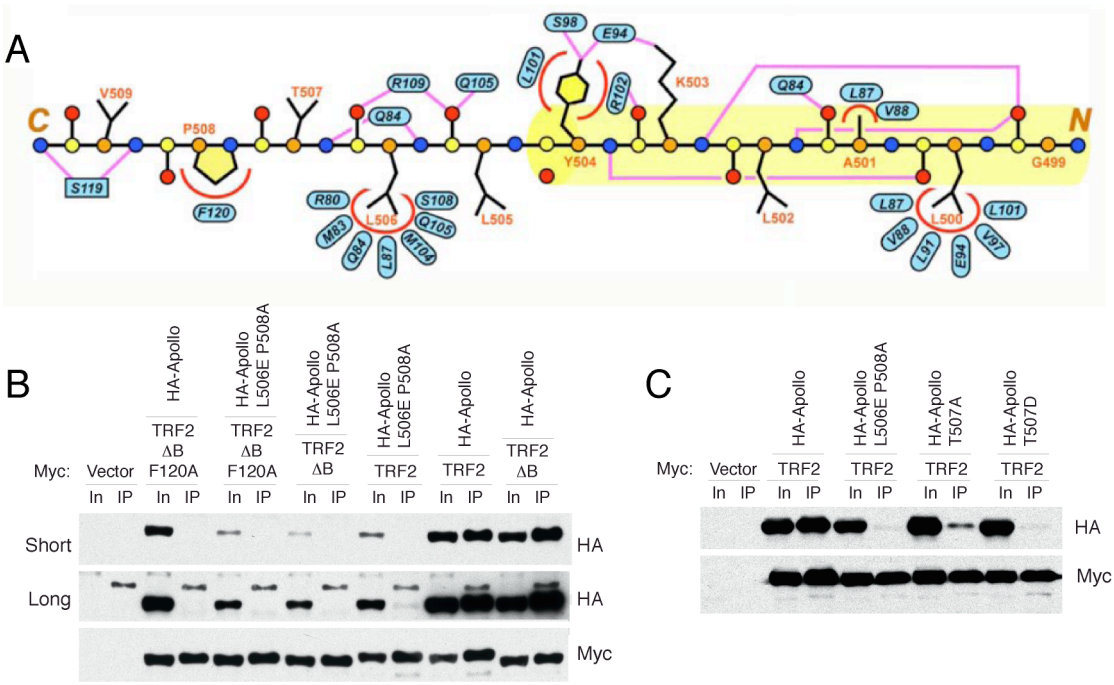

D

TRF2 F120 L3-L4 interaction motifs:

```
TIN2:          GRHFNLAPLGRRR
Apollo:        ALKYLLTPVNFFQ

putative:

XPF:           VGDYILTPEMCVE
ATM:           ESVYSLYPTLSRL
ATR:           DAEYLLGPLYAAL
PARP1:         NRFYTLIPHDFGM
Nbs1:          IPNYQLSPTKLPS
consensus         YxLxP
```

TRF1 F142 L3-L4 interaction motifs:

```
TIN2:          GRHFNLAPLGRRR

putative:

BLM:           EDCFILMPTGGGL
EST1A:         HEEFDLSPDQWRK
EST1B:         KRCFRLAPTFSNL
consensus         FxLxP
```

Figure 2-7. Apollo L506E P508A does not bind to TRF2.

(A) Linear representation of Apollo residues aa499-509 and the contacts they make with the TRFH domain in TRF2. (B) Apollo L506E P508A (ApolloΔTRF2) disrupts binding to TRF2. Co-IP of HA-Apollo and HA-Apollo L506E P508A with co-transfected myc-TRF2 and myc-TRF2 F120A. 293T cells were transiently transfected with the indicated pLPC constructs and IPs were performed with the 9E10 Myc antibody. IPs were analyzed by immunoblotting (IB) with the 9E10 Myc antibody for protein expression (bottom), and for interaction with Apollo (top-short exposure, middle-long exposure) with the HA.11 antibody. (C) Co-IP as in (A) with Myc-TRF2 and HA-Apollo mutated at a putative CDK1 site.(D) List of proteins that contain the YxLxP TRF2-TRFH interaction motif and the FxLxP TRF1-TRFH interaction motif.

Apollo has a putative CDK1 site in its TRF2 localization motif

Apollo has a potential CDK1 site (TP) within the TRF2 binding motif (CDK1 consensus site S/TPxK). Although tagged Apollo localizes to telomeres in a cell cycle independent manner, the possibility that endogenous Apollo might be cell cycle regulated cannot be excluded. Based on the TRF2-Apollo structure, phosphorylation of T507 in Apollo would increase the binding of Apollo to TRF2. Apollo T507 was mutated to T507D (phosphomimetic) and to T507A (abrogating phosphorylation) and the interaction of these mutants with TRF2 was examined in co-IP experiments. Inconsistent with the structure predictions, both the T507D and T507A largely abolished binding with TRF2. These mutations might destabilize the interaction of Apollo with TRF2 (Fig. 2-7C). This experiment does not rule out the possibility of cell cycle regulation of Apollo at telomeres, and it remains unclear whether T507 is a phosphorylation site for CDK1.

Apollo localizes to telomeres

To determine whether Apollo can associate with telomeres, we expressed Myc-tagged Apollo in hTERT-immortalized human BJ fibroblasts (BJ-hTERT) and determined its localization by indirect immunofluorescence (IF). Myc-tagged Apollo showed a homogeneous nuclear staining pattern. Extraction of soluble nucleoplasmic proteins with Triton-X-100 revealed numerous small Myc-Apollo foci that coincided with TRF1 and Rap1 signals (Fig. 2-8A), indicating that they represented telomeres. Tagged Apollo was also found in small foci that did not co-localize with telomeric markers. HA-tagged Apollo also colocalized to telomeres in BJ-hTERT using a DNA probe to detect telomeres $(CCCTAA)_3$ (Fig. 2-8B). Z-stack images taken of these cells indicate that Apollo localizes to the majority of

telomeres in BJ-hTERT cells. To further confirm Apollo's localization to telomeres, ChIP experiments were performed on BJ-hTERT cells expressing Myc-Apollo. Immunopreciptitation of Myc-Apollo resulted in a small but significant enrichment of telomeric DNA (Fig. 2-9A-B).

Figure 2-8. Tagged Apollo localizes to telomeres.

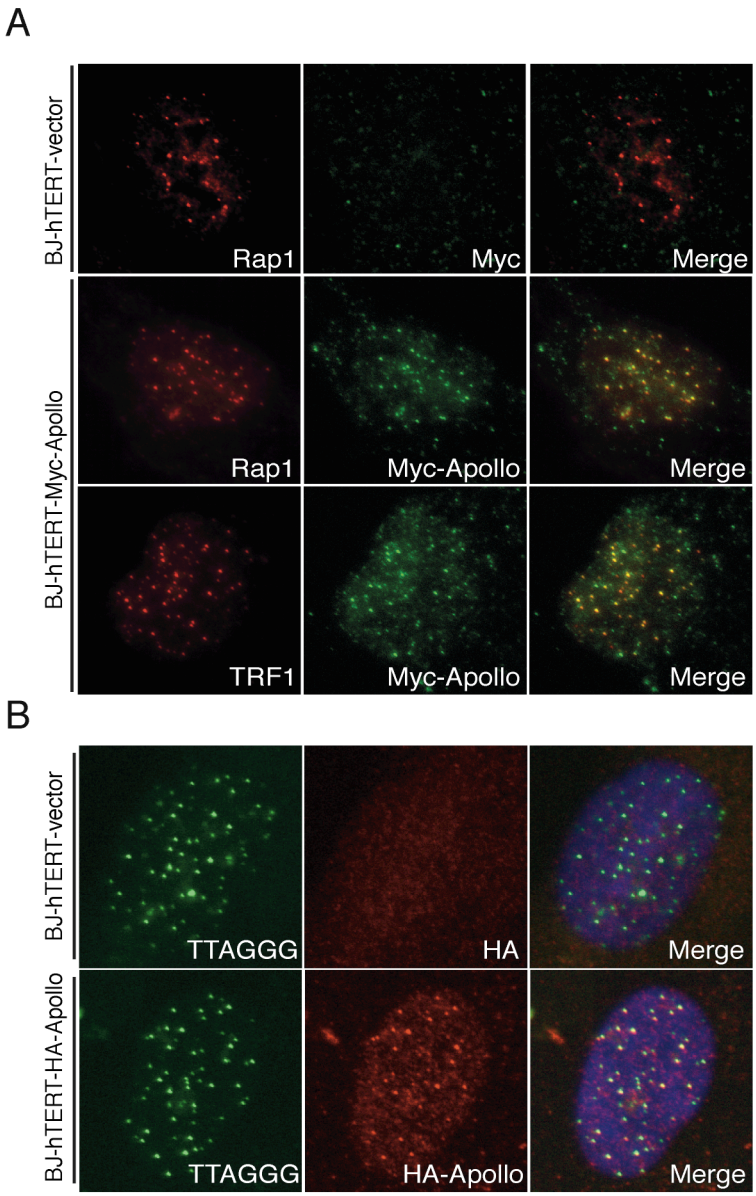

Figure 2-8. Tagged Apollo localizes to telomeres.

(A) Localization of retrovirally expressed Myc-tagged Apollo in BJ-hTERT cells. Apollo was detected using the 9E10 Myc Ab (Alexa 488, green). Rap1 was detected with Ab 765 (RRX, red). TRF1 was detected with Ab 371 (RRX, red). Cells were extracted with Triton-X-100 to remove soluble proteins. Top panels: BJ-hTERT cells infected with the empty pLPC vector. (B) Localization of retrovirally expressed HA-tagged Apollo in BJ-hTERT cells. Apollo was detected using HA.11 Ab (RRX, red). Telomeres were detected with a TTAGGG-specific FISH probe (FITC, green).

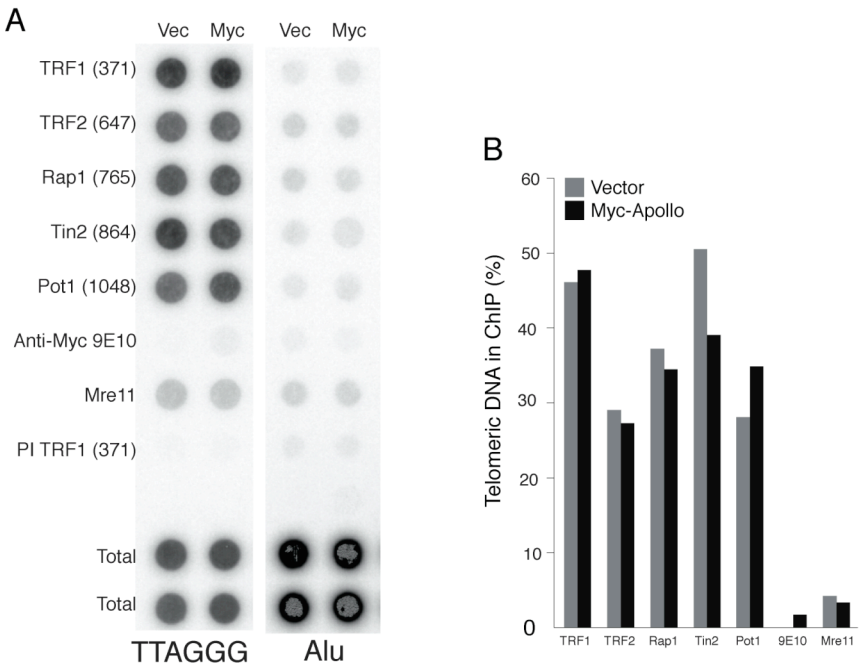

Figure 2-9. Apollo localizes to telomeres by ChIP.

(A) Telomeric ChIP on BJ-hTERT cells infected with pLPC-vector and pLPC-Myc-Apollo using the indicated antibodies or pre-serum (PI). Duplicate blots were probed for telomeric (TTAGGG) or Alu repeats. (B) Quantification of the data in (A) representing per cent TTAGGG repeat DNA recovered in each ChIP. Average duplicate signals obtained with total DNA samples were used at 100% value for the quantification.

The localization of Apollo to telomeres is dependent on TRF2

To test whether the localization of Apollo to telomeres was dependent on its interaction with TRF2, HA-Apollo and HA-ApolloΔTRF2 were expressed in BJ-hTERT cells and their patterns were analyzed by FISH-IF. As shown previously in Fig. 2-8B, HA-Apollo expressing cells have a punctate pattern that almost completely colocalizes with a probe recognizing TTAGGG (Fig. 2-10A). In contrast, HA-ApolloΔTRF2 has a diffuse nuclear staining without foci that colocalize with telomeres (Fig. 2-10A). This indicates that TRF2 is required for the recruitment of Apollo to telomeres.

Apollo vertebrate homologs have a strong conservation of this motif in the otherwise non-conserved/divergent C-terminus of Apollo (Fig. 2-10B).

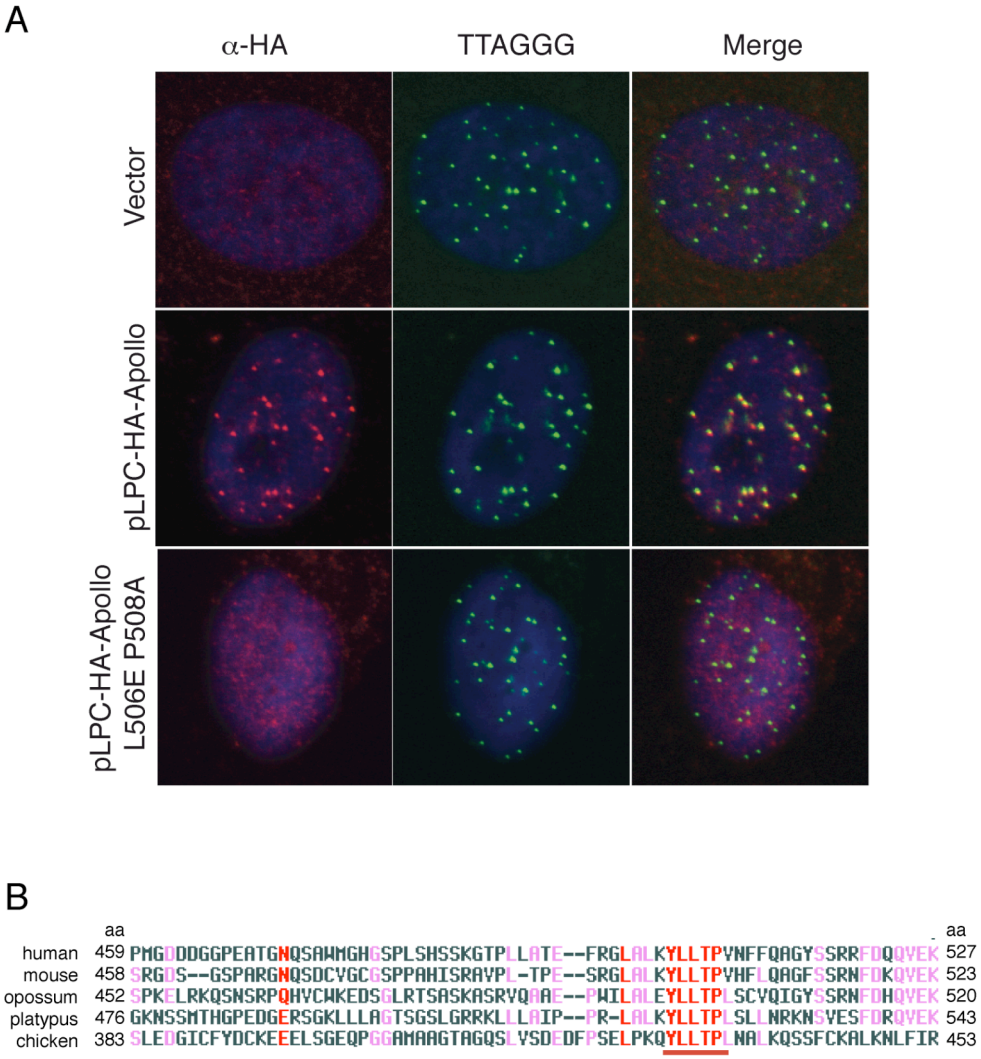

Figure 2-10. Apollo L506E P508A (ApolloΔTRF2) does not localize to telomeres.

(A) Localization of retrovirally expressed HA-tagged wildtype and L506E/P508A double mutant of Apollo in BJ-hTERT cells. Exogenous Apollo was detected with HA.11 (RRX, red). Telomeres were detected with a TTAGGG-specific FISH probe (FITC, green). Vector control top panels. (B) Alignment of vertebrate Apollo homologues to demonstrate the sequence conservation of YxLxP. Aligment was performed using MultAlin (http://bioinfo.genopole-toulouse.prd.fr/multalin/multalin.html)

Apollo antibodies

Attempts to detect endogenous Apollo by immunoblotting and IF using purified anti-peptide antibodies failed (Fig. 2-11A-C). As these α-Apollo antibodies detected retrovirally expressed Apollo by IF and in immunoblots, the failure to detect the endogenous protein is most likely due to its low abundance, which was noted previously for other members of the β-CASP family [133 138 139 138 139] (Fig. 2-11B-C). We further tested the antibodies by immunoblot using extracts from cells treated with the proteasome inhibitor MG-132. HA-Apollo and p53 were stabilized after treatment with this drug, but endogenous Apollo was still not detectable (Fig. 2-11C). A 60 kDa non-specific band, thought initially to be Apollo, did not diminish in extracts of cells treated for five days with an Apollo shRNA (UTR) (Chapter 3 Fig. 3-1B) (Fig. 2-11C). To determine whether Apollo expression might be limited to certain stages of the cell cycle, HeLa cells were synchronized using Aphidicolin and a double Thymidine block. Western Blotting for Cyclin B was used to determine the progression of cells into mitosis (Fig. 2-11D). The blot probed with anti-Apollo antibodies did not reveal any bands that increased in intensity over the course of the cell cycle (Fig. 2-11D). Furthermore, I was not able to IP endogenous Apollo or TRF2 with these antibodies (Fig. 2-8D). As described in the next chapter, Apollo can be detected by RT-PCR, indicating that Apollo is transcribed.

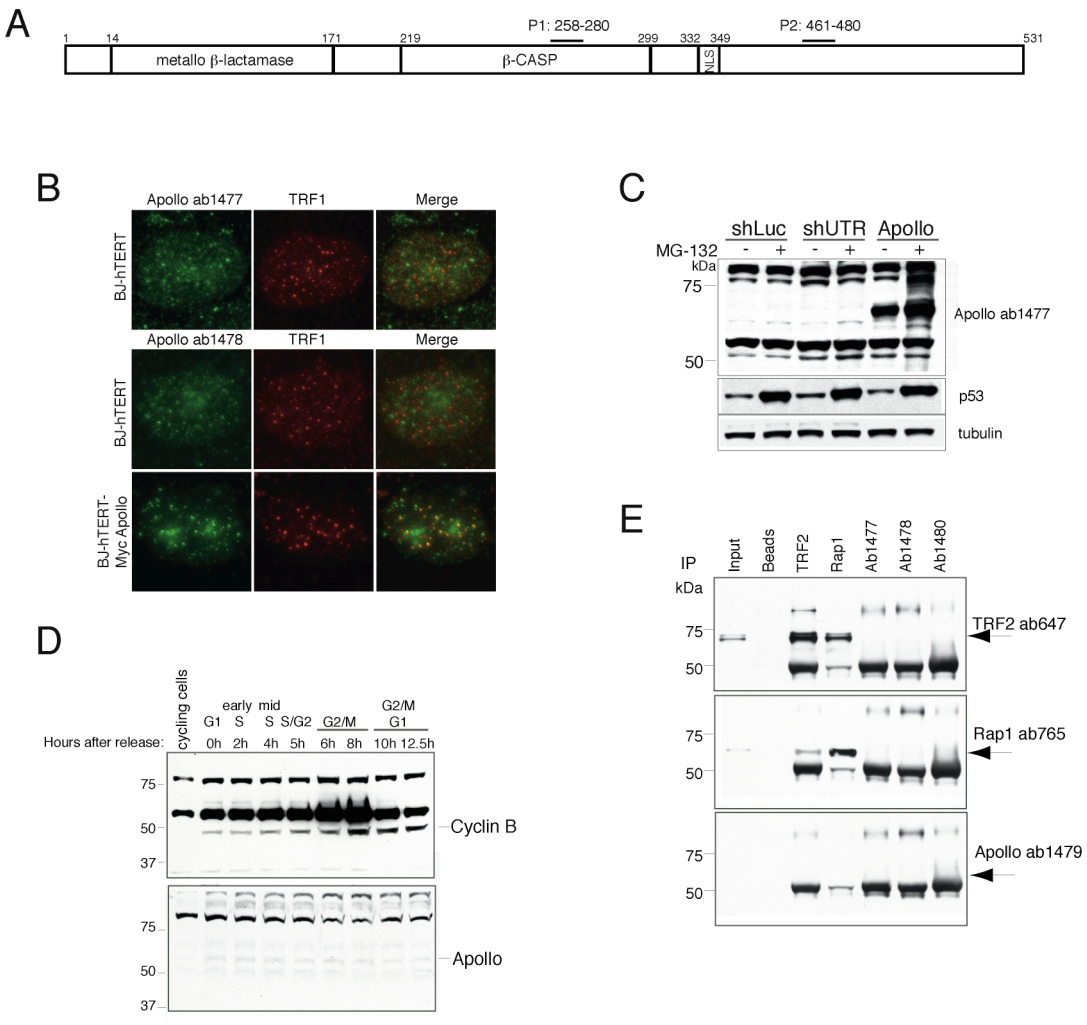

Figure 2-11. Apollo peptide antibodies recognize exogenous but not endogenous Apollo.

(A) Location of peptides used to generate Apollo antibodies. Abs 1477 and 1478 were generated by injecting two rabbits with P1. Abs 1479 and 1480 were generated by injecting two rabbits with P2. (B) IF staining in BJ-hTERT and BJ-hTERT Myc-Apollo using Apollo antibodies ab 1477 and ab 1478. (C) Immunoblot of IMR90 extracts treated with the proteasome inhibitor MG-132. Luc: Luciferase shRNA, UTR: Apollo shRNA targeting 3'UTR, Apollo: pLPC-HA-Apollo. Antibodies as indicated. (D) Immunoblot of synchronized HeLa cell extracts. Cell cycle stage and hours post-release as indicated. Antibodies: Cyclin B (Santa Cruz), Apollo Ab 1477. (E) HeLa cell extracts were immunopreipitated with the antibodies indicated at top (Ab 1477, Ab 1478, Ab 1480 all Apollo antibodies). Immunoblots using the indicated antibodies.

Apollo does not localize to sites of DNA damage

We investigated whether Apollo relocalizes to sites of damage. After exposure to a wide range of DNA damage inducing insults, the localization of HA-Apollo at telomeres remained unchanged (Fig. 2-12A). Furthermore, in contrast to what has been reported for SNM1A, a general re-localization of HA-tagged Apollo to sites of DNA damage (marked by γ-H2AX foci in our experiments) was not observed (Fig. 2-12A). The effect of DNA damage on HA-Apollo, TRF2, and TRF1 protein levels was tested by immunoblotting. IR and UV-induced damage did not have an effect on the levels of these proteins. However, TRF2 protein levels increased in cells treated with the DNA replication inhibitors Hydroxy Urea, and Aphidicolin as well as inter-strand crosslink-inducing drugs cisplatin and MMC (Fig. 2-12B). Cells treated with these drugs will accumulate in S-phase and will therefore have an increased protein concentration compared with cycling cells. Considering this, TRF2 levels are still increased by comparison with TRF1 and Apollo protein levels. HA-Apollo levels are mildly increased in response to cisplatin (Fig. 2-12B). As expected, Chk2 is phosphorylated in response to IR and Chk1 is phosphorylated in response to UV, replication stress, and ICL-inducing agents (Fig. 2-12B).

Fig. 2-12. Apollo does not relocalize to from telomeres to sites of DNA damage.

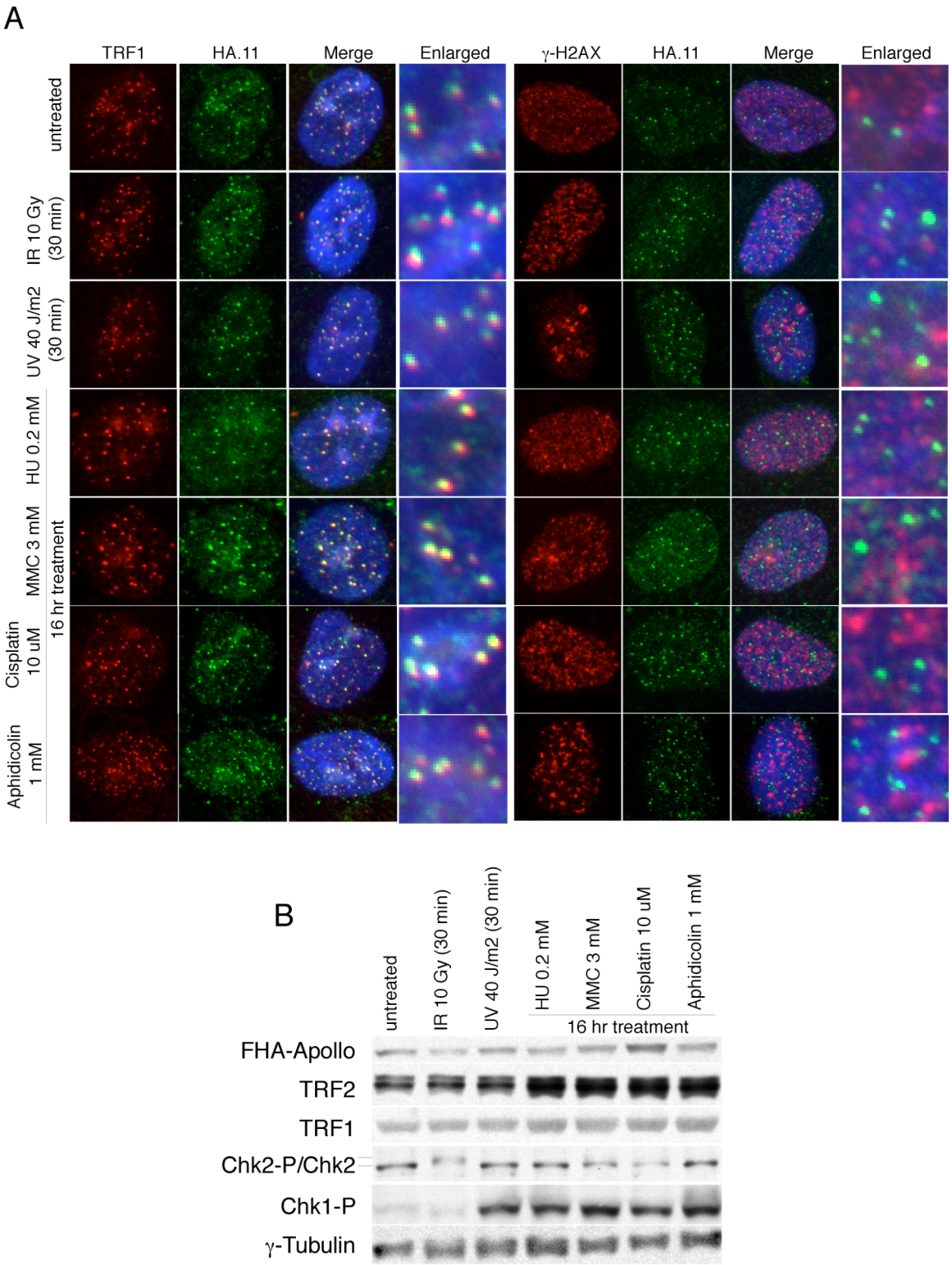

Fig. 2-12. Apollo does not relocalize to from telomeres to sites of DNA damage.

(A) Localization of retrovirally expressed HA-Apollo in BJ-hTERT cells after the indicated treatments (left). TRF1 (#371) and γ-H2AX (upstate) in red (RRX). HA-Apollo in green, (Alexa 488). Cells were pre-extracted with Triton-X-100. (B) Immunoblot of extracts taken from cells in (A). Antibodies, HA.11, TRF2 (647), TRF1 (371), Chk2 (BD Transduction), P-Chk1 (cell signalling), tubulin.

Discussion

The experiments discussed in this chapter reveal the binding of a novel factor at telomeres, the Apollo nuclease. Its low abundance at telomeres argues against Apollo being a component of the shelterin core complex. Hence, Apollo appears to be one of the shelterin accessory factors that are present as low copy number at telomeres and/or have a transient association with chromosome ends.

The localization of Apollo at telomeres is dependent on TRF2. Apollo is recruited to telomeres by interacting with a region around F120 in the TRFH domain of TRF2 using a putative TRF2-TRFH interacting motif, YxLxP. This motif is found in many known TRF2 interacting proteins, including Nbs1, PARP-1, ATM, and XPF. The multimeric organization of TRF2 might provide enough binding sites for all of these proteins in a single complex. Alternatively, TRF2 might bind to telomere accessory factors in discrete subcomplexes. Outside of the YxLxP motif and neighboring residues, the C-terminus of Apollo is not well conserved in vertebrate homologs (Fig. 2-4B, Fig. 2-7D).

Unlike SNM1A, tagged Apollo does not relocalize to sites of damage. This might indicate that Apollo performs a dedicated role at telomeres. Alternatively, telomeres might act as a sink for Apollo when overexpressed and a few molecules of tagged or endogenous Apollo might be sufficient at sites of damage and are not detected by IF. TRF2 protein levels are stabilized after treatment with replication inhibitors and ICL-inducing agents and tagged Apollo levels are increased after treatment with cisplatin. This observation suggests a possible role for these proteins in telomere replication, as discussed further in Chapter 3.

CHAPTER 3: APOLLO IS REQUIRED TO PROTECT TELOMERES IN S-PHASE

Shelterin prevents telomeres from being recognized as sites of damage

When telomeres become deprotected, proteins involved in DNA damage signaling and repair localize to telomeres forming foci called Telomere-dysfunction Induced Foci (TIF). TIFs occur in settings where TRF2 and Pot1 are compromised [86 77 63 149 150], and during replicative senescence[151] when shortened telomeres might lack sufficient shelterin to repress the DNA damage response.

DNA damage signaling after removal of TRF2 is dependent on the ataxia telangiectasia mutated (ATM) kinase [83 77 82]. The DNA damage response factors 53BP1 and γH2AX no longer localize to telomeres in TRF2-/- ATM-/- MEFs. Additionally, ATM deficient human fibroblasts show a reduction in apoptosis after treatment with a dominant negative allele of TRF2 [83]. To repress ATM at the telomere, TRF2 might act by restraining ATM locally through direct interaction [95]. Additionally, TRF2 might hide structures that would activate ATM such as the junction where the 5' end meets the base of the D loop in a t-loop conformation.

Single-stranded DNA in the D loop is another aspect of t-loops that may need sheltering. Pot1 binds to ssDNA at telomeres and inhibits signaling by the ATM-related Rad3 kinase (ATR) [82]. Chk1, the downstream effector kinase of ATR, is phosphorylated after Pot1 deletion and Pot1 deficient MEFs lacking ATR do not accumulate DNA damage response factors at telomeres. In response to replication stress, ATR and its associated protein ATRIP are loaded onto RPA-coated single stranded DNA [152]. Pot1

might act to suppress ATR by effectively competing with RPA for binding single-stranded telomeric DNA.

Telomeres fuse end-to-end in the absence of TRF2 [45]. Telomere fusion events are dependent on ATM and components of the NHEJ repair machinery [79 63 80 82]. In *S. cerevisiae* the telomere binding protein Rap1 is required to prevent NHEJ at telomeres [153]. Rap1 is conserved in vertebrates and its localization at telomeres is dependent on TRF2 [62]. In a biochemical assay to test DNA repair by NHEJ, human Rap1 prevents end joining of cut telomere-containing plasmid DNA [154]. Additionally, Rap1-/- mice show embryonic lethality before E10.5, suggesting that Rap1 might be required to suppress DNA damage signaling at the telomere (van Overbeek and de Lange unpublished results). Further testing using reconsititution experiments in TRF2-/- MEFs will be key in understanding the contribution of vertebrate Rap1 in preventing inappropriate repair at telomeres. Cells deficient for Pot1 do not exhibit a substantial amount of fusions [150]. However, telomeres fuse in an ATR dependent pathway in a Pot1 DKO, TRF2-/- ATM-/- setting [82]. This provides evidence that ATR can signal in the NHEJ pathway under certain conditions.

In addition to TIFs and telomere-telomere fusions, other indices of telomere dysfunction repressed by shelterin and shelterin associated factors include telomere sister chromatid exchanges, which are repressed by Ku80 in the mouse [155 156 80] , and telomeric DNA containing Double Minute chromosomes that may result from invasion of 3' overhang into interstial telomere related sequences in mouse cells in the absence of XPF/ERCC1[78].

Results

Apollo deficient primary cells have a growth defect

To determine the contribution of Apollo to telomere metabolism, Apollo transcripts were knocked down using RNAi. Target site algorithms were provided by the Whitehead Institute siRNA program (http://jura.wi.mit.edu/bioc/siRNAext/home). Off-target effects were minimized by excluding shRNAs that had non-Apollo targets based on BLAST search (targets shown in Fig. 3-1A). All five shRNAs were found to effectively reduce the Apollo mRNA levels as determined by RT-PCR (Fig. 3-1B). Two of the shRNAs were also tested for their ability to diminish the levels of Myc-tagged Apollo expressed from a retroviral construct using an Apollo specific antibody that recognizes overexpressed protein (Fig. 3-1C).

Figure 3-1. Structure, detection, and inhibition of Apollo.

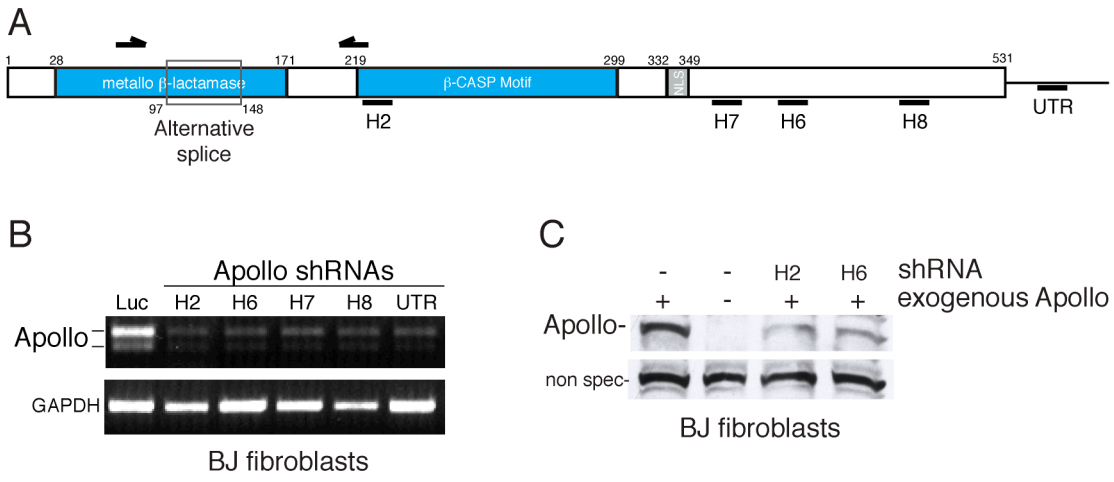

Figure 3-1. Structure, detection, and inhibition of Apollo.

(A) Schematic of Apollo indicating the PCR primers used for RT-PCR and the target sites of the shRNA hairpins used for Apollo knockdown. The RT-PCR strategy detects Apollo mRNA with and without inclusion of the indicated alternatively spliced exon. (B) Reduction of Apollo mRNA levels resulting from RNAi. RNA derived from cells infected with the indicated shRNA encoding retroviruses was processed to detect Apollo mRNA and GAPDH mRNA as a control using RT-PCR. The RT-PCR detects two versions of Apollo mRNA generated by alternative splicing (Luc, luciferase shRNA). (C) Immunoblot showing reduced expression of exogenous Apollo upon introduction of Apollo shRNAs H2 and H6. BJ cells were infected with a retrovirus expressing Apollo or the empty vector and subsequently infected with the indicated shRNA retroviruses. An antibody raised to an Apollo peptide (Ab 1477) was used to detect the overexpressed protein. This antibody did not detect endogenous Apollo in immunoblots or by IF.

Primary human IMR90 fibroblasts with diminished Apollo mRNA levels showed a clear growth defect (Fig. 3-2A). Within a week of introduction of Apollo shRNAs, the cells gradually slowed their proliferation and appeared to arrest. Reduced proliferation was also observed in BJ and BJ-hTERT cells (Fig. 3-3A-B). The reduced proliferation was due to the depletion of Apollo since it was rescued by co-infection with a retrovirus encoding a mutated version of Apollo lacking the target site for one of the shRNAs (Fig. 3-2B). The knockdown cell lines grew at different rates. The cells expressing UTR4 and H8 hairpins grew faster than cells expressing the H7, H6, and H2 hairpins, even though the RT-PCR levels show a similar knockdown for all of these hairpins. This difference might reflect off-target effects of the hairpins or small variations in the residual mRNA level not easily detected by RT-PCR. A growth defect was not observed when Apollo was down regulated in HeLa cells, consistent with data from other groups (Fig. 3-3C)[139 148].

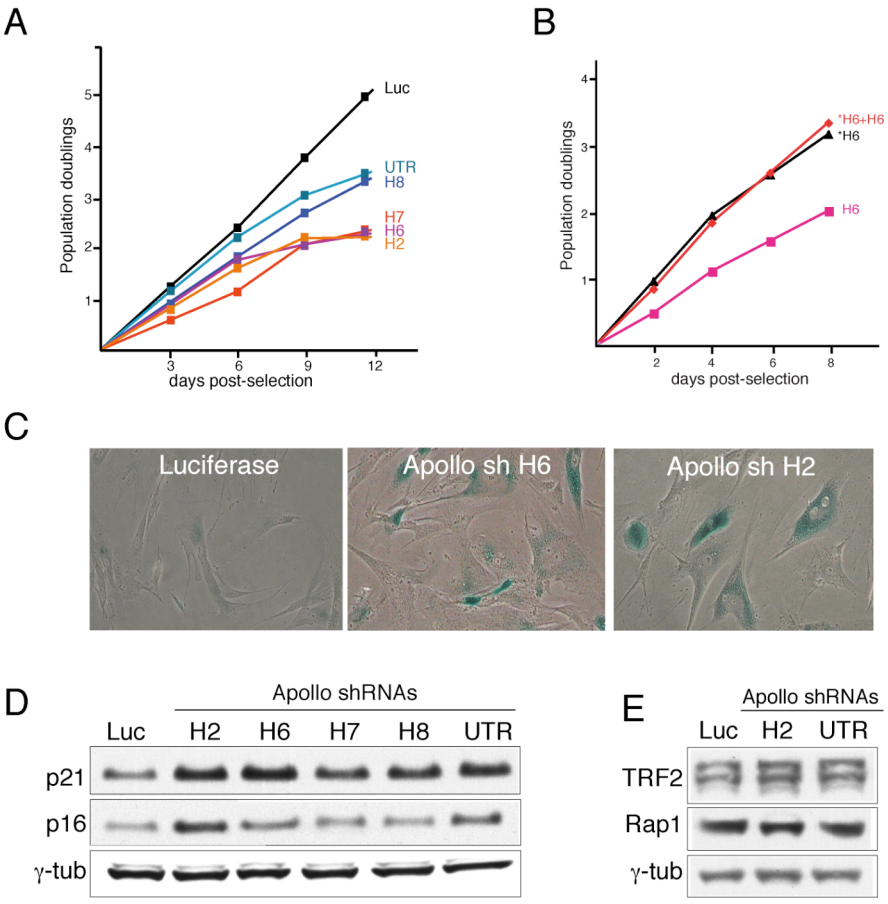

Figure 3-2. Diminished Apollo expression in human IMR90 fibroblasts results in a senescent-like phenotype.

(A) Diminished cell proliferation upon inhibition of Apollo. IMR90 cells were infected with the indicated shRNA retroviruses and subjected to puromycin selection for three days. Subsequently, cells numbers were measured at the indicated time points with day 0 representing the first day after puromycin selection. (B) Absence of the proliferation phenotype of Apollo shRNA H6 in cells that co-express shRNA-resistant Apollo (*H6). BJ cells were infected with the indicated shRNA retroviruses and subjected to puromycin selection for three days. Subsequently, cell numbers were measured at the indicated time points with day 0 representing the first day after puromycin selection. (C) Senescence-like phenotype of IMR90 cells with diminished Apollo expression. Twelve days after selection for the indicated shRNAs, cells were photographed after staining (37ºC, overnight) for SA-β-galactosidase. (D) Induction of p21 upon Apollo inhibition. Immunoblot of extracts from the cells shown in (B) at day 5 post-selection. (E) Apollo knockdown does not affect TRF2 and Rap1. Immunoblot of extracts from the cells shown in (B) at day 5 post-selection. Antibodies: TRF2 (647); Rap1 (765); γ-tubulin, GTU 488 (Sigma).

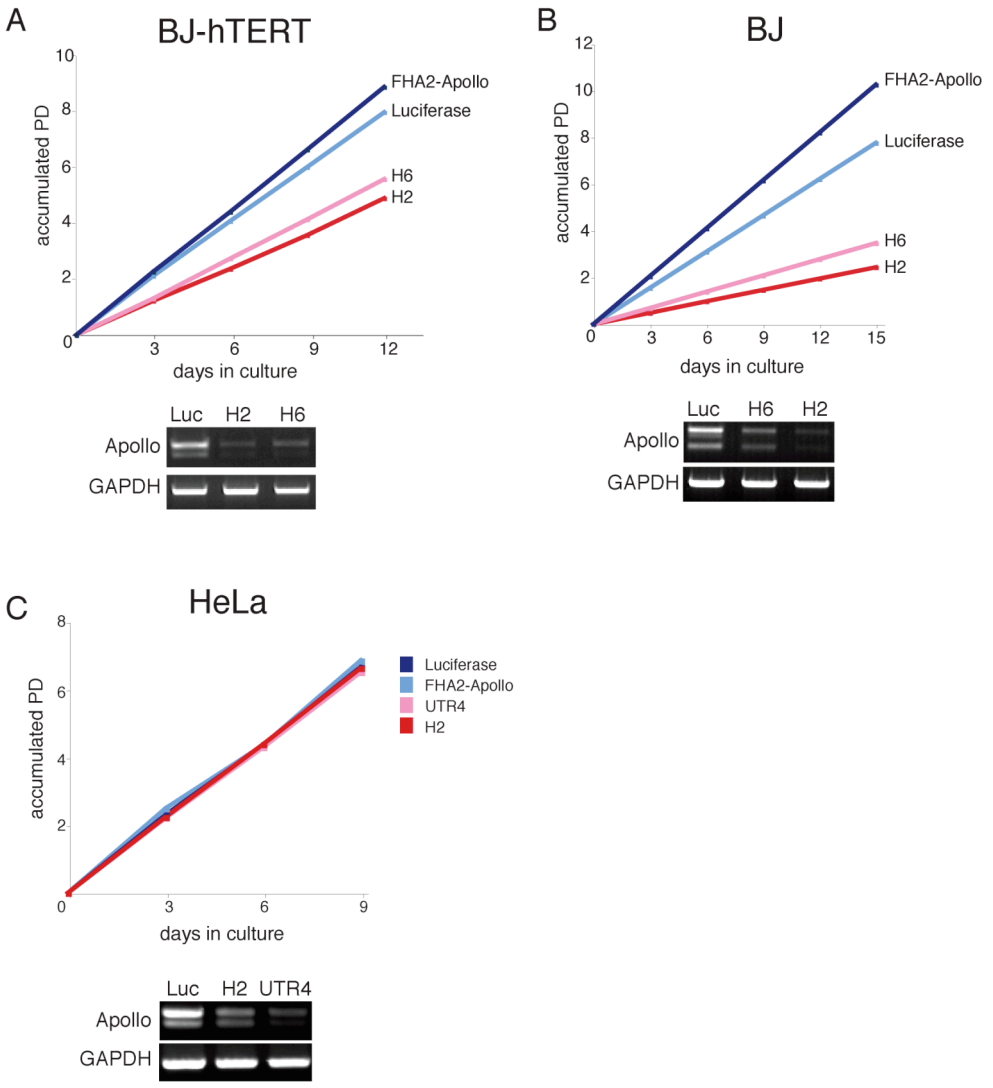

Figure 3-3. Diminished Apollo expression in human BJ and BJ-hTERT fibroblasts and not in HeLa cells results in a senescent-like phenotype.

(A-B) Diminished cell proliferation upon inhibition of Apollo in BJ and BJ-hTERT cells. (C) No growth defect upon inhibition of Apollo in HeLa cells. Cells were infected with the indicated shRNA retroviruses and subjected to puromycin selection for three days. Subsequently, cells numbers were measured at the indicated time points with day 0 representing the first day after puromycin selection. Apollo mRNA levels are indicated for each of the cell lines below the growth curve.

The Apollo knockdown cells had a senescent morphology and stained positive for SA-β-galactosidase, a marker for senescence (Fig. 3-2C). All Apollo shRNAs induced the upregulation of the CDK inhibitor p21, a read-out for p53 activation. Induction of p16, a second CDK inhibitor implicated

in senescence, only occurred with Apollo shRNA H2 and may therefore be an off-target effect (Fig. 3-2D). As cells deficient for TRF2 also have a senescent phenotype [45 63], we examined the TRF2 and Rap1 protein levels. The levels of these proteins were unaffected in Apollo knockdown cells, indicating that the senescence was not due to loss of TRF2 (Fig 3-2E). The data indicate that Apollo knockdown can induce a senescent-like phenotype.

Telomere Dysfunction-Induced Foci (TIFs) in Apollo deficient cells

The senescence resulting from Apollo knockdown is consistent with cells experiencing a persistent DNA damage signal. Diminished Apollo expression enforced by three independent shRNAs resulted in TIFs in ~20% of IMR90 cells (Fig. 3-4). The TIFs were obvious based on IF for γ-H2AX and 53BP1 and the co-localization of these DNA damage response factors with TRF1 (Fig. 3-4A). The median number of TIFs per nucleus was ~12 (Fig. 3-4C). The TIF phenotype associated with Apollo shRNA H6 was not observed if the cells co-expressed the version of Apollo resistant to this hairpin (Fig. 3-4E), showing that the DNA damage signal is the result of Apollo inhibition. Apollo knockdown also resulted in 53BP1 and γ-H2AX foci that were not obviously associated with telomeres, suggesting that Apollo is required for global genome integrity as well as telomere protection. However, more than half of the DNA damage response foci in Apollo knockdown cells were localized at chromosome ends (Fig. 3-4D), indicating that Apollo deficiency preferentially affected telomeres.

Figure 3-4. Induction of a telomere damage signal in cells with diminished Apollo.

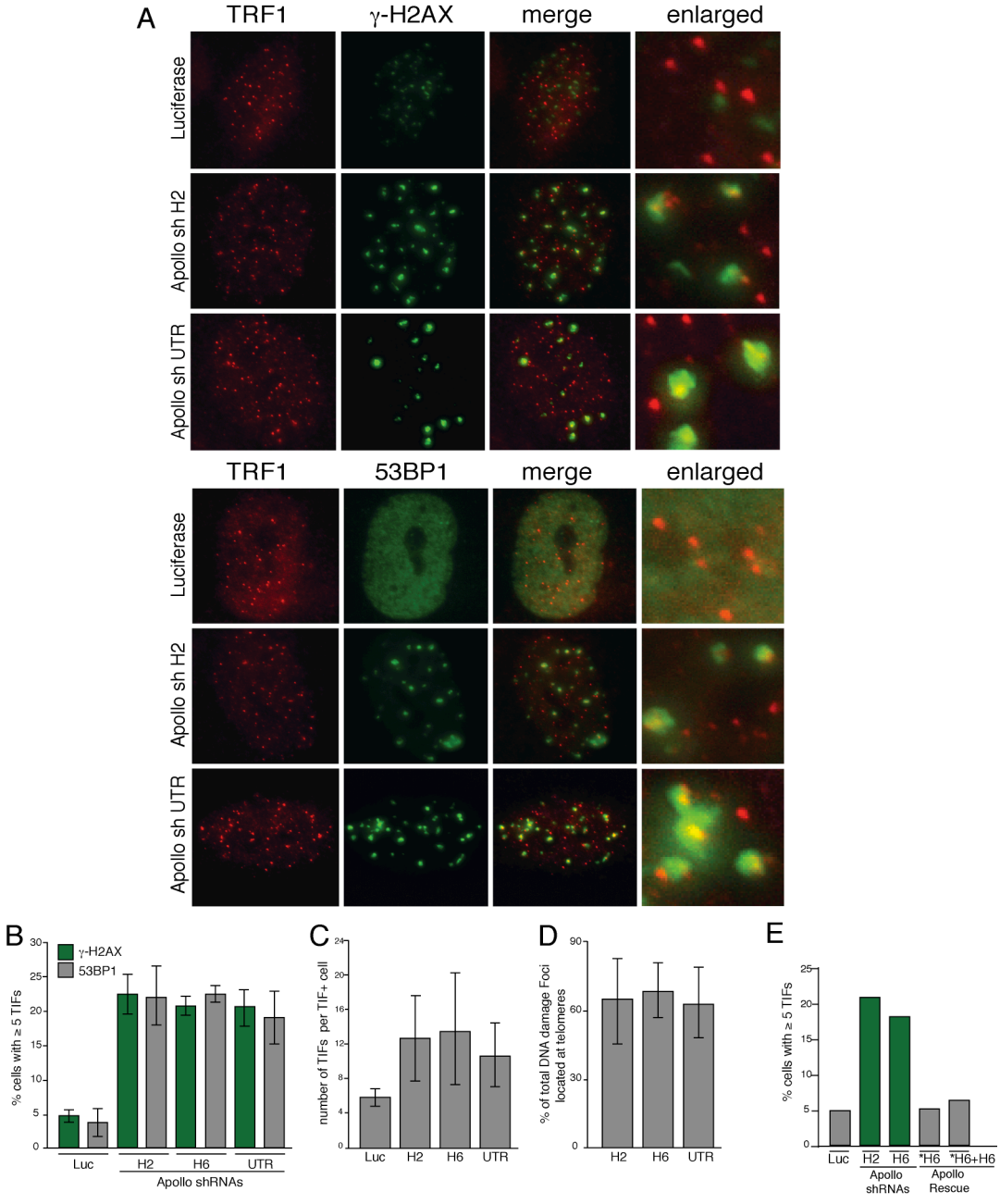

Figure 3-4. Induction of a telomere damage signal in cells with diminished Apollo.

(A) IF showing co-localization of γ-H2AX (top) and 53BP1 (bottom) foci with telomeric sites marked by TRF1 in IMR90 nuclei of cells treated with the Apollo shRNAs indicated on the left. Cells were processed at day 3 post-selection. (B) Quantification of the induction of TIFs by Apollo shRNAs. Cells were processed as shown in panel A and TIFs were scored based on co-localization of DNA damage factors with TRF1. The bargraph shows the percentage of cells (median and standard deviation based on n=3; >100 cells per data point) containing 5 or more TIFs for each of the indicated shRNAs. (C) Quantification of the number of TIFs per cell. Bar graph representing data derived from images as shown in (A). The percentage of foci co-localizing with TRF1 was determined in nuclei with ≥5 TIFs. (D) Quantitative analysis of the fraction of DNA damage foci that co-localize with telomeres. Cells were processed as in (A) and (B). For each TIF positive nucleus the percentage of foci co-localizing with TRF1 was determined. Data from γ-H2AX and 53BP1 IF were indistinguishable and pooled to generate the bargraphs.(E) Absence of the TIF phenotype of Apollo shRNA H6 in cells co-expressing shRNA-resistant Apollo (*H6). BJ cells were processed as shown in Fig. 3A and nuclei were inspected for TIFs based on co-localization of γ-H2AX with TRF1. The bargraph shows the percentage of cells containing 5 or more TIFs for each of the indicated cell lines.

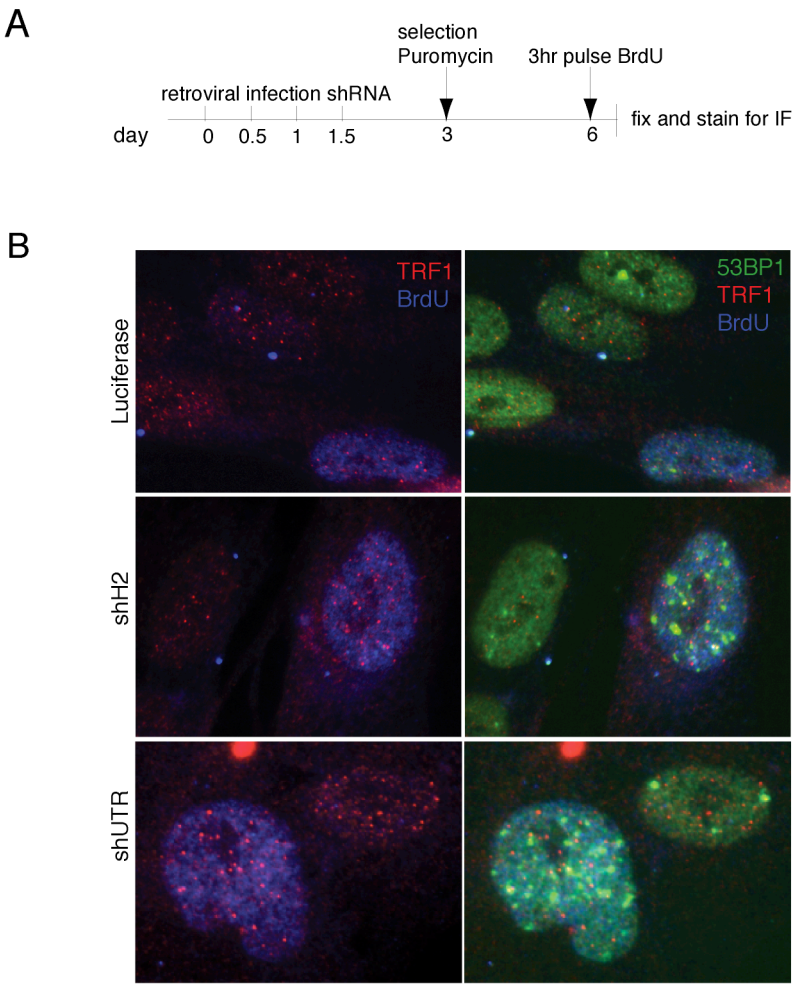

Figure 3-5. Telomere Dysfunction in Apollo knockdown cells occurs in S-phase.

(A) The experimental time line. IMR90 cells retrovirally infected with control shRNA and Apollo shRNAs H2 and UTR were pulsed with 10 μM BrdU for 3 hours, 3 days post selection. Cells were fixed and processed for TIF analysis, (B) Cells were stained for IF using antibodies to TRF1 (red), 53BP1 (right-green) and BrdU (blue).

Because the TIFs were only observed in ~20% of the Apollo knockdown cells, we asked whether they appeared in a specific stage of the cell cycle. Initial experiments suggested that the TIFs arose during or after DNA replication. Specifically, we noted that the TIF positive cells often had a subset of telomeric signals that appeared as doublets (Fig. 3-4A). This pattern suggested that the TIFs occurred in cells that had replicated some,

but not all of their telomeres. To test whether the TIFs were more prominent in S phase than in G1, we examined cells that had been cultured in the presence of BrdU for 3 hours (Fig. 3-5). Very few TIF positive cells lacked the ability to incorporate BrdU. The fraction of TIF positive cells that had incorporated BrdU was 91% and 83% for the Apollo shRNAs H2 and UTR, respectively (n≥150 for each) (Fig. 3-5). Collectively, the data suggest that Apollo contributes to the protection of telomeres during or soon after DNA replication. FACS analysis of BJ cells expressing hairpins H2 and H6 revealed an accumulation of cells in G2/M (~29% in knockdown cells compared with 18% in control cells and ~17% in cells overexpressing Apollo) (Fig. 3-6A-D).

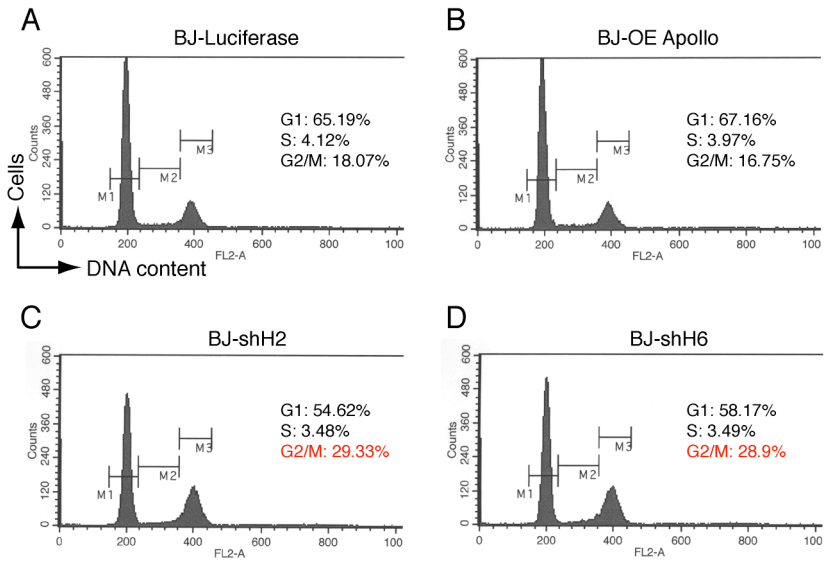

Figure 3-6. Apollo deficient BJ fibroblasts accumulate in G2/M.

FACS profile of Propidium Iodine stained BJ primary fibroblasts expressing (A) luciferase control hairpin (B) FHA2-Apollo (C) shRNA H2 and (D) shRNA H6 with the indicated percentages of cells in various stages of the cell cycle. The number of cells is represented on the y-axis and the DNA content is represented on the x-axis.

Multiple telomere FISH signal in Apollo deficient cells

Since knockdown of Apollo induced a DNA damage signal at telomeres, we evaluated the status of the telomeric DNA by Flouresence In-Situ Hybridization (FISH). The analysis of metaphase spreads derived from Apollo knockdown cells did not show significant levels of telomere aberrations (Fig. 3-7A), including telomere-telomere fusions[45], telomeric DNA containing Double Minute chromosomes, or extrachromosomal telomeric signals. However, we did observe a small but significant increase of chromatid ends with two or more distinct telomeric FISH signals instead of one (Fig. 3-7A and B). Telomere doublets at single chromatid ends have been noted previously in Atm-/- mouse cells, and have been recently observed in TRF1-/- mouse cells, and TRF2-/- mouse cells rescued with an allele of TRF2 that can no longer bind to Tin2 [157] (Agnel Sfeir, Jill Donigian, and Titia de Lange, unpublished results). They have also been described to occur at low frequency in unperturbed human fibroblasts and other human cells (Fig. 3-7B) [158]. The nature and origin of these aberrant telomere structures has not been established.

A

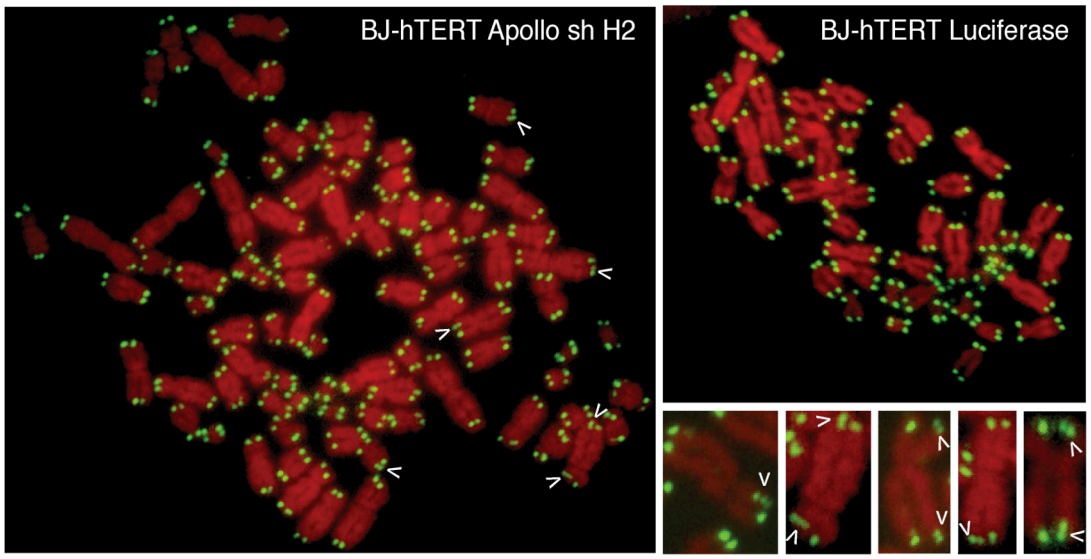

B

shRNA	Chromatid ends scored	Telomere doublets (% of ends)	
Luciferase	7544, 1544, 4616	1.9%, 1.3%, 1.0%	median 1.3±0.5%
H2	5324, 1056	4.7%, 3.8%	p<0.01
H4	3648, 1900	4.4%, 3.6%	
H6	4728	3.9%	median 4.0±0.4%
UTR	6144	4.2%	

Figure 3-7. Apollo shRNAs increase the occurrence of single chromatid multiple telomere signals

(A) Metaphase spreads illustrating presence of multiple telomere signals at single chromatid ends. Metaphase spreads were obtained from BJ-hTERT cells treated with the indicated shRNAs and processed for telomeric FISH (FITC, green). DNA was stained with DAPI (false colored in red). Arrowheads highlight chromatids with telomere multiple/doublet signals. Enlarged images (bottom right) are derived from BJ-hTERT cells and BJ cells expressing SV40 large T antigen both treated with Apollo shRNAs. Metaphases were harvested at day 3 post-selection. (B) Quantification of telomere doublets in BJ-hTERT cells treated with the indicated shRNAs. Metaphases were treated as in (A) and examined for the occurrence of double telomeric signals at each chromatid end. P value based on Student's t-test.

ApolloΔTRF2 mutant does not rescue telomere-specific phenotypes and partially rescues growth defect

A small portion of tagged Apollo localizes to sites other than telomeres and ~40% of damage foci in Apollo knockdown cells are not at telomeres. To test whether the Apollo knockdown phenotypes were due entirely to telomere dysfunction, rescue experiments were performed using an Apollo point mutant that cannot bind to TRF2 (ApolloΔTRF2, described in detail in Chapter 2). This mutant was expressed in BJ-hTERT and IMR90 cells where endogenous Apollo was simultaneously knocked down using a hairpin that targets its 3'UTR and is absent from the ApolloΔTRF2 construct. Neither the TIF phenotype nor the occurrence of multiple telomere signals was rescued by the expression of ApolloΔTRF2, whereas wild type Apollo fully rescued both phenotypes (Fig. 3-8A, Fig. 3-9A). Interestingly, cells overexpressing ApolloΔTRF2 showed TIFs and multiple telomere signals, although the phenotypes were less severe (Fig. 3-8A, Fig. 3-9A). This indicates that ApolloΔTRF2 may be a dominant negative allele that acts either by titrating limiting factors away from the telomere, or by dimerizing with endogenous Apollo and preventing it from binding to telomeres. The number of TIFs in TIF positive cells expressing both ApolloΔTRF2 and shUTR was greater than in cells expressing shUTR alone (Fig. 3-8C). Furthermore, TIFs accounted for ~75% of the damage foci in TIF positive cells expressing shUTR rescued with ApolloΔTRF2 compared with ~50-60% in TIF positive shUTR expressing cells (Fig. 3-8D). In contrast to the TIF and multiple telomere signal phenotypes, the growth defect of cells expressing ApolloΔTRF2 was not as severe as cells expressing the hairpin

alone (Fig. 3-9C). This data indicates that Apollo is required specifically at telomeres to suppress DNA damage signaling in S-phase.

Figure 3-8. TIFs are not rescued by expression of ApolloΔTRF2.

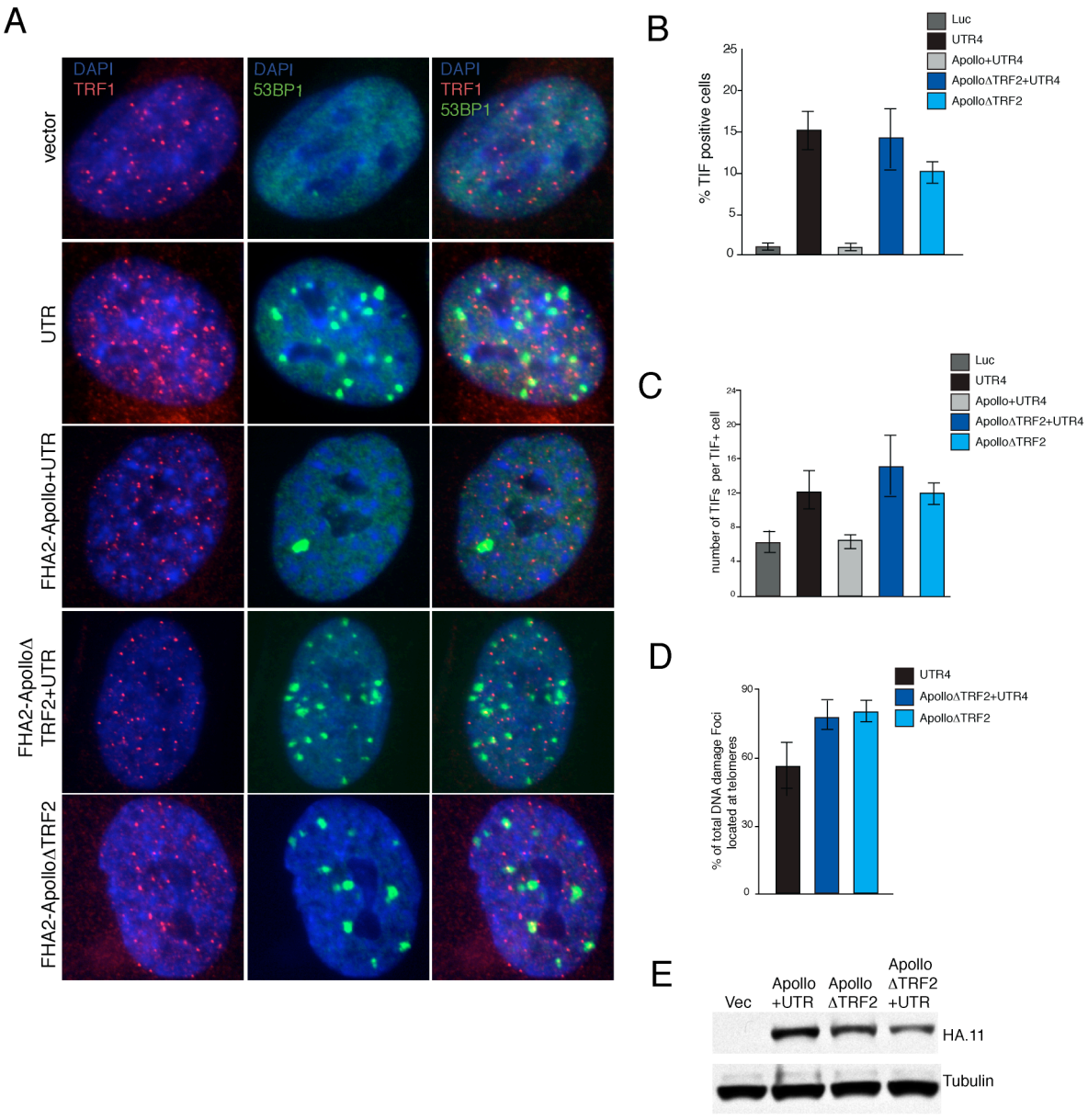

Figure 3-8. TIFs are not rescued by expression of ApolloΔTRF2.

(A) IF showing colocalization of 53BP1 (green) with telomeric sites marked by TRF1 (red) with DAPI staining to represent the nucleus (blue) in BJ-hTERT cells expressing an allele of Apollo that can not bind to TRF2 (indicated on the left). (B) Quantification of TIFs shown in (A). (C) Quantification of the number of TIFs per cell. Bar graph representing data derived from images as shown in (A). The percentage of foci co-localizing with TRF1 was determined in nuclei with ≥5 TIFs. (D) Quantitative analysis of the fraction of DNA damage foci that co-localize with telomeres. For each TIF positive nucleus the percentage of foci co-localizing with TRF1 was determined (E) Western Blot showing the relative expression of Apollo and ApolloDTRF2 with and without introduction of shRNA.

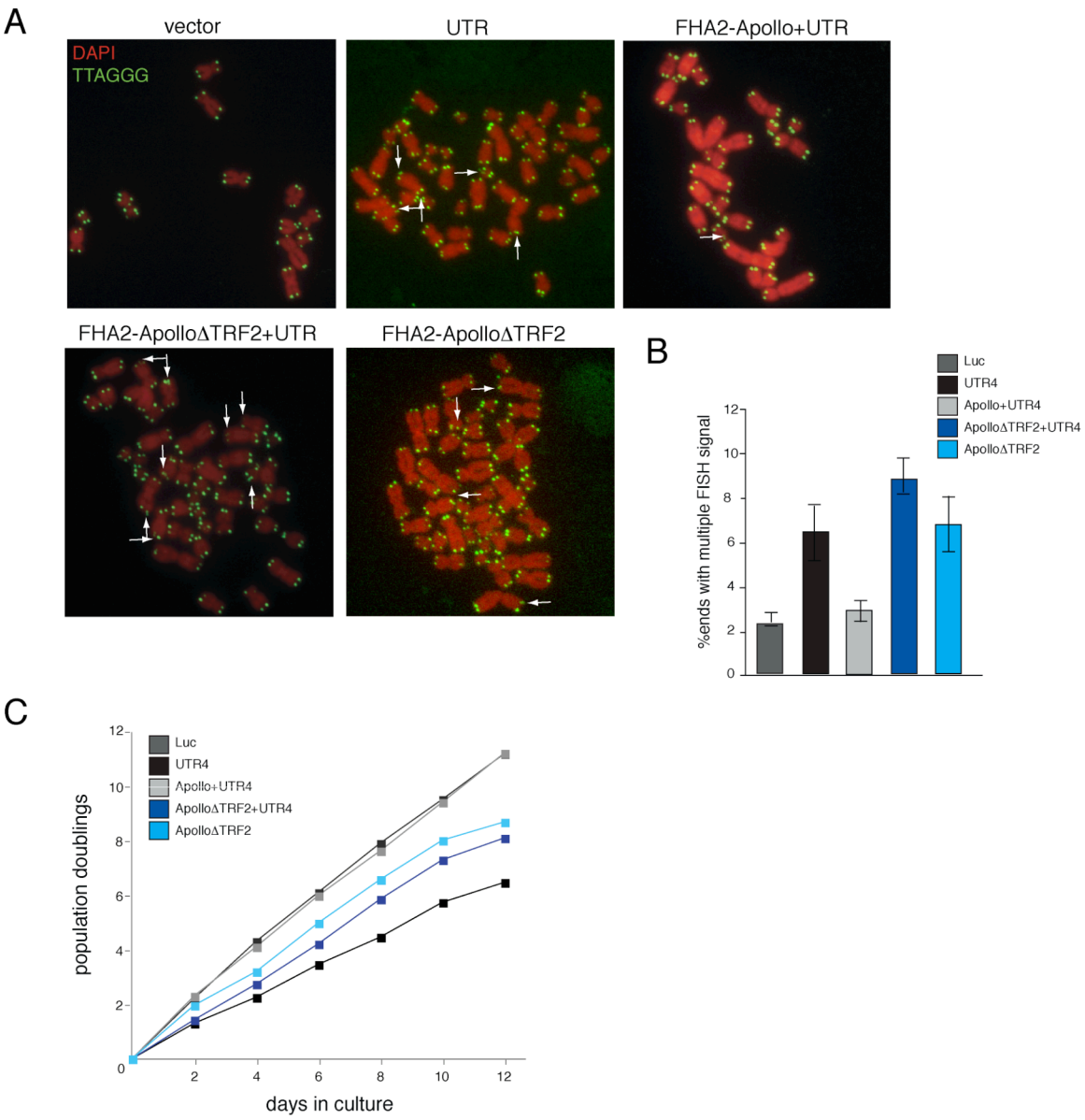

Figure 3-9. Multiple telomere signals on a single chromatid are not rescued by expression of ApolloΔTRF2.

(A) Metaphase spreads illustrating the presence of multiple telomere signals at single chromatid ends. Metaphase spreads were obtained from BJ-hTERT cells treated with the indicated shRNAs or mutants and processed for telomeric FISH (FITC, green). DNA was stained with DAPI (false colored in red). Arrowheads highlight chromatids with multiple telomere signals. (B) Quantification of multiple telomere signals shown in (A). (C) Growth curve of cell lines expressing Apollo and ApolloΔTRF2 . IMR90 cells were infected with the indicated shRNA retroviruses and subjected to puromycin selection for three days. Subsequently, cells numbers were measured at the indicated time points with day 0 representing the first day after puromycin selection.

Effect of replication inhibition on telomeres and Apollo

Because of the presence of S-phase specific telomere damage upon Apollo inhibition, we investigated whether the multiple telomere signals observed by FISH were also replication related, perhaps representing blocked replication forks. Cells were treated with Aphidicolin [0.3 μM] at a concentration that has been reported to induce expression of fragile sites [159], and monitored telomere status by FISH for the presence of multiple telomeric signals in metaphase chromosomes. Aphidicolin acts by competing with each of the four dNTPs for binding to a DNA polymerase α-DNA binary complex [160] and at fragile sites, aphidicolin induces gaps and breaks that lead to sister chromatid exchanges, translocations, and deletions [161 162]. Aphidicolin treatment resulted in a two-fold increase in the frequency of multiple telomere signals per chromosome end in Apollo knockdown cells as compared with Luciferase controls (Fig. 3-10A-B). Metaphase spreads from Apollo deficient cells treated with Aphidicolin were analyzed using Chromosome Orientation-FISH (CO-FISH) to examine the frequency of telomere sister chromatid exchanges (T-SCEs) [163]) (Fig. 3-11A). Although there was not a significant difference in T-SCEs in Apollo knockdown cells compared with Luciferase controls, all cells that were treated with Aphidicolin showed elevated levels of T-SCEs (9-10%) (Fig. 3-11B-C). Thus, Aphidicolin has two striking effects on telomeres. First, it increases the frequency of aberrant telomere structures in cells with diminished Apollo levels. Second, Aphidicolin induces a strong increase in T-SCE regardless of the Apollo levels in the cells.

A

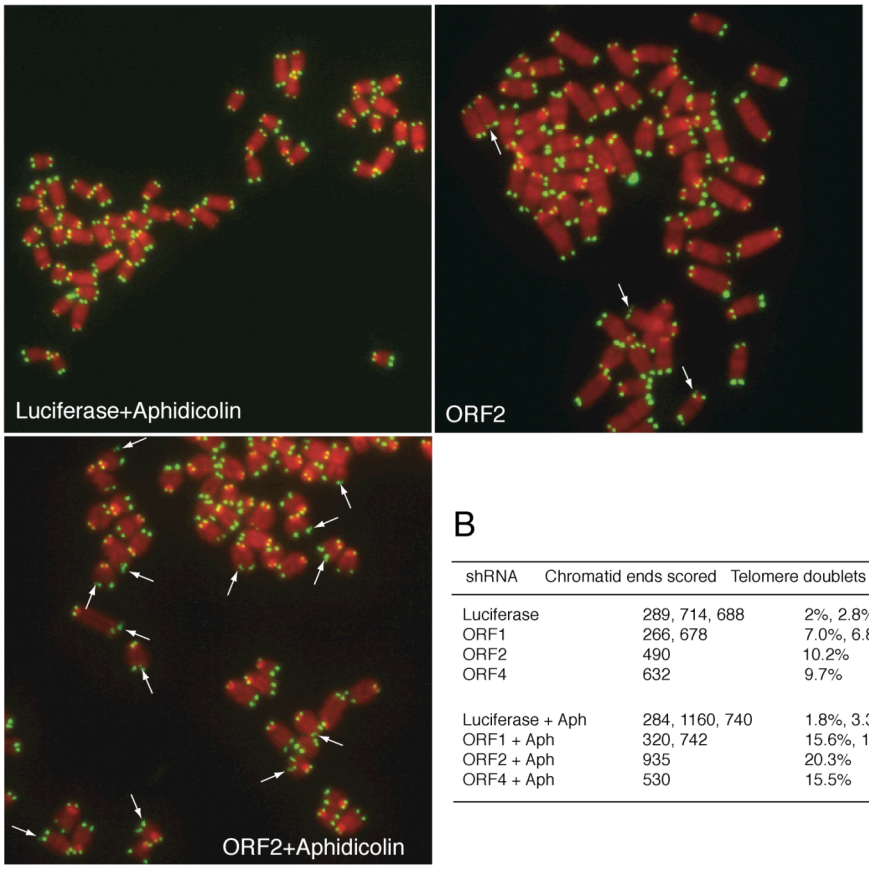

B

shRNA	Chromatid ends scored	Telomere doublets (% of ends)	
Luciferase	289, 714, 688	2%, 2.8%, 1.7%	median 2.2±0.6%
ORF1	266, 678	7.0%, 6.8%	median 8.4±1.8%
ORF2	490	10.2%	
ORF4	632	9.7%	
Luciferase + Aph	284, 1160, 740	1.8%, 3.3%, 2.6%	median 2.6±0.8%
ORF1 + Aph	320, 742	15.6%, 16.2%	median 16.9±2.3%
ORF2 + Aph	935	20.3%	
ORF4 + Aph	530	15.5%	

Figure 3-10. Aphidicolin treatment of cells expressing Apollo shRNAs increase the occurrence of multiple telomere signals on single chromatids.

(A) Metaphase spreads illustrating presence of multiple telomere signals at single chromatid ends. Metaphase spreads were obtained from p53-/- MEFs treated with the indicated shRNAs +/- Aphidicolin for 20 h [0.3 μM] and processed for telomeric FISH (FITC, green). DNA was stained with DAPI (false colored in red). Arrowheads highlight chromatids with multiple telomere signals. Metaphases were harvested at day 5 post-selection. (B) Quantification of single-chromatid multiple telomere signals in p53 -/- MEFs treated with the indicated shRNAs and +/- Aphidicolin for 20 h [0.3 μM].

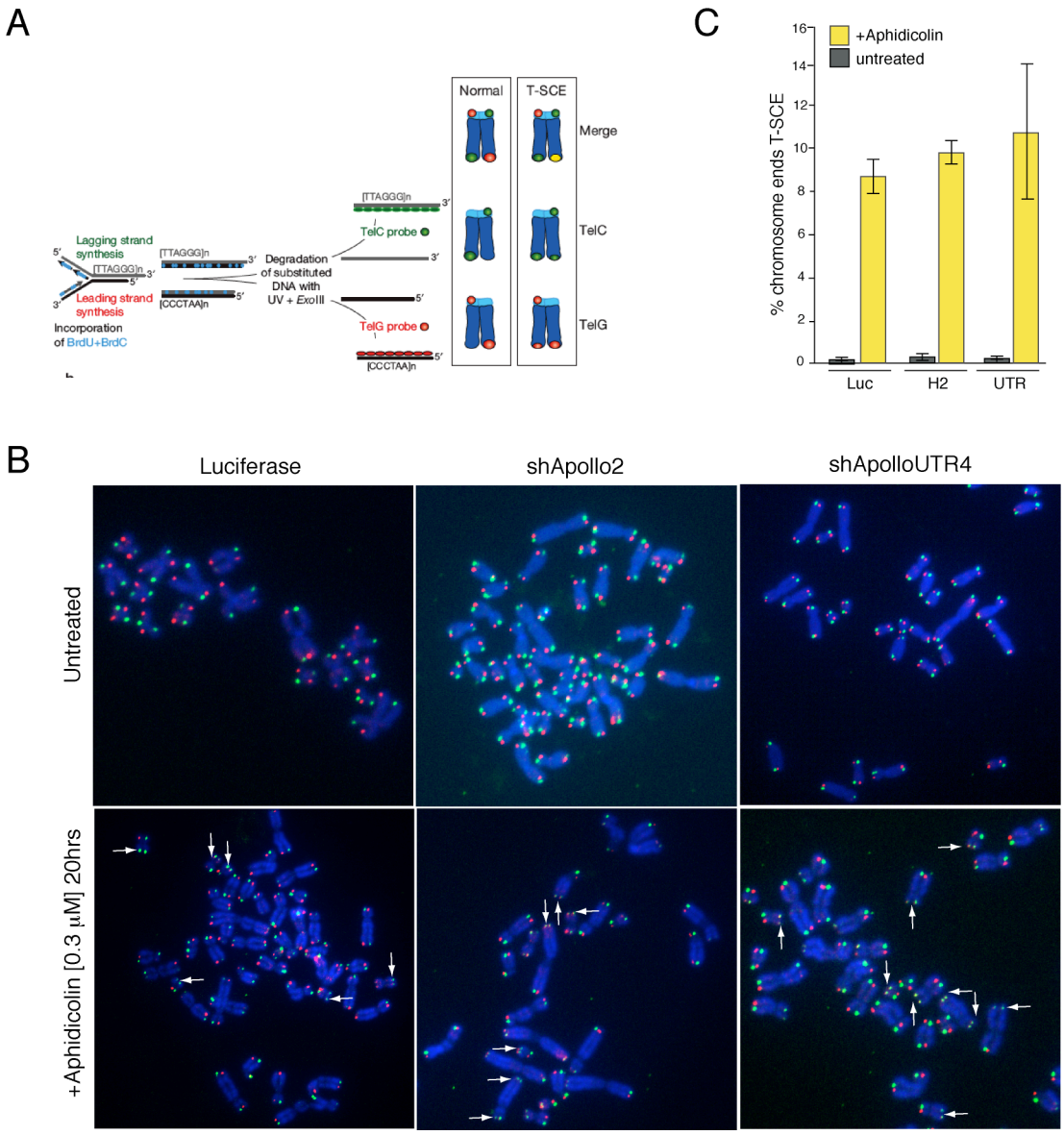

Figure 3-11. Treatment with Aphidicolin increases the occurrence of T-SCEs.

(A) Schematic representation of T-SCE detection using CO-FISH {Bailey et al., 1996, Mutagenesis, 11, 139-44}. (B) Metaphase spreads illustrating presence of T-SCEs in cells treated with Aphidicolin. Metaphase spreads were obtained from BJ-hTERT cells treated with the indicated shRNAs for 5 days and then treated with +/- [0.3 μM] Aphidicolin for 20 h and processed for CO-FISH. DNA was stained with DAPI. Arrowheads highlight chromatids with T-SCEs. (C) Quantification of T-SCEs from three independent experiments.

Apollo loss from the telomere does not induce T-loop HR

As described in Chapter 1, the overexpression of an allele of TRF2 that lacks its N-terminal basic domain (TRF2ΔB) leads to homologous recombination at the telomere with two products: short telomeres and telomere circles detected by 2-D gel electrophoresis [86]. We speculated that the multiple telomere signals on a single chromatid might represent the products of t-loop HR with the recombined t-loop still attached by telomeric cohesion [128] [164]. We therefore assayed for the presence of telomere circles in Apollo knockdown cells.

To assay for telomere circles, we employed a technique based on rolling circle amplification (RCA). In the Telomere Circle Amplification (TCA) technique, products of t-loop HR are annealed to telomere specific primers that serve as a template for RCA using the highly processive DNA polymerase Φ29 (Fig. 3-12A) [88]. The extension products are separated from bulk DNA by alkaline electrophoresis and detected by southern hybridization. The specificity of the reaction was tested by Exonuclease V treatment of samples, which hydrolyzes nucleotides from 3' and 5' ends of linear double-stranded DNA and single-stranded DNA. Bulk DNA was efficiently degraded by Exonuclease V and telomere circles from these reactions were resistant.

TCA assays on DNA extracted from BJ cells expressing TRF2ΔB consistently showed a 20-30 fold increase in t-circles compared to control cells, confirming in an independent experimental setting previous findings that TRF2ΔB overexpression results in t-loop HR [86] (Fig. 3-12B). In contrast, DNA from cells with decreased levels of Apollo or from cells expressing ApolloΔTRF2 showed a very mild increase in telomere circles

(2-4 fold) in comparison to control samples (Fig. 3-12B). As previously described in this section, cells that have been treated with Aphidicolin have an increase in the number of multiple telomere signals detected by FISH (Fig. 3-10A-B). DNA extracted from these cells was tested for the presence of telomere circles. There was no increase in telomere circles detected by TCA in Apollo knockdown cells treated with Aphidicolin indicating that the multiple telomere structures seen by FISH do not correlate with products of t-loop HR.

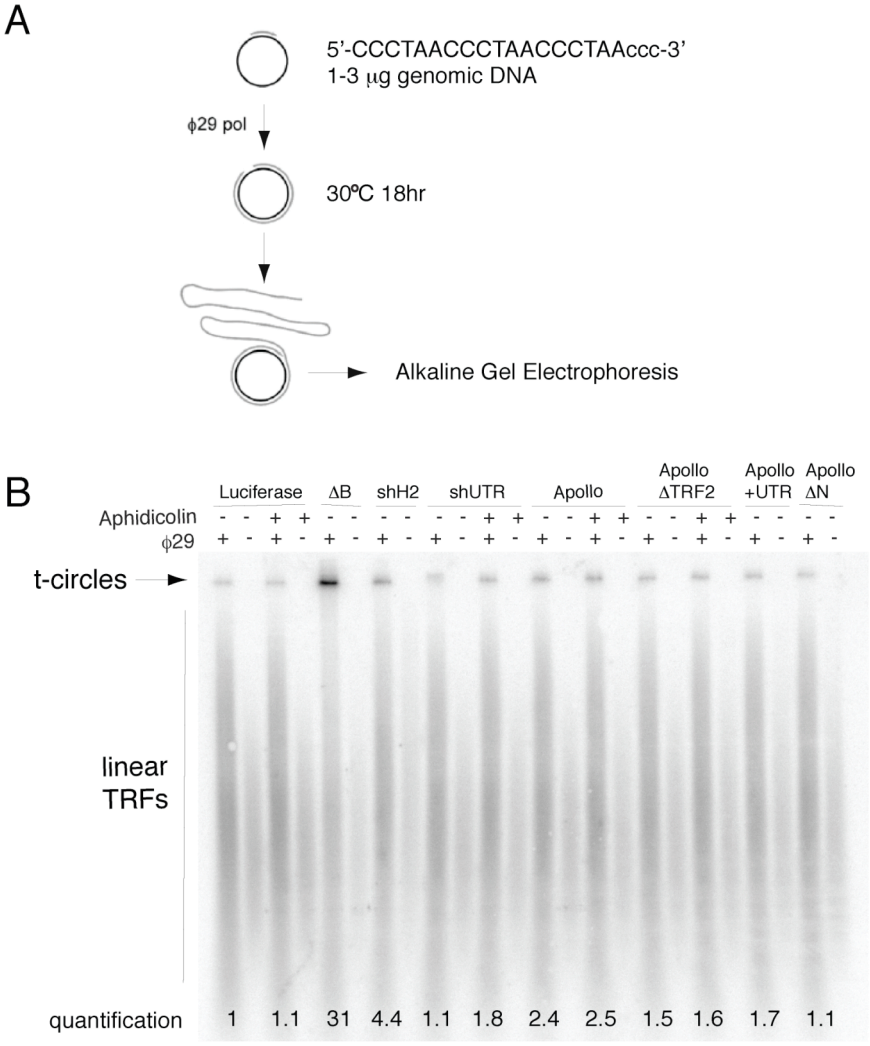

Figure 3-12. Telomere Circle Amplification (TCA) analysis of BJ cells expressing Apollo shRNA and Apollo mutant alleles.

(A) Schematic representation of primer elongation by the ϕ29 polymerase from a circular template [88].The lower case cytosines in the primer represent thiophasphate linkages between the three terminal nucleotides to prevent primer degradation by ϕ29 exonuclease activity. (B) Detection of t-circles in BJ fibroblasts. TCA reaction was performed +/- ϕ29 polymerase on 2 μg of digested genomic DNA annealed with 1 μM $(CCCTAA)_3ccc$ containing thiophosphate linkages at the 3' end. Extension products were separated by denaturing gel electrophoresis and hybridized to a 800 bp telomeric DNA probe (Sty11). Samples were harvested 5 days post-selection. Aphidicolin treated samples were incubated with [0.3 μM] Aphidicolin for 20 hours prior to harvesting. Quantification was performed using ImageQuant software. T-circle intensities were normalized to the linear TRF signal from neighboring samples that were not treated with ϕ29 polymerase.

Discussion

Experiments described in this chapter reveal that Apollo is required at telomeres to suppress DNA damage signaling during S-phase. Primary cells with reduced amounts of Apollo senesced and showed telomere dysfunction in S-phase. Additionally, a subset of telomeres in Apollo deficient cells showed multiple telomere signals by FISH that increased after treatment with Aphidicolin, possibly indicating an aberrant structure at chromosome termini. Together, these data indicate that Apollo has a role in processing telomeres during or after replication.

Telomeres represent 0.01% of the genome. Human cell cultures treated with [0.2 μM] Aphidicolin are reported to have 16-17 SCEs per cell, with ~80% of these events occuring at fragile sites [165]. If random, a T-SCE event would occur at one of every 625 telomeres in cells treated with Aphidicolin. Strikingly, 8-10% of telomeres have exchanges, providing strong evidence that telomeres behave like fragile sites and are likely to be difficult templates to replicate. Corroborating this finding, TIFs are also prevalent in p53-/- MEFs treated with Aphidicolin (K. Hoke and T. de Lange unpublished results).

The replication inhibitor Aphidicolin increased the frequency of multiple telomere signals in Apollo knockdown cells. These aberrant telomere structures have also been noted in MEFs from which TRF1 was deleted (A. Sfeir and T. de Lange, unpublished data). Taz1, the fission yeast ortholog of mammalian TRF1 and TRF2, is required for the replication of telomeres [112]. Taz1 is predicted to act by either altering the telomere complex to allow for replication fork passage or by recruiting proteins (e.g. the RecQ helicase) to unwind G-quartet structures on telomere repeats.

TRF1 and TRF2 might act in a similar fashion, where TRF2 recruits the Apollo nuclease to telomeres to resolve non-covalent structures that would impede the replication fork. Apollo might act also in the context of the genome in the repair of covalent lesions such as interstrand crosslinks or pyrimidine dimers.

CHAPTER 4: APOLLO AFFECTS THE AMOUNT OF SINGLE STRANDED DNA AT TELOMERES

Nuclease Processing of Telomeres

The Mre11 complex at telomeres in Saccharomyces cerevisiae

Without additional processing after replication, chromosomes are predicted to have one blunt end produced by leading strand synthesis and one end with a short G-rich overhang created by a gap at the 5' end of the newly lagging strand synthesized C-rich strand. Studies in *S. cerevisiae* show that yeast telomeres acquire 3' G-rich overhangs in S phase [166] and that these overhangs are detectable on both leading and lagging strand ends of linear plasmid DNA recovered from yeast [167], indicating that both ends of a newly replicated chromosome are likely to be processed by a nuclease. 3' G-rich telomere overhangs are present in cells lacking telomerase [168] and the passage of the replication fork through the telomere sequence has been shown to be required for their generation [169]. Studies in a variety of organisms show that a G-rich tail is a universal feature of all telomeres.

Telomeres in budding yeast deleted for any member of the MRX (Mre11-RAD50-Xrs2) complex are short but stable [170]. Cells with an MRX deletion combined with Mec1 (ATR) acquire an *est* (ever shorter telomere), characterized by progressive telomere shortening and eventual senescence. When combined with Tel1 (ATM), deficiency for MRX does not lead to an *est* phenotype, consistent with the view that Tel1 and MRX function in the same pathway [171]. The MRX complex was also found in the same epistasis

group as genes encoding telomerase components and was predicted to prepare ends for elongation by telomerase [172]. Mutation or deletion of MRX components leads to defects in homologous recombination and non-homologous end joining [173 174 175 170]. Mre11 has single stranded endonuclease activity and a 3'-5' exonuclease activity *in vitro* [176 177], while the MRX complex *in vivo* is implicated in 5'-3' resection of DSBs in budding yeast [178 176]. This dilemma could be explained if Mre11 recruits a different nuclease to sites of damage or uses its endonuclease activity in conjunction with a DNA helicase. In this regard, the human ortholog of Xrs2 (Nbs1) has been shown to display some low DNA helicase activity *in vitro* [179].

There are conflicting data regarding the role of the *S. cerevisiae* MRX complex in telomere resectioning after replication. In one report, *rad50*Δ, *mre11*Δ, and *xrs2*Δ strains show diminished loading of Cdc13 and reduced telomere addition at an HO cut [180]. This suggests that MRX is involved in generating the 3' G-rich overhang. In another report, wild type levels of Cdc13 were detected at telomeres by ChIP in *rad50*Δ, *mre11*Δ, and *xrs2*Δ strains [181]. Furthermore, senescence was suppressed in *mec1*Δ *mrx*Δ strains, and telomere lengthening occurs efficiently in *mec1 mrxΔ* and *mrx*Δ strains by targeting Cdc13-telomerase fusion proteins to telomeres, suggesting that G-tails are present in the absence of the MRX complex [181]. A third study found that short G-tails (10-15 nt) are present throughout the cell cycle and that these overhangs are shorter in *mre11*Δ, but not completely abolished [182].

The MRX complex has a further role in telomere maintenance in telomerase-deficient strains. Most yeast cells senesce in telomerase-deficient strains after ~80-100 generations, yet some cells survive and maintain their telomeres in a recombination-dependent manner [31]. The majority of such

survivors use a pathway (referred to as Type I) that leads to multiple tandem copies of the subtelomeric Y' element and short terminal tracts of $C_{1-3}A/TG_{1-3}$. Type I survivors are dependent on Rad51p as well as Rad52p. Telomeres in the Type II survivor pathway show progressive shortening followed by a single, rapid elongation event that is dependent on Rad52p and Rad50p but not Rad51p [32 33]. The maintenance of telomeres in the Type II survivor pathway has been proposed to involve rolling circle replication of extra chromosomal telomeric circles [32].

Mre11 complex and XPF/ERCC1 nucleases at human and mouse telomeres

Human and mouse telomeres possess long G-rich overhangs that are 45-275 nucleotides in length [183 184 185]. The presence of overhangs is not dependent on telomerase [186]. Recent studies have shown that overhangs generated in human primary cells by leading and lagging strand synthesis are asymmetrical, with longer overhangs at lagging strand ends [187]. This study suggests the possibility that leading and lagging strand telomeres are processed by different mechanisms. This asymmetry is not observed in telomerase-positive cells, indicating that either telomerase affects telomere processing differently on leading and lagging strand overhangs or that telomerase extends overhangs differently.

Mutations in the Nbs1 and Mre11 components of the human MRN complex cause Nijmegen Break Syndrome (NBS) and Ataxia-telangiectasia-like disorder (ATLD), respectively [188 189 190]. Patients afflicted with these disorders show radiation sensitivity, chromosomal instability, predisposition to cancer, and neurological abnormalities. Additionally, peripheral lymphocytes from NBS patients have shortened telomeres and Nbs1 has

been shown to promote telomerase-mediated telomere elongation [93]. The MRN complex is present at human telomeres where it binds to TRF2 [16].

A role for the MRN complex in the generation of the 3' overhang in human cells has been suggested by studies that show shorter overhangs in telomerase-positive cells treated with siRNA targeting Mre11, Rad50, and Nbs1 [191]. The 3' overhang was unaffected after depletion of the Mre11 complex in telomerase-deficient cells, suggesting that MRN might be involved in the recruitment of telomerase or that telomerase must be present for MRN activity at telomeres. The 5' terminal nucleotide is unaffected in Mre11-deficient cells (see below for 5' end details). These data suggest that multiple nucleases are likely involved in post-replicative processing of telomeres and generation of the 3' overhang [191].

The Nucleotide Excision Repair (NER) heterodimer XPF/ERCC1 is another nuclease recruited to telomeres by TRF2. ERCC1 in mouse cells prevents the generation of Telomere Double Minutes (TDMs), perhaps by inhibiting telomeres from strand invading interstitial telomere related sequences [78]. XPF/ERCC1 has also been implicated in clipping the 3' overhang from deprotected telomeres, creating a substrate for NHEJ [78].

The role of Pot1 in regulating nucleases at mammalian telomeres

Knockdown of human Pot1 results in a partial loss of the telomeric ssDNA signal (~30-40%) in telomerase-positive and negative cells [149]. This diminished G-strand signal might occur due to incomplete processing of the telomere after replication, possibly by insufficient end-resection by a C-strand specific nuclease. Alternatively, Pot1 deficient cells may form unstable t-loop structures leaving the G-rich strand more vulnerable to 3'-5' nucleases.

Whereas human telomeres have a single Pot1 gene, there are two mouse Pot1 genes, Pot1a and Pot1b [150]. Pot1a is an essential gene because it is required to suppress the DNA damage signal at mouse telomeres. Pot1b regulates the amount of single stranded DNA at mouse telomeres and is not essential [150]. Removal of Pot1b in conditional MEFs leads to a 2-3 fold increase in the amount of single stranded DNA at telomere termini. The enhanced shortening rate of Pot1b-/- MEFs is consistent with the 5' degradation model for telomere shortening proposed by Makarov et al. [183] indicating that Pot1b actively inhibits a nuclease from improper resectioning after telomere replication (Hockemeyer et al, unpublished data). The 5'-3' exonuclease Exo I was tested genetically to determine whether it was responsible for the excessive 5' resection observed after removal of Pot1b. Exo I does not play a role in 3' overhang generation in mouse cells, or is redundant with other nucleases, as there was no change in the rate or amount of overhang increase after Pot1b deletion in Exo I null MEFs (Hockemeyer et al, unpublished data).

Loss of human Pot1 leads to randomization of the 5' end sequence

Telomere ligation experiments by Sfeir et al. have determined that the 5' end of human chromosomes is extremely specific, ending more than 80% of the time with the sequence ATC-5', whereas there is no preference for a specific terminal nucleotide in the G-rich strand [8]. The telomere ligation assay used in these studies is a modified version of STELA (Single Telomere Ligation Assay)**,** where a limiting amount of genomic DNA is ligated to a set of primers specific for each of the six permutations of the telomeric sequence AATCCC. These “telorettes” contain a cassette 5' to their telomere sequences that can be PCR amplified. A PCR primer specific

to the subtelomeric region of the X-chromosome and the telorette are used to amplify individual telomeres (Fig. 4-2A).

Pot1 is responsible for determining the 5' nucleotide of chromosome ends as demonstrated by the randomization of the 5' end into all six permutations of the telomere repeat 3'-AATCCC-5' in Pot1 knockdown cells [149]. Pot1 may act by recruiting an endonuclease or a 5'-3' exonuclease to the telomere after replication and direct it to cleave specifically at the site 3'-AATC*CC-5'. Alternatively, Pot1 may specifically recognize ATC-5' and protect it from nucleolytic attack.

Apollo is predicted to have nuclease activity

In the experiments described in this chapter, the assumption is made that Apollo acts as a nuclease at telomeres. This assumption is made on the basis that Apollo is a member of the β-CASP (metallo- β-lactamase-associated CPSF Artemis SNM1/PSO2) family of proteins, part of the metallo–β-lactamase superfamily[130]. Other members of this family include Artemis, SNM1A (sensitivity to nitrogen mustard 1A), and CPSF (cleavage and polyadenylation specificity factor), whose activities are involved in DNA repair and RNA processing. The histidine and glutamic acid residues required for enzymatic activity and the coordination of Zn++ ions in the metallo-β-lactamase domain of Artemis are conserved in Apollo [142]. Artemis possesses intrinsic 5'-3' exonuclease activity and acquires endonucleolytic activity on 5' and 3' overhangs when in complex with DNA-PKcs [134]. Mutations in human Artemis cause RS-SCID (Radio sensitive severe combined immune deficiency), indicating that Artemis is required for V(D)J recombination and double strand break repair [133]. PSO2/SNM1 (Psoralen mutant 2/sensitivity to nitrogen mustard 1), the budding yeast ortholog of the

SNM1A/Apollo/Artemis family, has a role in interstrand crosslink repair [192] [193] [194]. Conservation of this function is evident in Apollo and SNM1A. HeLa cells with reduced levels of Apollo [139] and DT40 cells deleted for Apollo [195] show diminished survival when treated with the interstrand crosslink (ICL) inducing agents MMC and cisplatin. SNM1A-/- embryonic stem cells are highly sensitive to treatment with MMC but not other ICL inducing agents [138]. Finally, *in vitro* work by the Gilson lab has suggested that Apollo has 5'-3' exonuclease activity [148].

As described above and in Chapter 1, there are many events in telomere metabolism where a nuclease is required, including 5' end processing of chromosome termini and NHEJ of dysfunctional telomeres. We probe these aspects of telomere regulation in the following experiments and ask where the putative Apollo nuclease acts.

Results

Apollo negatively regulates the amount of ssDNA at telomeres

To assess the possible role of Apollo in creating the correct telomere terminus structure, we examined the status of the 3' overhang in BJ primary fibroblasts treated with an Apollo shRNA-UTR4 that was previously shown to be effective (Fig. 3-1). After growth for 5 days (~4 PD) with lowered Apollo levels, there was no detectable change in the amount of telomeric ssDNA compared with control cells (Fig. 4-1A-B). In contrast, BJ cells that overexpress wild type Apollo or ApolloΔN have a mild reduction in the amount of ssDNA (75-90% of control signal). This difference was statistically significant ($p<0.01$) and observed in three independent experiments. Overexpression of ApolloΔTRF2 consistently increased the

amount of ssDNA at telomeres (~125% of control signal, p<0.001) (Fig. 4-1A-B). This result would suggest that Apollo is a negative regulator of overhang generation and that ApolloΔTRF2 acts to interfere with this function. Such a dominant effect for ApolloΔTRF2 has also been documented in Chapter 3.

Figure 4-1. Overexpression of Apollo alleles affect the status of the 3' overhang.

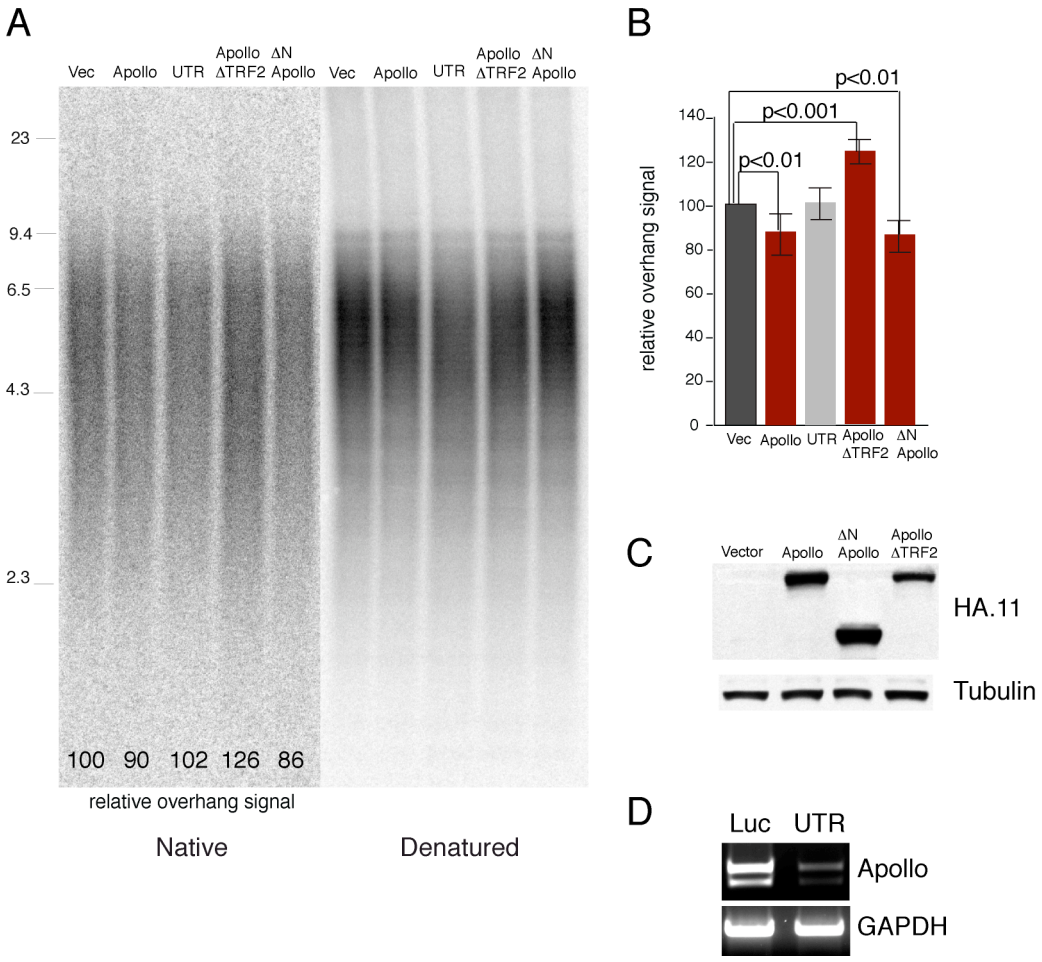

Figure 4-1. Overexpression of Apollo alleles affect the status of the 3' overhang.

(A) Telomeric DNA analysis. (Left) In-gel assay detecting 3' overhang in BJ fibroblasts expressing Vector control, Apollo shRNA UTR, pLPC-FLAGHA$_2$-Apollo, pLPC-FLAGHA$_2$-ApolloΔTRF2, and pLPC-FLAGHA$_2$-ΔNApollo. In-gel hybridization to a $(CCCTAA)_4$ probe to detect ssTTAGGG repeats (native). (Right) The DNA was denatured in situ and rehybridized to the same probe to detect the total TTAGGG signal (denatured). Overhang signals were quantified with ImageQuant software and normalized to the total TTAGGG signal in the same lane. The numbers below the gel represent the percentage of normalized overhang signals compared with the normalized overhang signal for vector control treated cells. Numbers on the left indicate the size of telomere fragments in Kb (B) Quantification of telomeric overhang 5 days post infection in three independent experiments compared with vector control. Student's t test was performed to generate p values (C) Immunobloting for expression of Apollo alleles in BJ fibroblasts. (D) RT-PCR analysis with primers for Apollo and GAPDH loading control.

Apollo does not define the 5' end sequence of chromosomes

To test the possibility that Apollo is involved in determining the 5' terminal sequence, we collaborated with the Wright and Shay Lab (UT Southwestern) to execute STELA assays in order to monitor the ends of chromosomes in cells that either overexpress Apollo or cells that were knocked down for Apollo. STELA indicated that the 5' end of chromosomes from BJ cells with altered Apollo levels harvested five days post selection did not show any evidence of randomization (Fig. 4-2B). The experiment was repeated in BJ-SV40 cells, which tolerate Apollo knockdown without senescing, allowing assays at later time points. Fourteen days after selection there was no randomization of the 5' end under these conditions in Apollo knockdown cells, whereas Pot1 knockdown resulted in the expected loss of the 5' end specificity (Fig. 4-2C).

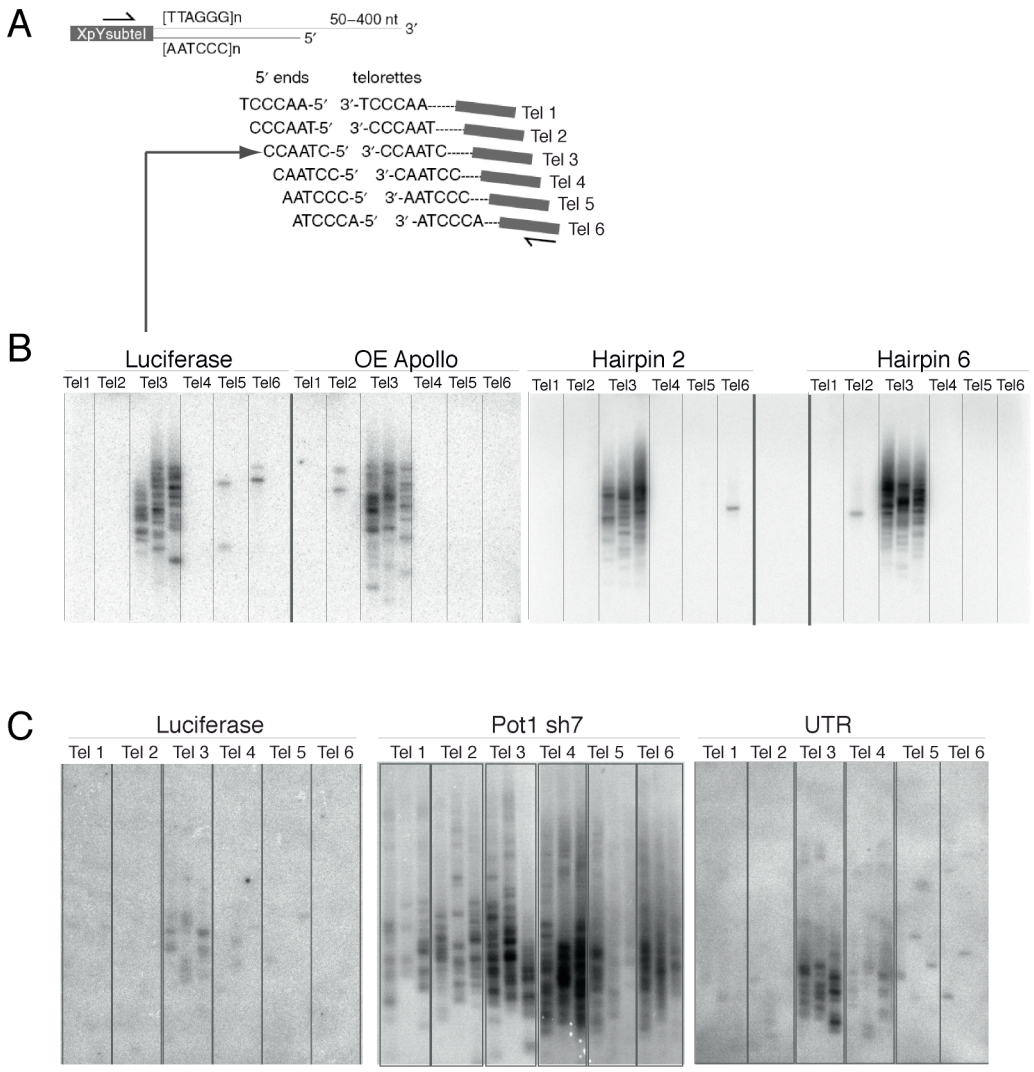

Fig. 4-2. No change in the 5' end sequence of human chromosomes in Apollo deficient cells.

(A) Schematic of the ends of human chromosomes and the 5' telorette assay. The six telorettes and the 5' ends to which they can ligate are shown. PCR primers used for amplification are shown schematically. (B) Products of the 5' telorette assay in BJ fibroblasts expressing pLPC-FLAGHA$_2$-Apollo, control shRNA or Apollo shRNAs H2 and H6. Cells were harvested five days post selection. Each telorette was used for 2-3 independent assays and the products were run in separate lanes. (C) Products of the 5' telorette assay in BJ-SV40 cells expressing Luciferase control shRNA, positive control Pot1 shRNA and Apollo shRNA UTR. Cells were harvested 14 days after selection. Each telorette was used for three independent assays and the products were run in separate lanes. The telorette corresponding to the 5' end detected is shown above the lanes.

To further test the possibility that Apollo affects the 5' end sequence, we looked in a setting where Pot1 was knocked down which leads to loss of 5’ end specificity. Cells were treated with Pot1 shRNA for a time period sufficient to induce randomization of the 5' end and subsequently treated with Apollo shRNA for two weeks to determine if the randomization would be reversed. Knocking down Apollo in Pot1 deficient cells did not rescue randomization (Fig. 4-3A). Finally, we asked whether randomization of the 5' end upon Pot1 loss could occur in a setting with reduced Apollo. Apollo levels were decreased for ten days prior to introduction of Pot1 shRNA. Randomization of the 5' end in cells expressing Apollo, ApolloΔTRF2, and the Apollo hairpin shUTR was not impeded (Fig. 4-3B). Apollo does not appear to have a role in determining the 5' end in the experimental settings described above.

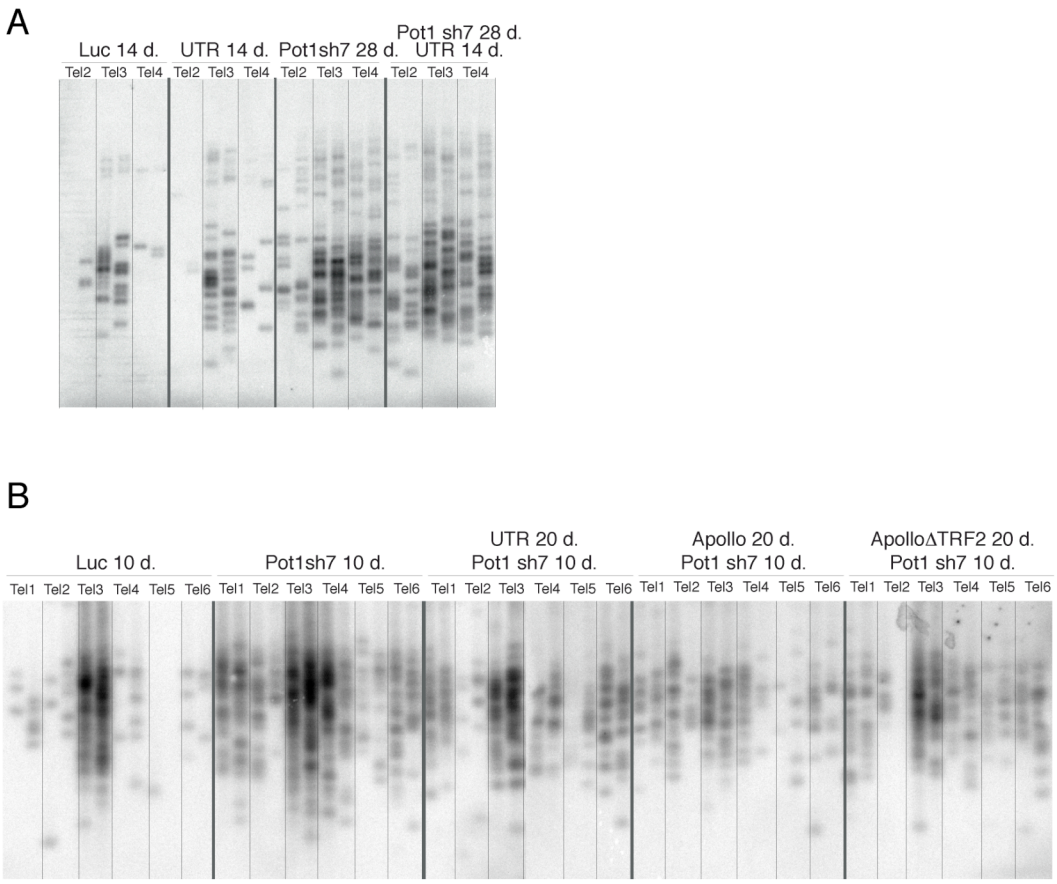

Figure 4-3. Apollo deficiency does not rescue randomization of the 5' end in Pot1 deficient cells.

(A) Products of the 5' telorette assay in BJ-SV40 cells expressing Luciferase control shRNA, Apollo shRNA UTR , Pot1 shRNA, and Pot1 shRNA/Apollo shRNA UTR. Luciferase and Apollo shRNA UTR expressing cells were harvested 14 days after selection, Pot1 shRNA expressing cells were harvested 28 days after selection. Each telorette was used for two independent assays and the products were run in separate lanes. The telorette corresponding to the 5' end detected is shown above the lanes. (B) Products of the 5' telorette assay in BJ-SV40 cells expressing Luciferase control shRNA, , Pot1 shRNA, Pot1 shRNA/Apollo shRNA UTR, Pot1 shRNA/Apollo and Pot1 shRNA/ApolloΔTRF2. Cells were harvested at 10 days (Luciferase and Pot1 shRNA) and 20 days (Pot1 shRNA/Apollo shRNA UTR, Pot1 shRNA/Apollo, and Pot1 shRNA/ApolloΔTRF2) post selection. Each telorette was used for two independent assays and the products were run in separate lanes. The telorette corresponding to the 5' end detected is shown above the lanes.

Diminished 5' end resection upon Apollo inhibition in Pot1b null cells

To determine whether Apollo is the nuclease that causes excessive 5' resection after removal of mouse Pot1b, mApollo was knocked down in Pot1b Stop/Flox conditional MEFs (Fig. 4-4D). The effect of Apollo shRNAs was consistent with findings at human telomeres, there is no change in the 3' overhang status in MEFs with reduced Apollo levels (Fig. 4-4A-B). Cre recombinase was added 5 days after selection for Apollo knockdown to take away the remaining allele of Pot1b and cells were harvested 3-7 days later. As expected, removing Pot1b resulting in a 2.6-3.2 fold increase in the amount of ssDNA at telomeres. In contrast, in Apollo knockdown cells there was only a 1.4-2 fold increase in ssDNA after removing Pot1b (also expressed as 70% of the increase in telomere ssDNA observed in Luciferase control cells deleted for Pot1b) (Fig. 4-4A-B). In the reverse setting, where Apollo is downregulated in cells already deleted for Pot1b, there is a consistent, but very mild reduction in the ss-DNA signal generated from Pot1b loss (88-90% of Pot1b+Luciferase levels) (Fig. 4-4E-F). These results suggest that, at least in one setting, Pot1b acts to reduce the access of Apollo to the 5' end of mouse telomeres.

Figure 4-4. mApollo participates in the degradation of the 5' end after removal of Pot1b.

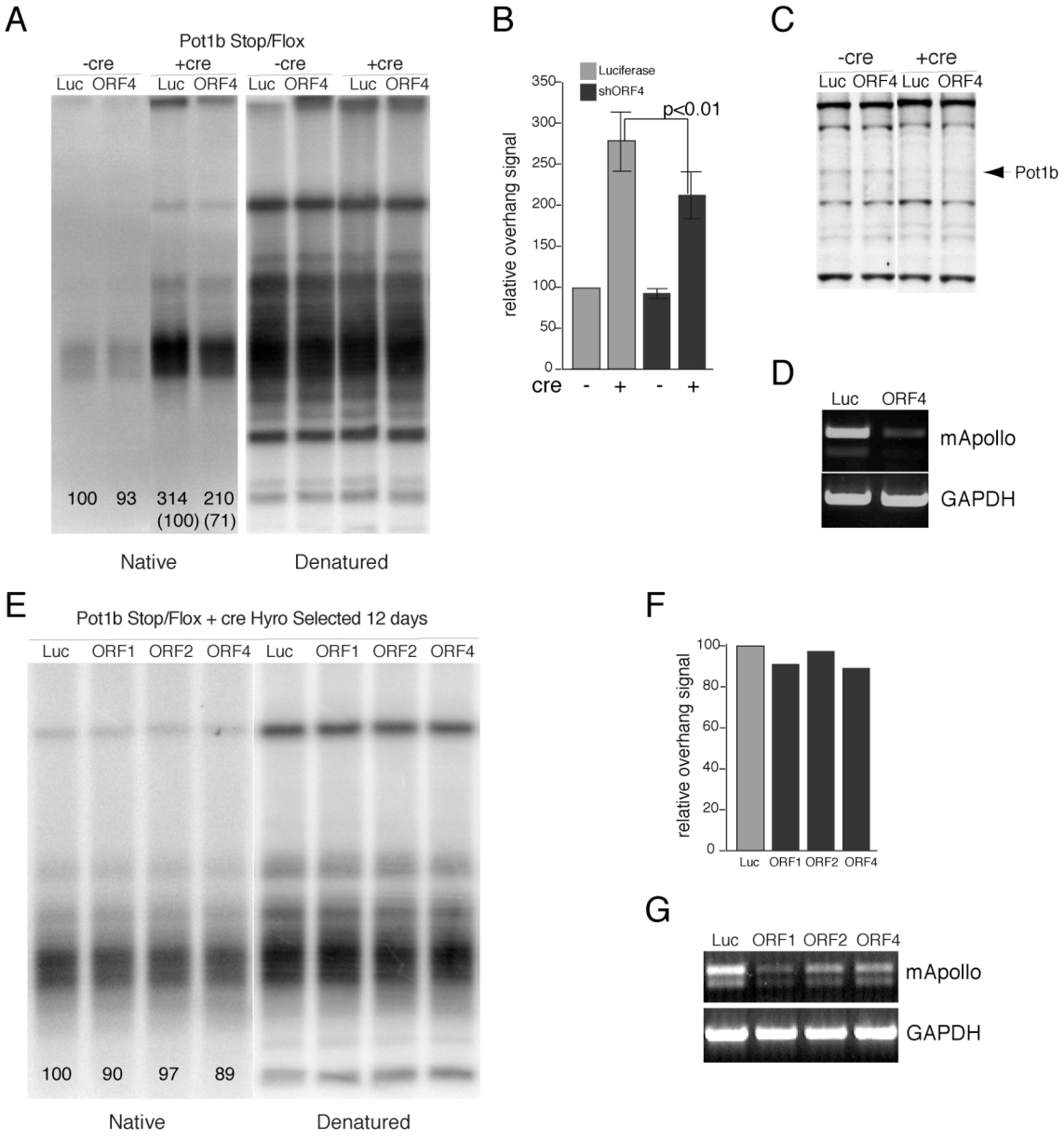

Figure 4-4. mApollo participates in the degradation of the 5' end after removal of Pot1b.

(A) Telomeric DNA analysis. (Left) In-gel assay detecting 3' overhang of Pot1bStop/Flox SV40 MEFs expressing control Luciferase or Apollo shRNA ORF4. Cells were harvested six days post-infection with cre and processed with in-gel hybridization to a $(CCCTAA)_4$ probe to detect ssTTAGGG repeats (native). (Right) The DNA was denatured in situ and rehybridized to the same probe to detect the total TTAGGG signal (denatured). Overhang signals were quantified with ImageQuant software and normalized to the total TTAGGG signal in the same lane. The numbers below the gel represent the percentage of normalized overhang signals compared with the normalized overhang signal for the same cells not treated with cre and the relative overhang increase of shRNA treated cells compared to Luciferase treated cells six days after cre introduction (bottom in parenthesis). (B) Quantification of telomeric overhangs in three independent experiments compared with +/- cre and Luciferase control. Student's t test was used to generate p value. (C) Immunobloting for mPot1b in Pot1b Stop/Flox MEFs +/- cre. (D) RT-PCR analysis with primers for mApollo and GAPDH loading control. (E) Telomeric DNA analysis as in (A) in Pot1b Stop/Flox MEFS infected with pWZL-cre and selected for Pot1b deletion in hygromycin-containing medium for 12 days and subsequently infected with control shRNA and Apollo shRNAs ORF1, ORF2 and ORF4. (F) Quantification of telomeric ssDNA from (E). (G) same as in (D).

Apollo does not affect overhang loss after TRF2 deletion

We tested whether the loss of Apollo had any influence on the rate of telomeric ssDNA loss after TRF2 deletion. mApollo was knocked down in TRF2 Flox/null conditional MEFs. Cells were harvested at 72 and 96 hours after the introduction of Cre recombinase. The overhang signal was monitored by native in-gel hybridization and normalized to the total telomeric DNA in the same lane. There was no change in the rate of overhang loss between control and Apollo knockdown cell lines (Fig. 4-5A). Additionally, there was no obvious difference in the extent of telomere fusions as detected by the appearance of larger telomeric DNA fragments at the different time points (Fig. 4-5A). These results suggest that Apollo does not affect the amount of ssDNA at deprotected telomeres.

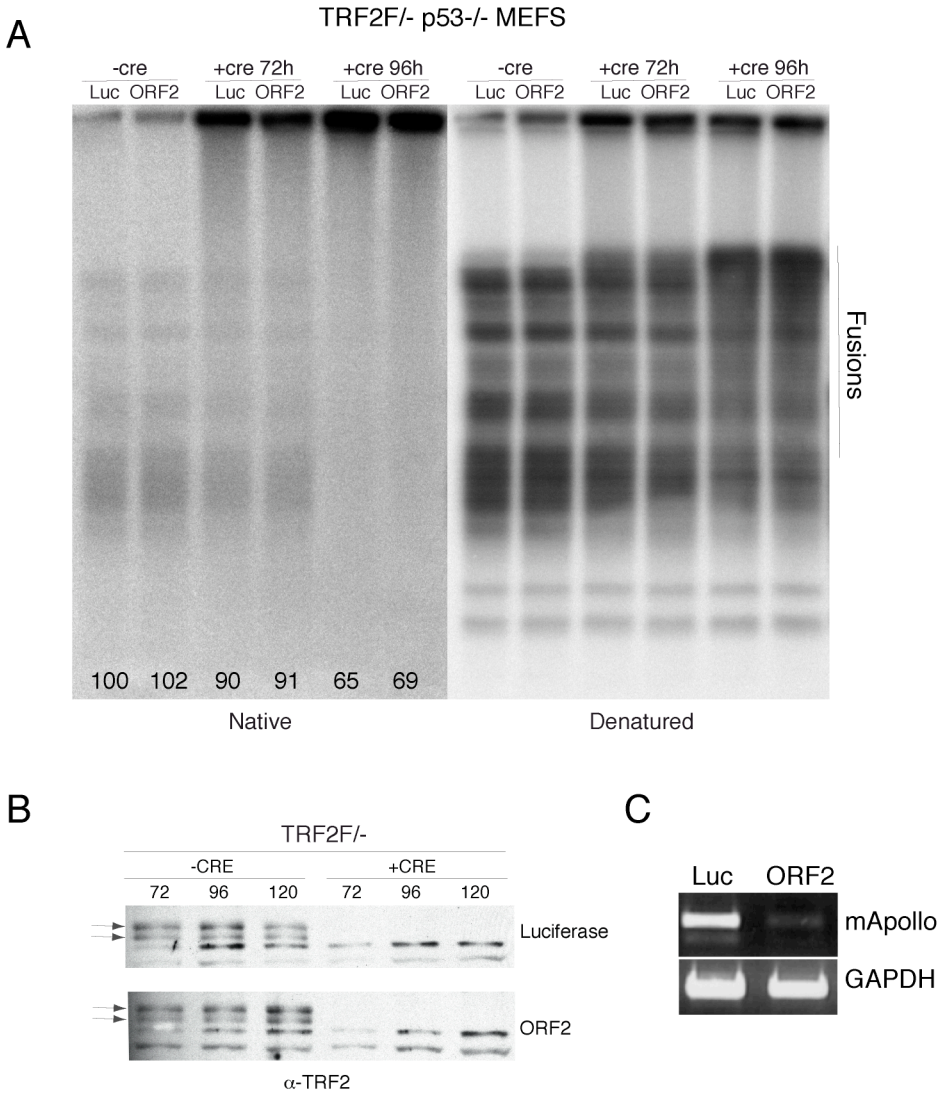

Figure 4-5. Apollo deficiency does not affect overhang loss in cells deleted for TRF2.

(A) Telomeric DNA analysis. (Left) In-gel assay detecting 3' overhang of TRF2F/-p53-/- MEFs expressing control Luciferase or Apollo shRNA ORF2. Cells were harvested 72 h and 96 h post-infection with cre and processed in-gel hybridization to a (CCCTAA)4 probe to detect ssTTAGGG repeats (native). (Right) The DNA was denatured in situ and rehybridized to the same probe to detect the total TTAGGG signal (denatured). Overhang signals were quantified with ImageQuant software and normalized to the total TTAGGG signal in the same lane. The numbers below the gel represent the percentage of normalized overhang signals compared with the normalized overhang signal for the same cells not treated with cre. (B) Immunobloting for mTRF2 in MEFs at the indicated time points after cre introduction. (C) RT-PCR analysis with primers for mApollo and GAPDH loading control.

Discussion

The experiments discussed in this chapter addressed the possibility that Apollo might contribute to the generation or removal of single stranded telomeric DNA. No evidence emerged to support a role for Apollo in defining the 5' sequence of chromosome ends or in the same pathway as XPF/ERCC1 in removing the 3' overhang at deprotected telomeres. As the experiments employed a shRNA knockdown and overexpression strategies, such negative results are not interpretable. In contrast, Apollo affects the amount of ssDNA at telomeres in settings where different alleles of Apollo are overexpressed and after removal of Pot1b in mouse cells. The implications of these results are discussed below.

The terminal structure of chromosomes implies that there is extensive post-replicative processing of telomeres. We found that Apollo negatively regulates the amount of ssDNA at human telomeres. Apollo could function by inhibiting resection of the 5' end or by preventing extension of the 3' end of the overhang. Expression of ApolloΔTRF2, a point mutant that cannot be recruited to telomeres, results in an increase in overhang signal, interfering with this function possibly by titrating factors required for the negative regulation of ssDNA away from the telomere. In human and mouse cells, Apollo deficiency alone does not change the amount of ssDNA at telomeres.

In Pot1b null MEFs less of the 5' end is resected in the absence of Apollo, suggesting that Pot1b functions in part by inhibiting the activity of Apollo at the 5' end. In the reverse setting, Apollo knockdown only mildly affects the amount of ssDNA at telomeres. The 12 day period between Pot1b deletion and mApollo knockdown might provide a sufficient window where

other nucleases might act instead of Apollo. Only through genetic experiments will we be able to answer definitively whether Apollo is the principal nuclease involved in the 5' resection of mouse telomeres.

CHAPTER 5: THE APOLLO COMPLEX

Introduction

To gain insight into the pathway(s) Apollo functions in, we sought to identify interacting proteins. We found DBC-1, the translesion bypass polymerase polη, and Rad51 in the Apollo complex. The biological pathways relevant to these factors are discussed in this introduction.

DBC-1

The gene encoding DBC-1 was originally identified during a search for candidate tumor suppressor genes in a frequently deleted region in breast cancers on human chromosome 8p21 [196]. However, after a more refined deletion analysis it appeared that DBC-2 is more likely to be the candidate tumor suppressor gene. In support of this conclusion, the authors found that in contrast to DBC-2, DBC-1 expression was not diminished in any type of cancer tissue tested. Furthermore, the Oncomine database (www.oncomine.org) revealed that DBC-1 is actually upregulated in breast carcinoma versus normal breast tissue and in breast ductal carcinoma versus other tissues [197]. Little is known about the molecular function of DBC-1. Full-length-nuclear DBC-1 undergoes caspase-dependent processing during TNF-α-mediated death signaling, producing two N-terminally truncated versions that localize to the cytoplasm [198]. However, its localization is primarily nuclear in healthy cells [198]. Recently, DBC-1 was found to bind directly to the steroid hormone estrogen receptor-α (ER-α) in a ligand independent manner [197]. Estrogen has been shown to induce and promote

breast cancer in animal models and ER-α is a target for endocrine therapy with antiestrogens such as tamoxifen and Icl in breast cancer patients. In the absence of a ligand, siRNA against DBC-1 reduced the level of ER-α in the cell, implicating DBC-1 in the stabilization of unliganded ER-α.

DBC-1 contains a Leucine Zipper motif, an EF hand domain, and a C-terminal coiled coil domain (Fig. 5-2A). Interestingly, a DBC-1 phosphorylated peptide containing T454 was recovered in a screen of HeLa nuclear proteins [199]. This site was independently predicted to be a phosphorylation target of a PIKK kinase [200].

Cajal Bodies

As shown in this chapter DBC-1 localizes to Cajal bodies. Cajal bodies (CBs) are dynamic subnuclear domains implicated in the biogenesis and maturation of several classes of small ribonucleoproteins (RNPs). The human telomerase RNA subunit (hTR) has been recently found to localize to Cajal bodies [201 202]. hTR contains a Cajal body box (CAB) motif found in small Cajal body-specific RNAs (scaRNAs). Mutation of the CAB motif abolishes the localization of hTR to CBs [201]. This permitted experiments to ask what role Cajal bodies have in telomerase function. Studies by Cristofari et al. [203] found that there was no change in the *in vitro* telomerase activity of CAB-mutated hTR compared with wild type hTR using a primer extension assay. However, HT1080 and HeLa cells co-overexpressing hTERT and mutant hTR had impaired telomere elongation. Additionally, hTERT was detectable by ChIP at telomeres in cells co-overexpressing hTERT and wild type but not mutant hTR. These data suggest that while Cajal bodies may be dispensable for telomerase biogenesis, they contribute to telomerase recruitment at telomeres. This might occur in two nonexclusive ways. A

maturation step essential for the productive association of telomerase RNP with telomeres might occur in Cajal bodies or the telomerase RNP might associate with a protein in Cajal bodies that can recruit telomerase to telomeres.

Rad51 and Translesion Bypass Polymerase Polη

Rad51 is part of the RecA/RAD51 family of recombinases that have key functions in homologous recombination (HR). Members of this family have the unique ability to search for homologous sequences and to catalyze the exchange of DNA strands between two molecules. HR is used by mitotic cells to repair collapsed replication forks and double strand breaks and in meiosis, HR is required for the exchange of genetic information. Double strand break repair by HR is generally error free and takes place in S/G2 when a sister chromatid is present. The first step involves 5'-3' resection of broken ends (possibly by the MRN complex), and stabilization of ssDNA by RPA binding. Subsequent displacement of RPA by Rad51 filament formation occurs on ssDNA. Rad52 and BRCA2 [204] facilitate this step. The Rad51 filament then performs a search for homologous sequences to use as a template for repair. A D loop is created by the subsequent invasion of the Rad51 filament into double stranded DNA. This reaction is promoted by Rad54. Next, a DNA polymerase synthesizes DNA using the undamaged sister chromatid as a template. The resulting double Holliday Junction is resolved to finalize the HR reaction.

Polη is part of the Y-family of lesion bypass polymerases that includes Polι, Polκ, and Rev1. These specialized polymerases have more open active sites than canonical DNA polymerases [205]. This feature allows this family of polymerases to negotiate distorted DNA templates. Polη is

able to replicate across DNA lesions such as cisplatin-induced inter-strand crosslinks and UV-induced cyclobutane pyrimidine dimers (CPDs) [206] [207] [208] [209] [210]. Polη is thought to be recruited to the replication machinery through monoubiquitination of PCNA that results in replication across CPDs [211]. Polη has low intrinsic processivity and is predicted to switch out shortly after replicating opposite a lesion. Deficiency in polη is the cause of XP-V (Xeroderma Pigmentosum Variant) [206] [207], an inherited disorder whose patients exhibit a dramatic increase of sunlight induced cancers. Cells derived from XP-V patients are deficient in their ability to replicate across UV-damaged DNA [206].

More recently, a role in the DNA synthesis step of homologous recombination has been proposed for polη. A DNA polymerase is expected to synthesize DNA in the dynamic D loop created by strand invasion during homologous recombination. It was not known whether conventional DNA polymerases performed this function or if specialized polymerases were involved. McIlwraith et al. [212] were able to purify an active fraction from HeLa nuclei that could extend D loops *in vitro*. Immunoblotting of this fraction revealed the presence of polη and polδ but not other DNA polymerases. Further tests showed that purified polη, but not polδ, was able to extend D loops *in vitro*. D loop extension was severely impaired when tested using polη deficient XP-V extracts compared with HeLa extracts. Electromobility shift assays (EMSA) demonstrated that polη can bind D loops better than forked DNA and ss- and ds-DNA substrates. Interestingly, a direct interaction between polη and Rad51 was observed in HeLa cells after exposure to UV irradiation [212]. Furthermore, Rad51 stimulated polη

extension of D loops at low concentrations of polη suggesting a mechanism for the recruitment or stabilization of polη at the stand invaded 3' end.

Results

Most soluble Apollo is complexed at 1:1 stoichiometry with TRF2/Rap1

We isolated the Apollo protein complex using the high salt, nuclear extraction technique described in Chapter 2. The isolated complex was analyzed by Coomassie staining after gel-electrophoresis. Individual bands were excised, digested with trypsin, and analyzed by MS/MS. Three bands of equal intensity appeared between the 75 and 50 kDa MW makers that corresponded with tagged Apollo, TRF2, and Rap1 (Fig. 5-1A), indicating that most of Apollo in the nuclear extract of these cells is associated with TRF2/Rap1. The relative abundance of other shelterin components was analyzed by western blot. Pot1 and Tin2 were present in relatively high amounts in both N-terminally tagged and C-terminally tagged Apollo isolates (Fig. 5-1B). In contrast, TRF1 was underrepresented in this Apollo complex (Fig. 5-1B).

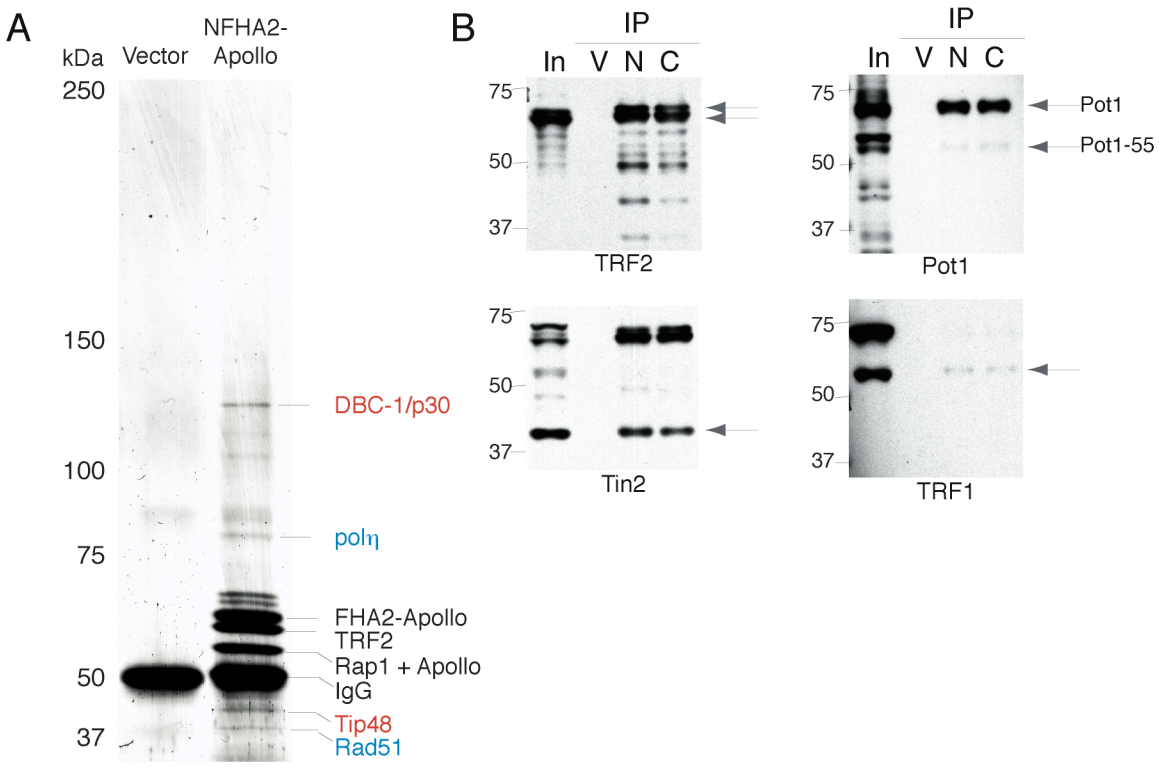

Figure 5-1: The Apollo Complex.

(A) Coomassie stained gel of the Apollo complex after tandem purification using FLAG and HA epitopes. Vector control cell line subjected to the same nuclei isolation and purification protocol at left. Proteins identified by mass spectrometry are identified in red and proteins identified by immunoblotting are in blue. (B) Immunoblotting for the presence of shelterin components in the isolated Apollo complex. TRF2 (647), Tin2 (864), Pot1 (979), TRF1 (371). Both full length Pot1 and an alternatively spliced form of Pot1 lacking its N-terminal OB-fold (Pot1-55) are present in the Apollo complex. Input (IN), Vector (V), $NFHA_2$-Apollo (N), Apollo-FHA_2C (C). Input is 2.5% of IP.

Deleted in Breasted Cancer-1 (DBC-1) directly interacts with Apollo

Mass spectrometry identified a protein in the Apollo complex migrating at 130 kDa as DBC-1 (Deleted in Breast Cancer-1) (Fig. 5-1A). Eighteen different peptides from DBC-1 were recovered in MS/MS analysis

(Fig. 5-2C). To verify the presence of DBC-1 in the complex, immunoblots were performed on Apollo complexes isolated from HeLa S3 cells expressing N- and C-terminally tagged Apollo. Immunoblotting showed an obvious enrichment for DBC-1 in the Apollo complexes compared to the control (Fig. 5-2B). Roughly 2% of total DBC-1 was recovered in association with the Apollo complexes. To determine whether DBC-1 interacts directly with Apollo, co-IP experiments were performed on 293T cells transiently transfected with DBC-1, Apollo, and shelterin factors. These experiments demonstrate that DBC-1 directly interacts with Apollo but not with any of the shelterin components (Fig. 5-2D). Although Apollo binds DBC-1 directly, it is not required for DBC-1 protein stability, as DBC-1 protein levels were unchanged in extracts made from Apollo knockdown cells (Fig.5-2E).

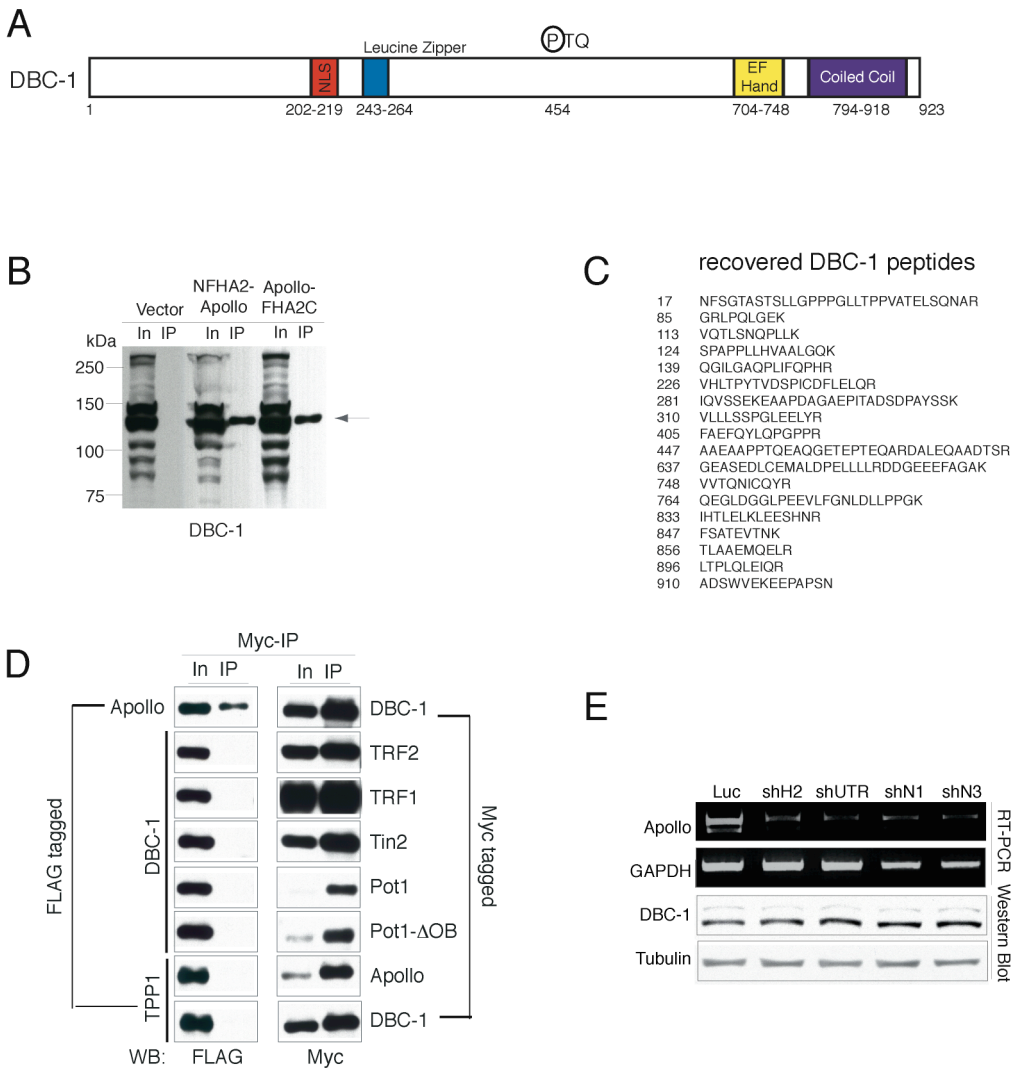

Figure 5-2: DBC-1 interacts with Apollo.

(A) Schematic of DBC-1 indicating domain structure and PIKK phosphorylation site. (B) Immunoblot confirming the presence of DBC-1 in the Apollo complex after tandem purification using Flag and HA epitopes, α-DBC-1 (Bethyl Labs). (C) Peptides recovered from Apollo complex identifying DBC-1. (D) Co-immunoprecipitation experiments indicating a direct interaction of DBC-1 with Apollo and not with any shelterin component. Flag-DBC-1 was co-transfected with Myc-shelterin in 293T cells (tags reversed for TPP1/DBC-1 co-IP). Myc-IPs were probed for the the presence of DBC-1 (or TPP1 in DBC-1 IP) by immunoblot with Flag antibody. (E) Immunoblot analysis of DBC-1 protein stability in cells with reduced levels of Apollo (monitored by RT-PCR).

DBC-1 localizes to Cajal Bodies

We performed IF on BJ-hTERT cells expressing tagged DBC-1 to determine its nuclear localization. Myc-DBC-1 localizes to 7-15 nuclear foci, some of which colocalize with telomeres (marked with TRF1) (Fig. 5-3A). This pattern is reminiscent of Cajal bodies [213] [214]. To test for the presence of DBC-1 in Cajal Bodies, co-immunoflouresence was performed with Coilin, a widely used molecular marker for Cajal bodies [215]. DBC-1 clearly and almost exclusively co-localizes with Coilin (Fig. 5-3B). We conclude that DBC-1 is a component of Cajal bodies. Considering that Apollo and DBC-1 have only partially overlapping subnuclear localizations, their interaction is likely to be regulated.

Figure 5-3: DBC-1 localizes to Cajal bodies.

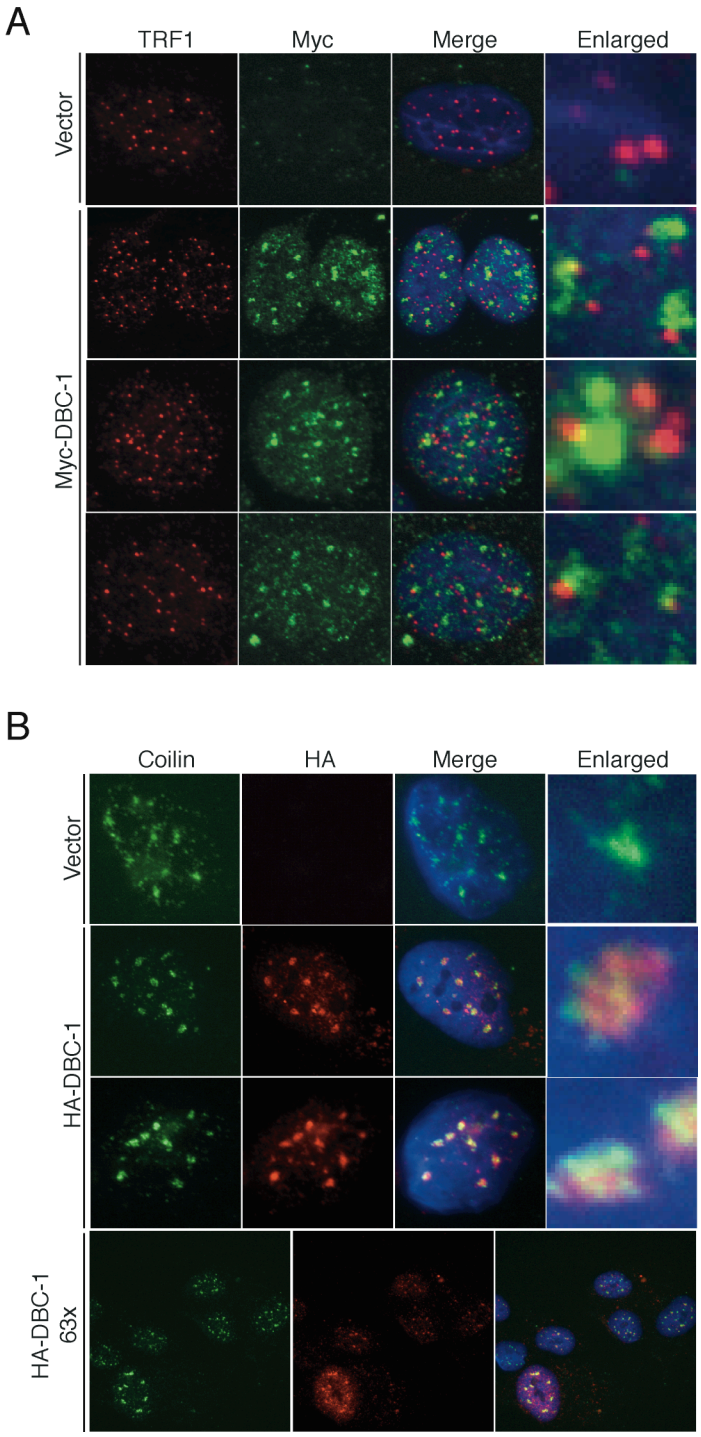

Figure 5-3: DBC-1 localizes to Cajal bodies.

(A) Immunoflouresence (IF) analysis of the localization of Myc-DBC-1. Telomeres are marked with TRF1 (371) (red, RRX). DBC-1 is detected with Myc antibodies (9E10) (green, Alexa 488). (B) IF analysis showing the localization of DBC-1 to Cajal bodies. Coilin is used to detect Cajal bodies (Sigma) (green, Alexa 488). DBC-1 is detected with HA antibodies (HA.11) (red, RRX). Lower panels show a field captured with a 63x objective. All other fields were captured at 100x. In both (A) and (B) cells were extracted with Tx-100 prior to fixation to remove soluble proteins. Upper panels in both (A) and (B) show vector control cells stained with either Myc or HA antibodies.

Polη and Rad51 are part of a TRF2-independent Apollo complex

Peptides identifying Tip48, a member of the Tip60 chromatin remodeling complex, were present in the isolated Apollo complex (Fig. 5-1A). Tip48 was detected by immunoblot in affinity purified extracts expressing tagged Apollo and not in extracts expressing a vector control (Fig. 5-4B). Tip48 does not, however, directly interact with Apollo by co-IP. (Fig. 5-4C). Ku70, Ku80, and HSP 70 were also identified in the Apollo pulldown. Since each of these proteins are common contaminants in mass spectrometry analysis I did not pursue them further.

Several bands visible by Coomassie staining of the isolated Apollo complex failed to reveal their identity by mass spectrometry. To determine the identities of these bands, I tested by immunoblot for the presence of factors in pathways that Apollo might be involved in: ICL repair (FANCD2); DNA replication (ATRIP); polη and polι; WRN; BLM; homologous recombination (Rad51, Rad51C, BRCA1, BRCA2, Rad54), and NHEJ (DNA-PKcs) (Fig. 5-4A-B). Among these proteins, Rad51 and polη were the only proteins that were enriched in the Apollo complex (Fig. 5-4B). I tested whether these proteins could interact directly with Apollo. As previously observed, TRF2 and DBC-1 interact directly with Apollo but not TRF1 in co-IP experiments. Co-IP experiments show that polη and Rad51 do not interact directly with Apollo (Fig. 5-4C). I next tested whether the association of Rad51 and polη with Apollo was mediated by TRF2 or Rap1, both abundant components of the Apollo complex. In order to test this possibility, I used the allele of Apollo that does not bind TRF2/Rap1 (Chapter 2). Co-IP experiments showed that ApolloΔTRF2 can associate

with Rad51 and polη, establishing that these factors interact with the Apollo complex in a TRF2-independent manner (Fig. 5-4D).

Figure 5-4: Rad51 and polη interact with the Apollo complex in a TRF2-independent manner.

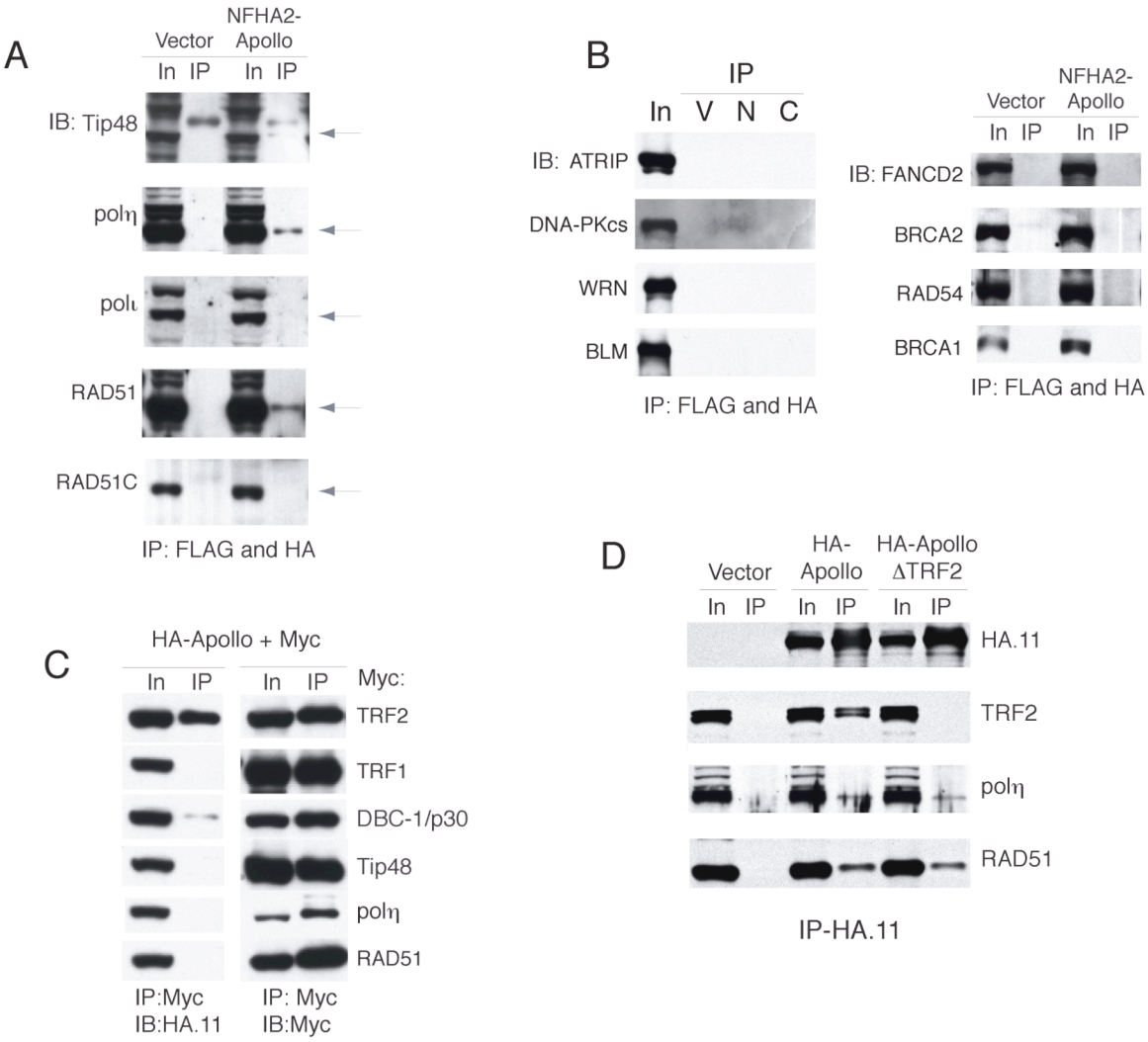

Figure 5-4: Rad51 and polη interact with the Apollo complex in a TRF2-independent manner.

(A) Immunoblot indicating the presence of polη and Rad51 in the Apollo complex after tandem purification using Flag and HA epitopes and not in vector control IPs. (B) Immunoblot of extracts for proteins suspected to be in the Apollo complex. IP performed tandemly from HeLa S3 cells using Flag and HA epitopes and subsequently blotted for the presence of proteins listed on the left. Input (IN), Vector (V), $NFHA_2$-Apollo (N), Apollo-FHA_2C (C). (C) Co-IP experiment indicating that Rad51 and polη do not interact directly with Apollo. HA-Apollo was co-transfected with cDNA encoding Myc-tagged proteins listed on the right. Myc IP was performed and immunoblotting of IPs was performed with Myc antibodies to verify expression (right) and HA to look for the presence of Apollo (left). (D) Immunoblot analysis of polη and Rad51 binding to Apollo complexes with (HA-Apollo) and without (HA-ApolloΔTRF2) the presence of TRF2/Rap1. 293T cells were transfected with either contruct listed above. The presence of the proteins listed on the left in the IPs was analyzed by Immunoblot with antibodies to the endogenous protein (except HA). Input is 2.5% of IP. Specific antibodies listed in Material and Methods.

Discussion

In this chapter we uncovered interactions of Apollo with DBC-1, polη and Rad51 in an Apollo complex that is independent of TRF2. As the Apollo complex we isolated contains stoichiometric amounts of TRF2/Rap1, the results point to a shelterin subcomplex that contains these factors.

Polη and Rad51 have both been implicated in homologous recombination, specifically the extension of the D loop structure after 3' strand invasion into duplex DNA. In complex with these proteins, Apollo might be involved in t-loop formation (discussed further in Chapter 5). Curiously, Rad54, a factor shown to promote 3' Rad51 filament invasion into duplex DNA, was not recovered in the Apollo IP.

The localization of DBC-1 to Cajal bodies and its direct interaction with Apollo is highly suggestive of a function for Apollo in telomerase recruitment at telomeres. This hypothesis is currently being tested by examining the effect of DBC-1 knockdown in a telomerase recruitment assay that examines the rate of telomere elongation in Pot1ΔOB expressing cells. Additionally, co-IP experiments are being performed with DBC-1 and hTERT to test this hypothesis.

Apollo has been implicated in ICL repair. ICL repair is a multistage process that involves converting an ICL into a DSB, localization of the FANCD2-FANCI complex to the site of damage, NER processing, homologous recombination, and potentially translesion synthesis and chromatin remodeling. Factors involved in some of these processes have been isolated in the Apollo complex. However, due to the diverse pathways these proteins are involved in, we are unable to place Apollo in a specific stage of ICL repair.

CHAPTER 6: DISCUSSION

Preamble

The most important function of a telomere is to prevent the chromosome end from being recognized as a break and processed inappropriately by DNA repair enzymes. Telomeres fulfill this role by providing a platform of telomere repeats onto which specific telomere DNA binding proteins can load to form a protective cap. The telomere can ensure its maintenance by regulating telomerase with its binding proteins. In mammals, shelterin performs this protective role with its six protein components. Shelterin recruits telomere accessory factors to shape the telomere structure. Paradoxically, the enzymes and proteins that shelterin recruits have activities that shelterin is meant to protect against, such as non-homologous end joining and homologous recombination. This implies a tightly regulated interaction between shelterin and factors involved in DNA transactions.

In this thesis I describe the identification of a new shelterin accessory factor, Apollo. Apollo is recruited to telomeres by TRF2 and it interacts with TRF2 on a molecular surface that other telomere accessory factors are predicted to bind. Abolishing this interaction or reducing the amount of endogenous Apollo by shRNA results in telomere dysfunction in S-phase. Our findings suggest that Apollo has a role in telomere replication, the generation of ssDNA at the telomere, and potentially a role in t-loop formation and regulation of telomerase. In this discussion I will briefly review my findings and speculate on the role of the Apollo nuclease in telomere metabolism.

Apollo localizes to telomeres and interacts with TRF2

In our efforts to find TRF2/Rap1 binding partners we discovered an interaction with hSNM1B/Apollo, a member of the β-CASP family of nucleases. Apollo was identified in the affinity purified TRF2/Rap1 complex by mass spectrometry. Apollo was found to interact directly with the TRFH domain of TRF2 through co-IP experiments. Consistent with co-IP data, ITC measurements show a strong binding of Apollo with TRF2-TRFH (Kd, 0.12 μM). Although the TRFH domains of TRF1 and TRF2 are nearly identical structurally, Apollo does not interact with TRF1. To understand why Apollo interacts specifically with TRF2 and not TRF1, structural analysis was performed with a peptide from the C terminus of Apollo (aa498-509) and the TRFH domain of TRF2. Analysis of this interaction revealed that the folding of alpha helices 2 and 3 in TRF1-TRFH does not provide space for Apollo residues L500 and Y504. Tin2 can bind to the same molecular surface as Apollo in TRF2-TRFH yet with a Kd of 6.5 μM. The specific strong interaction with TRF2 by Apollo and not Tin2 can be partially explained by the electrostatic interactions made by Y504, whereas Tin2 has a phenylalanine at the equivalent position. A putative motif for interaction with the TRFH domains in TRF1 and TRF2 in the loop between alpha helix 3 and 4 arose from this study where TRF1 binding proteins have an FxLxP motif and TRF2 interacting proteins have an YxLxP motif. As explained in Chapter 2, the L and P position of Tin2 and Apollo bind in an almost identical manner. Consistent with this finding, many known TRF2 interacting factors contain an YxLxP motif.

Using this information we can examine how much of the protective function of TRF2 at telomeres is mediated by accessory factors. It will be

interesting to look at the phenotypes of TRF2 deficient MEFs rescued with the TRF2 point mutation that cannot bind to Apollo and potentially a set of other repair proteins (TRF2F120A). Are telomere accessory factors in competition for this single binding site in TRF2? Or does the multimeric organization of TRF2 offer enough binding sites for all of the enzymes and proteins predicted to bind to TRF2? Because of the tight binding of Apollo to TRF2 (Kd, 0.12 μM), one might expect Apollo to be an effective competitor for TRF2 binding with other accessory factors in a setting where Apollo is overexpressed. Cells readily overexpress Apollo and these cells do not have any phenotypes associated with defects at the telomere by FISH and TIF analysis. However, there is a decrease in the amount of ssDNA at the telomere in cells that overexpress Apollo. In this setting, Apollo might occupy the TRF2-TRFH binding site of a protein required for the regulation of ssDNA at the telomere, Mre11, for example.

When overexpressed, Apollo localizes to most telomeres in individual cells and at telomeres throughout the cell cycle in primary and tumor cell types. This observation indicates that the localization of Apollo to telomeres is not cell cycle regulated and that Apollo could act at most telomeres within a cell. Due to lack of an antibody we were unable to track endogenous Apollo at telomeres. It is possible that the localization of endogenous Apollo at telomeres is cell cycle regulated or its protein levels are cell cycle regulated. Until an antibody that recognizes endogenous Apollo is made, real time PCR methods can be used to determine whether the transcription of Apollo mRNA is cell cycle regulated.

DNA damage response occurs at telomeres in the absence of Apollo

In Apollo knockdown cells, telomeres are dysfunctional and the DNA damage factors γH2AX and 53BP1 localize to telomeres. These TIFs arise specifically in S-phase, indicating that they are a result of aberrant replication of telomeres or the presence of an inappropriate structure after telomere replication. The nature of the TIFs has not been examined. This will be critical to understanding what type of damage is being sensed in the absence of Apollo. If ICLs are being sensed, proteins involved in ICL repair such as the ID complex (FANCD2 and FANCI) and homologous recombination proteins like BRCA1, BRCA2 will be present at TIFs. If the lesions are Thymine dimers one would expect to find NER proteins localized to TIFs. If the damage is due to stalled or collapsed replication forks, ATR and RPA might be present. Consistent with a telomeric DNA damage response, human primary cells with reduced levels of Apollo have a growth arrest, senescent morphology, an induction of the CDK inhibitor p21, and stain positive for SA-β-galactosidase. However, this growth defect is largely rescued by the expression of ApolloΔTRF2. This finding implies two possibilities. Either Apollo deficiency in a non-telomeric role is the cause of the growth defect seen in Apollo knockdown cells or alternatively, ApolloΔTRF2 might still bind minimally to telomeres. A large fraction of Pot1 was recovered in the Apollo complex. A few molecules of Apollo might associate with Pot1 at the telomere terminus and regulate ssDNA but cannot bind along the length of telomeres (hence the absence of telomere foci in cells that overexpress ApolloΔTRF2).

Telomeres are sensitive to Aphidicolin treatment

Treatment with low doses of Aphidicolin slows replication and induces the expression of common fragile sites as evidenced by chromosome breaks and SCEs. Fragile sites are classified as rare or common, based on their induction and frequency within the population. Rare fragile sites often have a proximal expansion of repeat sequences [216]. For example, the rare fragile site FRA16B has a block of telomere-like repeats adjacent to it [217]. In wildtype cells and cells treated with Apollo shRNA, T-SCEs occurred at a large proportion of telomeres after treatment with low doses of Aphidicolin (9-10%). This finding corroborates work from K. Hoke showing a high incidence of TIFs in MEFs after Aphidicolin treatment (K. Hoke and T. de Lange unpublished results). This provides evidence that telomeres are challenging templates to replicate and are induced like fragile sites upon Aphidicolin treatment. Yet, in contrast to telomeres, fragile sites are often late replicating. The sensitivity of telomeres to Aphidicolin might be due to secondary DNA structures like G-quadruplexes or the susceptibility of telomeres to DNA lesions.

Multiple telomere signal phenotype of Apollo knockdown cells is replication related

In cells with reduced levels of Apollo and in cells expressing ApolloΔTRF2, we observed a significant increase in the incidence of multiple telomere signals on a single chromatid end. The frequency of these aberrations is increased when Apollo knockdown cells are treated with Aphidicolin, suggesting they are replication related. What do these structures represent? The FISH signal we observe on a chromatid with multiple signals

is roughly the sum of the sister signal, indicating that there is no loss or gain in the telomeric DNA content. This diminishes the possibility that these structures represent stalled or reversed replication forks at the telomere. Additionally, substantial telomere loss is not observed in cells with diminished levels of Apollo. Finally, our data suggests that these structures are not recombined t-loops still attached to telomeres.

A telomere transcript (termed telomeric repeat-containing RNA (TERRA)) ranging in size from 100 bp and 9 kb has recently been reported to localize to telomeres [218]. The function of this RNA at telomeres is not known but its presence appears to be negatively regulated by the nonsense mediated messenger RNA decay pathway [218]. Considering the putative RNA metabolizing domain in Apollo, Apollo might be involved in regulating TERRA at telomeres. The multiple telomere signals we observe might be a result of detection of TERRA at telomeres. Apollo might be required to process TERRA to allow the replication fork to pass. To test the possibility that Apollo is involved in regulating TERRA, the localization and abundance of TERRA can be followed using an RNA probe in settings with different levels of Apollo.

It is unknown what fraction of telomeres form t-loops. G-quadruplex structures have been suggested to protect telomeres from degradation. These structures might form on chromosome ends that do not form t-loops. If Apollo deficient cells, or cells expressing ApolloΔTRF2 are impaired in their ability to form t-loops, G-quadruplex structures might form with a greater frequency. This might explain the multiple telomere signals seen in wild type cells and the moderate increase of these signals seen in Apollo deficient cells.

Preliminary CO-FISH analysis of the multiple telomere signals showed that Apollo loss affects both sister telomeres generated by leading or lagging strand DNA synthesis. However, the total number of multiple telomere signals observed in wildtype and Apollo knockdown cells was reduced compared with FISH analysis. These experiments must be reexamined to determine whether our reasoning for the potential role of Apollo in regulating TERRA or the relative abundance of G-quartets is consistent. TERRA is composed of UUAGGG repeats and would be detected with the product of leading stand synthesis by CO-FISH. G-quadruplexes would be detected on the product of lagging strand synthesis by CO-FISH.

Apollo affects the amount of ssDNA at human and mouse telomeres

The nuclease(s) that generates the 3' ssDNA overhang after telomere replication and defines the 5' end of chromosomes is unknown. We tested whether Apollo was involved in these processes.

We found that Apollo does not define the sequence of the 5' end of chromosomes. As theses studies were performed using a knockdown strategy and expression of exogenous proteins, the results are not conclusive. It is possible that in the absence of Pot1, attack on the 5' end would occur by multiple nucleases, masking the effect of a single nuclease that is normally regulated by Pot1.

We assayed whether Apollo has a role in the generation or removal of ssDNA at telomeres and found that it acts to negatively regulate the amount of ssDNA at human telomeres. Overexpression of Apollo and ApolloΔN in human cells resulted in less ssDNA at the telomere, whereas overexpression

of ApolloΔTRF2 increased the amount of ssDNA. This data suggests that Apollo negatively regulates ssDNA at telomeres. This could occur by preventing 3' overhang extension, preventing 5' end resection, or by promoting 3' end degradation. In an Apollo knockdown setting, there was no change in the amount of ssDNA at the telomere. These results suggest that in a knockdown setting there is sufficient Apollo at the telomere to regulate the amount of ssDNA at the telomere, whereas ApolloΔTRF2 might act as a dominant negative allele.

We examined the effect of Apollo knockdown on 5' end resection in mouse cells after removal of Pot1b. In this setting, Apollo promotes 5' end resection as the amount of ssDNA was reduced after Pot1b removal in Apollo knockdown cells. As Apollo knockdown does not have an effect on the overhang in Pot1b proficient cells, it is difficult to interpret this finding. Apollo might be one of many nucleases that act in 5' end resection, all regulated by Pot1b. Examination of the 3' overhang in Pot1b-/- Apollo-/- MEFs will show whether Apollo is the principal nuclease involved in 5' end resection.

The negative and positive affects of Apollo on ssDNA generation can be reconciled in the following model. In Pot1 proficient cells, the action of Apollo at the 3' end is regulated by TRF2 and Pot1 (Fig. 6-1C). Pot1 acts to promote 5' resection at the telomere terminus in conjunction with Apollo. When ApolloΔTRF2 is overexpressed in Pot1 proficient cells, Apollo can still associate with Pot1 at the telomere terminus, unregulated by TRF2. This inappropriate association might lead to increased amounts of ssDNA at the telomere by increased 5' end resection (Fig. 6-1D). In Pot1 deficient cells,

Apollo , and potentially other nucleases, bound to TRF2 would act to resect the 5' end of telomeres (Fig. 6-1E).

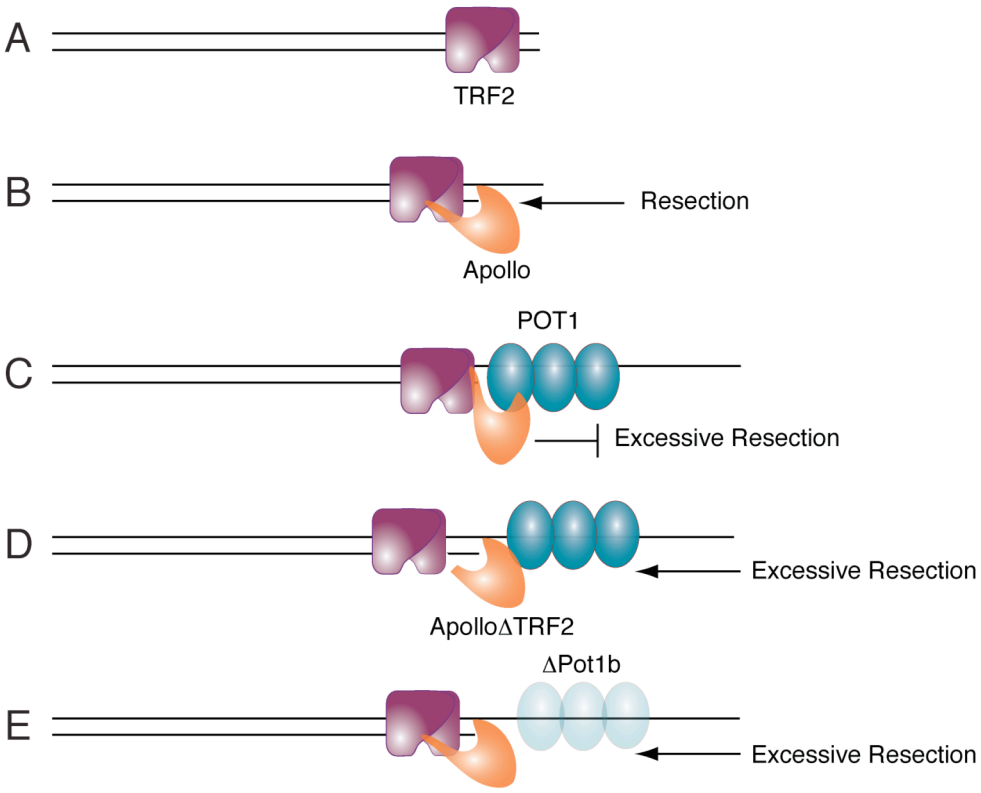

Figure 6-1: Apollo affects the amount of ssDNA at mammalian telomeres

(A) In this model TRF2 binds to newly replicated telomeres. (B) Apollo is recruited to TRF2 and participates in generating the 3' overhang. (C) POT1 binds to ssDNA preventing further resectioning by inactivating Apollo. (D) Excessive 5' resectioning is observed when an allele of Apollo that can no longer bind to TRF2 (ApolloΔTRF2) is expressed. (E) In the absence of Pot1b in mouse cells, Apollo participates in excessive resectioning of the 5' end. In summary, the presence of both TRF2 and POT1 are required to prevent inapproriate resection at the telomere by Apollo.

This model can be further tested by discovering and perturbing the connection between Apollo and Pot1b. We would expect that overexpressing a mutant form of Apollo that can no longer bind to Pot1b (ApolloΔPot1b)

would result in excessive resection at the telomere whereas the overexpression of the double mutant, ApolloΔTRF2ΔPot1b, would not affect the resection of the 5' end.

Apollo interacts primarily with TRF2/Rap1

In the isolated Apollo complex, Apollo, TRF2, and Rap1 are present in roughly equal stoichiometry. This leads to the possibility that Apollo is a resident telomere-specific nuclease kept exclusively in complex with TRF2/Rap1. Also, exogenous Apollo does not relocate from telomeres to sites of DNA damage, indicating that Apollo might not play a role in telomere unrelated pathways. However, two points of evidence argue against an exclusive role at telomeres for Apollo. The first is that non-telomeric DNA damage foci in Apollo knockdown cells can be partially rescued by ApolloΔTRF2. Secondly, ApolloΔTRF2 expression largely rescues the growth defect observed in Apollo knockdown cells, suggesting that loss of Apollo in non-temoleric roles is detrimental for the cell. These data indicate that Apollo performs essential functions in the cell independently of TRF2/Rap1. Apollo has been implicated in ICL repair as Apollo knockdown cells show sensitivity to ICL agents [138 139].

Apollo has a direct interaction with DBC-1 which localizes to Cajal bodies

Apollo interacts with DBC-1 in co-IP experiments. This interaction is unique to Apollo, as DBC-1 does not directly interact with shelterin. In this work, we find that the principal localization of DBC-1 in the nucleus is in Cajal bodies. The telomerase RNA subunit, hTR, has been recently shown to

accumulate in these subnuclear structures. Cajal bodies are not required, however, for the enzymatic activity of telomerase and are instead implicated in the recruitment of telomerase to telomeres. In the simplest model, Apollo would be required to resect the 5' end after telomere replication to generate a primer for telomerase (Fig. 6-2B). DBC-1 would then bind to Apollo and situate telomerase on the 3'end (Fig. 6-2C). An interaction between TPP1 and hTERT has been reported and TPP1 bound to Pot1 increases the proccessivity of telomerase *in vitro* [74] [73]. These two pathways, recruitment of telomerase and stimulation of telomerase, could act together to ensure the maintenance of telomeres by telomerase (Fig. 6-2D).

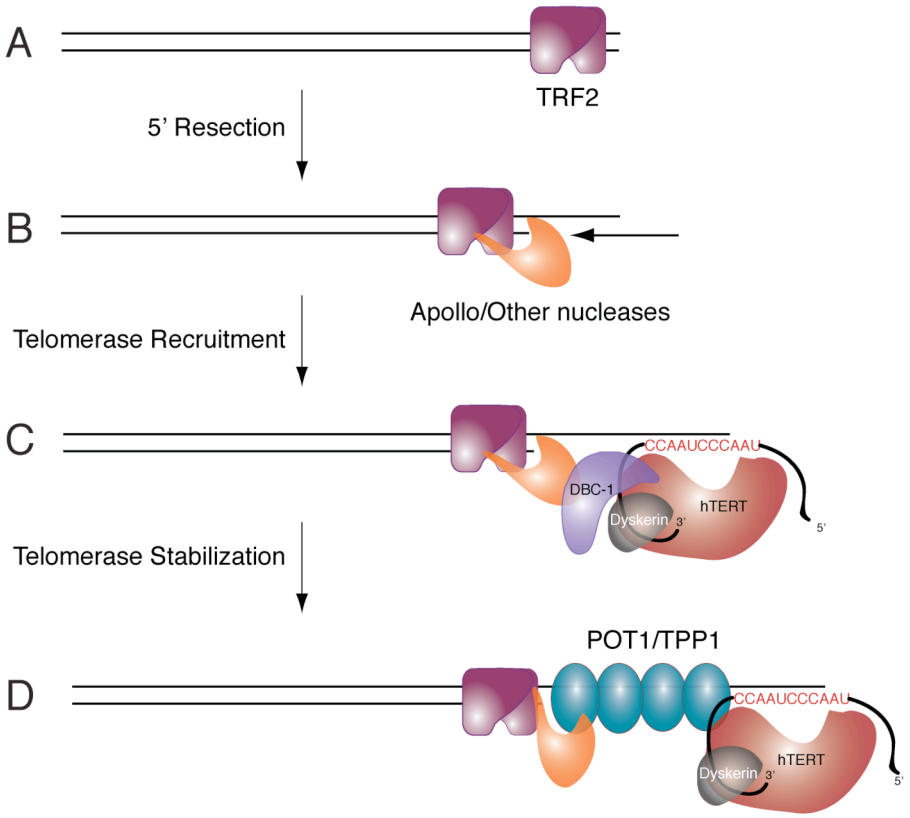

Figure 6-2: Model for telomerase recruitment to human telomeres.

(A) TRF2 binds to telomeres after replication and (B) recruits Apollo and other nucleases which participate or facilitate 5' resectioning of chromosome ends. (C) Considering the localization of DBC-1 to Cajal bodies and the direct interaction of Apollo with DBC-1, DBC-1 might mediate the recruitment of telomerase to telomeres. (D) POT1/TPP1 bind to ss-DNA and stimulate telomerase processivity after telomerase recruitment through a direct interaction between hTERT and TPP1.

This model predicts that DBC-1 deficient cells would have a telomere shortening phentoype in telomerase positive cells. We are currently testing DBC-1 in a telomerase recruitment assay that takes advantages of the rapid elongation of telomeres observed in cells that overexpress Pot1ΔOB {Loayza and de Lange, 2003, Nature, 424, 1013-8}. If DBC-1 is important for the recruitment of telomerase to telomeres, knockdown of DBC-1 in this assay will result in reduced telomere elongation in Pot1ΔOB expressing cells.

Factors involved in D loop extension are part of the Apollo complex

Homologous recombination has been proposed to shape the telomere into a t-loop conformation [16]. Work presented in this thesis describes Rad51 and polη as part of the Apollo complex. Polη has been found to extend D loops *in vitro*, possibly through recruitment by Rad51[212]. Apollo, Rad51, and polη could cooperate in the following model: To form a t-loop, the Apollo complex is recruited after replication to resect the 5' end and form a transient Rad51 filament on the exposed 3' end (Fig. 6-3B). Further steps would include invasion of the 3' end into duplex telomeric DNA (Fig. 6-3C). Polη would act to extend the 3' end in the D loop and thereby stabilize the structure (Fig. 6-3D). Apollo might regulate this step so as not to allow polη to extend the 3' overhang too far. This regulation step might explain the increase in telomeric ssDNA observed after expressing ApolloΔTRF2. After t-loop formation, Pot1 can be loaded onto the ssDNA of the D loop**.**

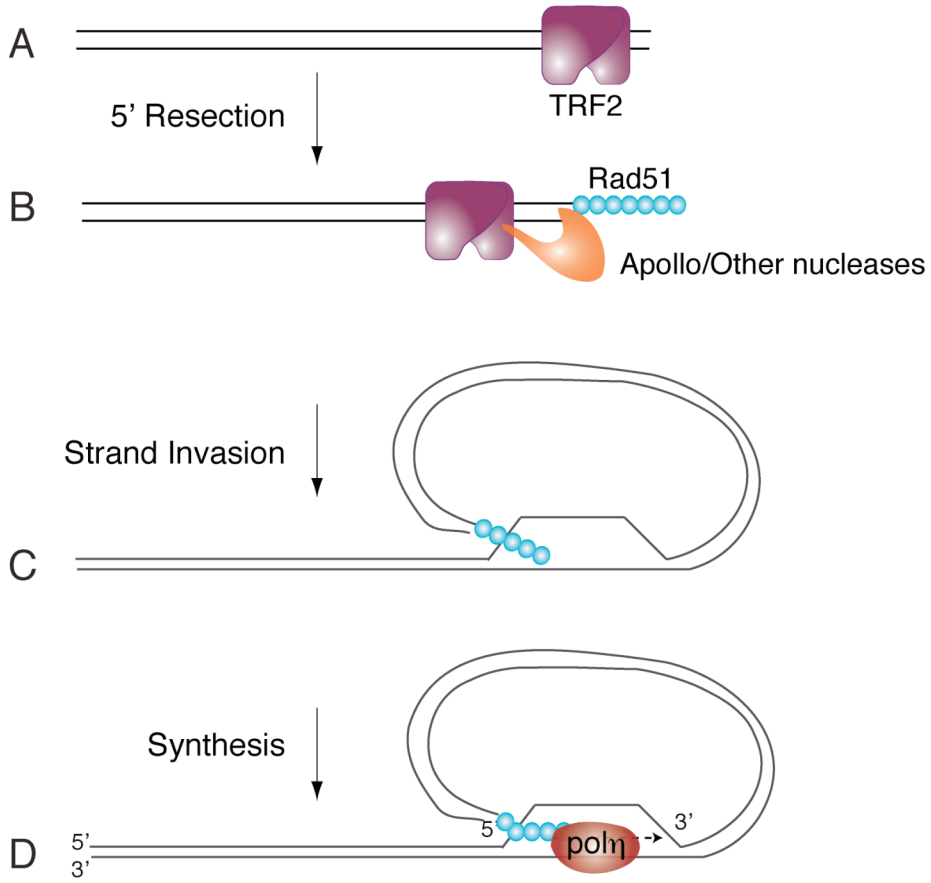

Figure 6-3: Model for t-loop formation.

(A) TRF2 binds to telomeres after replication and (B) recruits Apollo and other nucleases to resect the 5' end of chromosomes. In this model, Rad51 forms a transient filament on newly generated ssDNA. (C) The Rad51 filament facilitates invasion of the 3' end into ds-DNA, generating a displacement loop (D loop). (D) Through a direct interaction with Rad51, polη is recruited to extend and stabilize the D loop. Pot1 would displace the Rad51 on ss-DNA after t-loop formation due to its higher affinity for telomeric DNA (not shown).

Rad51 has been reported to be at telomeres in late S/G2 in ChIP experiments [219]. However, in these experiments cells were synchronized with Aphidicolin. As I show in Chapter 4, Aphidicolin induces a high incidence of DNA damage at telomeres and this would recruit Rad51 to

telomeres specifically in response to this drug. The findings of Verdun and Karlseder may therefore not be applicable to normal telomere metabolism. I tried unsuccessfully to ChIP polη and Rad51 at telomeres in settings with different levels of Apollo. These experiments are worth pursuing to understand if Apollo associates with these proteins for activities at the telomere and to determine whether their recruitment to the telomere is dependent on Apollo.

The model presented above predicts that t-loop formation and stabilization would be impaired in cells deficient for either polη or Apollo. It will be interesting to look at t-loops isolated from Apollo null mouse cells and see whether Apollo has a role in their formation or maintenance. Additionally, the overhang in polη deficient XP-V cells can be examined and would be expected to be shorter. Finally, if the Rad51 filament invades the subtelomere to form a t-loop, sequences from this region will be used as a template for extension of the 3' end in the D loop by polη. The sequence of the 3' overhang can be examined for the presence of non-canonical telomere repeats.

Diversity in SNM1 gene number

As discussed in Chapter 2, there are three SNM1 genes in vertebrates involved in diverse processes such as ICL repair, NHEJ, hairpin opening activity during V(D)J recombination, and as described in this thesis, telomere metabolism. We examined the number of SNM1 genes in other organisms to glean insight into the age of these genes and to understand when the diversity of function arose, or as we speculate below, might have been lost.

At the root of the phylogenetic tree presented in Fig. 6-4, the ciliate *Tetrahymena thermophila* and the plants *Arabidopsis thaliana* and *Oryza sativa* (not shown) have three SNM1 genes. This suggests that a common ancestor required the function of three SNM1 genes. Alternatively, it could suggest that both of these branches evolved to require the presence of three SNM1 genes. Presumably the processes of NHEJ and ICL repair would require the presence of at least two SNM1 genes. It will be interesting to see whether the third gene is involved in telomere metabolism in these organisms.

Diversity in the number of SNM1 genes is seen in Fungi. Both budding and fission yeast have only one SNM1 gene, wheras *Neurospora crassa*, *Candida albicans* (not shown) and *Apergillus fumigatus* have two. The single SNM1 gene in *S. cerevisiae* and *S. pombe* is required for ICL repair. The Mre11 nuclease appears to take the place of Artemis in *S. cerevisiae* during NHEJ, and might take have removed the requirement for a SNM1 gene in this process. Furthermore, Artemis is active in conjunction with DNA-PKcs, a PIKK kinase absent from the *S. cerevisiae* and *S. pombe* genomes. Again, it will interesting to see whether the yeast species with two SNM1 genes use one in telomere maintenance.

There are also a diverse number of SNM1 genes in metazoans. Vertebrates and Echinoderms have three separate genes whereas, the arthropod *Drosophila melanogaster* has a single gene and the nematodes *Caenorhabditis elegans* and *Caenorhabditis briggsae* have one and two genes, respectively. In *Caenorhabditis briggsae*, the two genes are very similar (~70% identity) and might represent a recent gene duplication event after the initial loss of two SNM1 genes. Interestingly, the SNM1 proteins in

nematodes are a fusion of an N-terminal OB fold (a single-stranded DNA binding motif also found in POT1) and a C-terminal metallo-β-lactamase domain. It has been recently reported that *C. elegans* have both G-rich and C-rich overhangs at their chromosome ends {Raices et al., 2008, Cell, 132, 745-57}. This novel combination of a metallo-β-lactamase domain and a ss-DNA binding domain might be involved in this unique processing event.

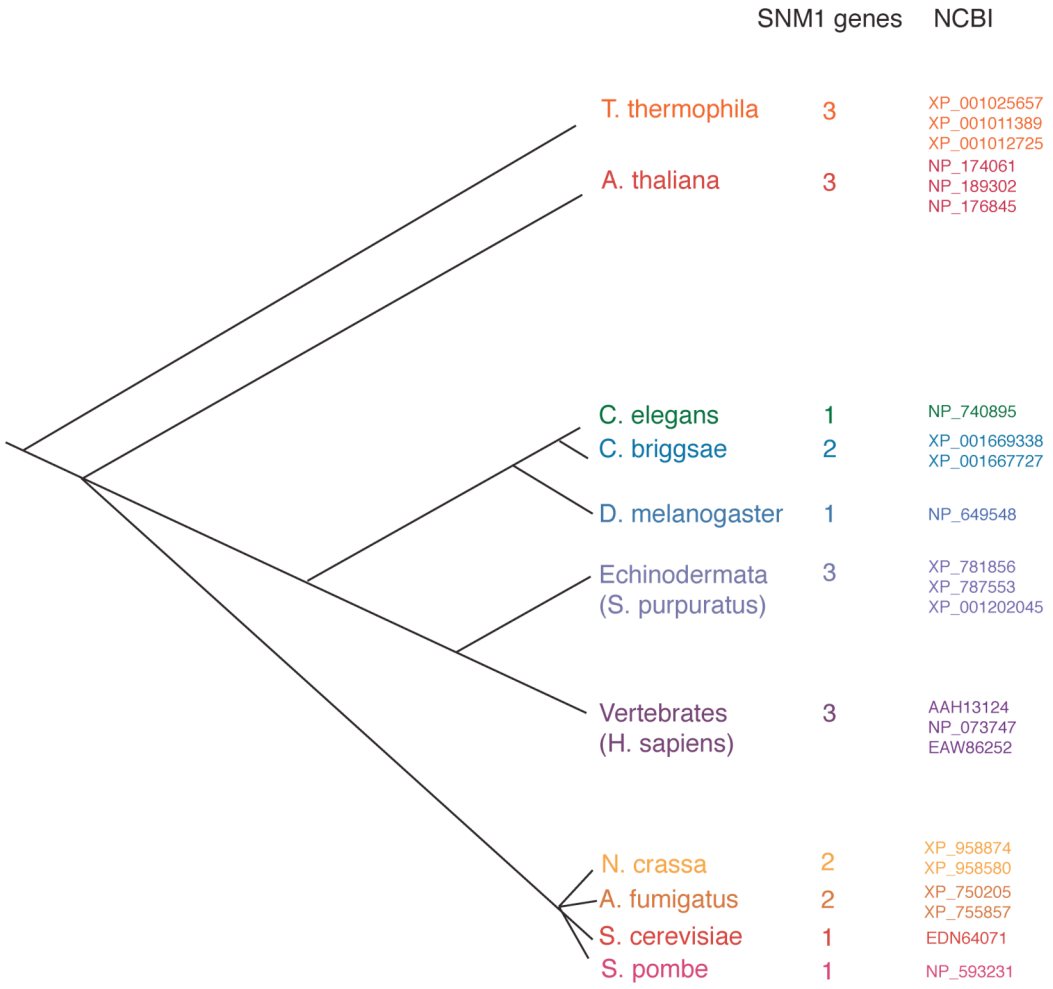

Figure 6-4. Diversity in SNM1 gene copy number.

Phylogenetic tree listing representative organisms and the number of SNM1 genes present in their genome with corresponding NCBI accession numbers. Branching is not drawn to scale.

It appears that there were orignially three SNM1 genes and Fungi and some Metazoans (arthropods and nematodes) lost one or two copies during their evolution. The process of recombinatorial assembly of lymphocyte receptors in adaptive immunity, which requires Artemis, did not arise until the class Agnatha (jawless fish). In classes that predate the evolution of adaptive immunity, a gene was likely required for the NHEJ repair pathway. In *S. cerevisiae* and *S. pombe*, the single SNM1 gene is required for ICL repair. In vertebrates, this role is primarily performed by SNM1A. The presence or absence of a third SNM1 gene, like Apollo in mammals, might reflect different strategies in solving problems related to telomere maintenance.

Apollo and disease

Mutations in DNA repair proteins underlie many cancer predisposition syndromes in humans. Mutations in telomere accessory factors such as Mre11, Nbs1, ATR, ATM, WRN, XPF, and BLM lead to cancer predisposition. Mutations in Artemis, a protein related to Apollo, were discovered as the underlying cause of RS-SCID. Mutations in Apollo have not been linked to human disease. Perhaps because most Apollo mutations are predicted to be lethal, mutations leading to a leaky phenotype or a disassociation of function might be rare.

We cannot presently ascribe a precise function to Apollo at the telomere. In this thesis, we have shown that Apollo is involved in the protection of telomeres during or after replication, generation of ssDNA at the telomere, and potentially in t-loop formation and telomerase regulation.

Analysis of the Apollo knockout mouse will clarify the roles of Apollo at telomeres.

MATERIALS AND METHODS

Cell culture

IMR90 primary lung fibroblasts (ATCC), HeLa, $p53^{-/-}$ and SV40 transformed MEFs, 293T cells, Phoenix ecotropic and amphotrophic packaging cell lines were grown in DMEM supplemented with 100 U/ml penicillin (Sigma), 0.1 μg/ml of streptomycin (Sigma), 2.0 mM L-glutamine (Invitrogen), 0.1 mM non-essential amino acids (Invitrogen), and 10% Fetal Bovine Serum. BJ fibroblasts (Clontech) and BJ-hTERT were grown in 4:1 DMEM/199 media supplemented with 15% fetal bovine serum, 100 U/ml penicillin (Sigma), 0.1 μg/ml of streptomycin (Sigma), 2.0 mM L-glutamine (Invitrogen), 0.1 mM non-essential amino acids (Invitrogen), and 1 mM sodium pyruvate (Sigma). All cells were grown at 37°C, 5% CO_2, and 95% relative humidity. Cells were passaged by pre-rinsing with room temperature PBS followed by incubation in Trypsin-EDTA (Gibco, 0.25%) for 2-5 min. Cells were seeded as indicated in text. Cells were counted with a Counter Counter Z1 Particle counter. For growth curves, 300,000 cells were plated on a 10 cm dish and grown for 72 hrs. Cells were harvested using trypsin and recovered in 4 ml of media, and the total cell number was determined. 300,000 cells were plated in a new 10 cm dish. At specified times, extra cells were plated in order to obtain protein and DNA samples for analysis. Population doublings were determined by the following formula: PD = original PD + [ln(# cells at passage/#cells seeded)/ln(2)] using Excel.

Calcium phosphate transfection of 293T cells for IPs and co-IPs

16-24 hrs. prior to transfection, 3-4 x 10^6 293T cells were plated in 10 cm dishes. Cells were transfected with 10 μg total DNA of the appropriate plasmids using $CaPO_4$ coprecipitation. For each plate, 428 μl H_20, 62 μl 2M $CaCl_2$, and 10 μg total plasmid DNA was mixed with an equal amount of 2X HBS (50 mM HEPES pH 7.05, 10 mM KCl, 12 mM dextrose, 280 mM NaCl, 1.5 mM Na_2PO_4) while being mixed by blowing air through a 2 mL pipette with a Pipet-aid (Drummond). Media was refreshed 5-8 hrs. after transfection. 48 hrs. after transfection, cells were harvested in media, counted, washed with PBS, and resuspended in 200-500 μl of lysis buffer (50 mM Tris-HCl pH 7.4, 1% Triton X-100, 0.1% SDS, 150 mM NaCl, 1 mM EDTA, 1 mM DTT, 1 mM PMSF, with a complete mini-protease inhibitor tablet [Roche] per 10 ml). The NaCl concentration was raised to 400 mM, and the lysate was incubated on ice for 5 min. The NaCl concentration was reduced to 200 mM with an equal volume of cold water, cell debris was removed by centrifugation at 13K for 10 min. at 4°C.

Immunoprecipitations

For immunoprecipitation of proteins expressed by transient transfection in 293T cells, transfection and harvesting was performed as above. 50 μL of 2X Laemmli buffer was added to 50 μL of lysate and set aside as the "Input." Antibody (anti-FLAG (M2), 4–6 μg; anti-HA (HA.11),1.0–1.2 μg; antimyc (9E10, Oncogene), 0.6–1.0 μg) was added to 800 μL of lysate. Samples were nutated at 4°C for 5 hrs. 60 μL of a Protein G sepharose slurry (50% [v/v] Protein-G sepharose [Amersham] in PBS in 1 mg/ml BSA) were added and samples were nutated at 4°C for an additional 60 min.

Beads were washed 4 times at 4°C with lysis buffer, and immunoprecipitated protein was eluted with 60 μL 2X Laemmli buffer. Samples were boiled for 5 min before loading onto SDS-PAGE gels.

Retroviral gene delivery

16-24 hrs. prior to transfection, 3-4 x 10^6 Phoenix packaging cells (293T derived cell lines) were plated in 10 cm dishes. For infection of mouse cells, Phoenix ecotropic cells were used. For infection of human cells, Phoenix amphotropic cells were used. Phoenix cells were transfected with 20 μg of the appropriate plasmid DNA by $CaPO_4$ coprecipitation (described above). The media was refreshed 5-8 hrs. later, and again 24 hrs. later. 36 hrs. after transfection, media was filtered through a 0.4 μm filter and polybrene was added to a final concentration of 4 μg/mL. Fresh media was added to the virus producing cells. This procedure was repeated 3 additional times at 12 hr. intervals. If appropriate, 12 hrs. after the final infection, fresh media was added containing antibiotics for selection (puromycin 2 μg/ml, hygromycin 90 μg/ml) for 3-8 days until uninfected control cells were completely dead.

Cell synchronization

HeLa cells (1 x 10^6) were plated on coverslips in a 10 cm culture dish and treated with 2 mM thymidine 24 h later. After 14 h, cells were washed three times with prewarmed PBS and provided with fresh medium for 11 h before adding 2 mM final concentration of thymidine. After 14 h, cells were washed with prewarmed PBS and again provided with fresh medium. Cells were harvested at the indicated time points for immunoblotting.

Expression of Cre Recombinase

Cre was introduced into MEFs using pMMP Hit & Run Cre-GFP retrovirus or pWZL-Cre retrovirus (containing the hygromycin resistance gene) using the retroviral infection technique described above.

Isolation of clonal lines

HeLa S3 cells expressing FHA_2-Rap1 were plated at low density (500-2000 cells/10 cm dish) and grown for approximately 2 weeks until clonal populations were visible under the light microscope. Clonal populations of cells were isolated by trypsinizing cells in cloning cylinders. Clonal populations were transferred to a well of a 96 well plate. When the cells reached confluence in the well, the clonal population was expanded.

Purification of the TRF2/Rap1 and Apollo complexes

For isolation of TRF2/Rap1 complexes from HeLaS3 cells, two retroviral vectors based on pLPC were generated by introducing a FLAG-HA-HA tag (FH2) in a N- or C-terminal position. Human Rap1

cDNA was PCR-amplified and cloned separately into either the N or C

terminally tagged constructs and sequenced. Apollo (SNM1B) cDNA was obtained from Invitrogen, and tagged versions of Apollo were generated by using standard PCR cloning into the pLPC retroviral vectors.

These constructs were transfected into amphotrophic Phoenix cells using calcium phosphate and the retroviral stocks were prepared for infection of semi-adherent HeLaS3 cells. Clones expressing tagged hRap1 were selected using puromycin (2 μg/ml) and isolated with cloning cylinders. The

efficiency of N- and C-terminally tagged hRap1 in forming a complex with endogenous TRF2, were tested by co-immunoprecipitations (IP).

HeLa S3 clones that expressed tagged hRap1 at a level 1-2-fold above that of endogenous hRap1 protein were selected for purification. For isolation of the TRF2/Rap1 and Apollo complexes, cells were grown in suspension culture (10 liters) at 37 °C to a density between 1.5-1.8 x 10^6 cells/mL. Cell harvest, extraction of nuclear proteins, sequential binding to affinity matrix, and peptide elutions were performed according to published procedures (Ogawa et al. 2002, Science) except that commercial affinity resins were used (anti-FLAG M2 resin from Sigma and anti-HA 3F10 resin from Roche). Eluted proteins were separated by SDS-PAGE on home made gradient gels (5%–15%). Coomassie staining was performed using Colloidal Blue Kit (Invitrogen) and silver staining was performed using the SilverQuest kit (Invitrogen).

Mass Spectrometry

In collaboration with the Chait Lab

The entire gel lane was sliced into 29 2-mm pieces, and the proteins in each gel piece were subjected to trypsin digestion. The resulting peptides were extracted and the proteins identified using a combination of two different mass spectrometers. First, tryptic mass maps of proteins from each gel piece were obtained using an in-house-constructed MALDIQqTOF mass spectrometer, and second, fragmentation spectra of all the discernable tryptic peptides were obtained using an in-house-constructed MALDI-ion trap

mass spectrometer (Krutchinksy et al. 2000, Anal Chem; Krutchinsky et al. 2001, J. Am. Soc. Mass Spectrom). Accurate masses of the tryptic peptides and the masses of their fragments were used to identify proteins in each gel piece with the computer search engine XProteo.

Rockefeller University Proteomics Resource Center

To identify Apollo and to examine the Apollo complex, individual bands were excised and subjected to trypsin digestion. The resulting peptides were extracted, and the protein was identified using the Applied Biosystems QSTAR XL tandem mass spectrometer at the Rockefeller University Proteomics Resource Center.

shRNA

shRNAs were generated in pSUPER-retro (OligoEngine), and retroviral infections were performed as described. The sequences of the shRNA targets are as follows:

H2, 5′-GAAGCTGCCCACCAGATTG-3′;

H6, 5′-GACTCTGTACAGCAATACA-3′;

H7, 5′-GATCAATCTCAAGCTGACA-3′;

H8, 5′-GATGGAGGTCCAGAAGCCA-3′; and

UTR, 5′-GGTCCTCGTGCCTATGGAA-3′.

The Luciferase control hairpin is 5′-CGTACGCGGAATACTTCGA-3′. The target sequence of shRNA H6 was changed to 5′-GACTCCGTCCAACAATACA-3′ by standard site-directed mutagenesis to create pLPC-Myc Apollo*H6.

RT-PCR

RT-PCR was performed with the oligo-dT ThermoScript RT-PCR system (Invitrogen). RNA was isolated from approximately 10^6 cells with the Qiagen RNAeasy kit. Three to four micrograms RNA was reverse transcribed with the ThermoScript RT-PCR system (Invitrogen) by using oligo dT priming and the protocol provided by the manufacturer. The primers used for PCR after cDNA synthesis are as follows: Apollo RT1 (forward GACTCCAACCCTACCACCATGAATG, reverse CAGTAGCTGTACCAACTCCAGGCGC) and GAPDH (forward TGAA GGTCGGAGTCAACGGATTTGGT, reverse CATGTGGGCCATGAGGTCCACCAC).

Radiation and drug treatment of cells

For γ-irradiation, cells were seeded in 6 cm culture dishes and exposed to a Ce source. Cells were allowed to recover in the incubator for the indicated amount of time before harvesting. For UV radiation, media was removed and reserved. Cells were subjected to the indicated dose of UV radiation in a Stratalinker 1800 (Stratagene). Reserved media was added back to cells and cells were allowed to recover in the incubator for the indicated amount of time before harvesting. Cells were treated with the indicated amounts of aphidicolin (Sigma), hydroxyurea (Sigma), MMC (Sigma), and cisplatin (Sigma) for the indicated amounts of time.

Whole cell lysates and western blots

For whole cell lysates, cells were harvested, washed with PBS, counted and resuspended in 2X Laemmli buffer at a concentration of 10,000 cells/μl.

Lysates were boiled for 5 min. and DNA was sheared through a 28 gauge insulin syringe. Protein samples were separated by SDS-PAGE and blotted onto nitrocellulose membranes. Membranes were blocked in 5% milk in PBST (0.5% Tween-20 in PBS) for 30 min. at RT and nutated with primary antibodies in 5% or 0.1% milk in PBST overnight at 4°C. Membranes were washed 3 times in PBST, nutated in secondary antibody in 5% milk in PBST for 45 min. at RT, and washed 3 times with PBST at RT. ECL (Amersham) was applied to membranes for 10 min. before exposure to film.

Fluorescence activated cell sorting (FACS) analysis

Cells were harvested from a 10 cm dish by trypsinization, washed with PBS, and resuspended in 100 µl PBS. Two ml ice cold 70% ethanol was added dropwise while vortexing. Cells were stored at 4°C. For FACS, cells were resuspended in propidium iodide solution (500 µl PBS, 100 µg RNase, 25 µg propidium iodide) and incubated at RT for 30 min. Cells were analyzed on a Becton Dickinson FACS – Scan II.

Immunofluorescence

Cells were plated in dishes on coverslips. Cells were rinsed with PBS, fixed with 2% paraformaldehyde in PBS for 10 min. at RT, wash twice with PBS for 5 min. Cells were either stored in PBS with the addition of 0.02% azide or processed immediately. If extraction was desired, prior to fixation, cells were treated with Triton X-100 extraction buffer (0.5% Triton X-100, 20 nM HEPES-KOH pH 7.9, 50 mM NaCl, 3 mM $MgCl_2$, 300 mM sucrose). Extracted cells were fixed with 3% paraformaldehyde, 2% sucrose for 10 minute at RT, and washed twice with PBS. Cells were permeabilized with

Triton X-100 buffer after fixation. After permeabilization, cells were washed three times with PBS and blocked with PBG (0.2% (w/v) cold water fish gelatin (Sigma), 0.5% (w/v) BSA (Sigma) in PBS) for 1 hr. at RT. Cells were incubated with primary antibody diluted in PBG 2 hrs at RT or overnight at 4°C, washed 3 times with PBG at RT, incubated with secondary antibody diluted 1:250 in PBG for 1 hr. at RT, and washed 3 times with PBS. To the second PBS wash 0.1 μg/ml 4,6-diamidino-2-phenylindole (DAPI) was added. Coverslips were sealed onto glass sides with embedding media (ProLong Gold Antifade Reagent, Invitrogen).

BrdU-TIF analysis

For the analysis of the cell-cycle stage of TIF induction, IMR90 cells were pulsed with 10 μM BrdU for 3 hr, fixed in 3% paraformaldehyde, and stained first for TRF1 and 53BP1 and then with rabbit-RRX (Jackson), mouse-Cy5 (Molecular Probes), and rat anti-BrdU conjugated to FITC (Axyll) in a buffer containing 10% goat serum, 3 mM MgCl2, and 100 U/ml DNaseI.

Metaphase spreads

Cells were grown to approximately 40% confluence on 10 cm dishes and incubated for 1-2 hrs. in 0.1 μg/ml colcemide (Sigma). Cells were harvested by trypsinization, centrifuged at 1K for 5 min., and resuspended in 0.075M KCL prewarmed to 37°C. Cells were incubated at 37°C for 15 min. with occasional inversion. Cells were centrifuged at 1K for 5 min. and supernatant was decanted. Cells were resuspended by tapping in the remaining (~200 μl) supernatant. 500 μl of cold 3:1 methanol:glacial acetic

acid fixative was added dropwise while cells were mixed gently on a vortexer (<1000 rpm). Another 500 µl fixative was added slowly while cells were being mixed. Tubes were then filled to 10 mL with the fixative and stored at 4°C overnight or longer. Cells were centrifuged at 1K rpm for 5 min. and supernatant was decanted. Cells were resuspended in the remaining fixative (~300 µl) and dropped from approximately 6 inches onto glass slides which had been soaked in cold water. Slides were washed with fresh fixative and placed on a humidified heating block set to 70°C (42°C for CO-FISH) for 1 minute. Spreading efficiency was checked under a light microscope. Slides were dried overnight. If only DAPI staining was required, slides were rehydrated in PBS for 5 min., stained with DAPI in PBS for 5 min., washed in PBS for 5 min., and allowed to dry before mounting.

CO-FISH

For CO-FISH cells were grown in the presence of BrdU:BrdC (3:1, 10 µM final) for 12-14 hrs. and supplemented with 0.1 µg/ml colcemide (Sigma) for the final two hrs. Metaphases were harvested as described above. Cells were treated with 0.5 mg/ml RNase A (in PBS, DNase free) for 10 min. at 37°C. Slides were then stained with 0.5 µg/ml Hoechst 33258 (Sigma) in 2X SSC for 15 min. at RT. Slides were then exposed to 365-nm UV light in a Stratalinker 1800 UV irradiator for 30 min. (equivalent to 5.4×10^3 J/m^2). Strands which had incorporated BrdU and BrdC were digested with 80 µl of 10 units/µl Exonuclease III (Promega) under a coverslip for 10 min. at RT. Exonuclease III digestion was repeated. Slides were washed in PBS and dehydrated in an ethanol series: 5 min. each 70%, 85%, 100%, and air dried.

Slides were incubated with the TAMRA-TelG 5'-$[TTAGGG]_3$-3' PNA probe (Applied Biosystems) diluted 1:5000 in 80 µl of hybridization mix (10 mM Tris-HCl pH 7.2, 70% deionized formamide, 0.5% blocking reagent [Boehringer Mannheim]) under a coverslip for two hrs. at RT in the dark. Slides were washed for several seconds in Wash I (70% formamide, 10 mM Tris-HCl pH 7.2, 0.1% BSA). Slides were incubated with the FITC-TelC 5'-$[CCCTAA]_3$-3' PNA probe (Applied Biosystems) in hybridization mix as described above. Slides were washed in Wash I twice for 30 min. each with a stir bar on a magnetic stir plate. Slides were then washed three times for 5 min. each in Wash II (0.1M Tris-HCl pH 7.2, 0.15M NaCl, 0.08% Tween-20) with a stir bar on a magnetic stir plate. DAPI was added to the second wash. Slides were dehydrated in an ethanol series: 5 min. each 70%, 95%, 100%, air dried, and mounted.

FISH

FISH was performed according to the same protocol as CO-FISH with the following exceptions. Cells were not incubated with BrdU/BrdC prior to collection of metaphase spreads. After metaphase spreads were dropped, slides were placed on a heating block set to 70°C (not 42°C as for CO-FISH). Hybridization was only performed with the FITC-TelC 5'-$[CCCTAA]_3$-3' PNA probe at 1:1000 and slides were placed on a heating block set to 80°C for 3 min. to denature DNA.

IF-FISH

Cells were plated in dishes with coverslips. Cells were rinsed with PBS, fixed with 2% paraformaldehyde in PBS for 10 min. at RT, washed twice

with PBS for 5 min. each. Cells were either stored in PBS with the addition of 0.02% azide or processed immediately. Coverslips were blocked for 30 min. in blocking solution (1 mg/ml BSA, 3% goat serum, 0.1% Triton X-100, 1 mM EDTA in PBS) and incubated for 1 hr. in primary antibody diluted in blocking solution. Cover slips were washed 3 times 5 min. each in PBS before incubation in secondary antibody diluted in blocking solution. Cover slips were washed 3 times 5 min. each in PBS, dehydrated in an ethanol series: 5 min. each 70%, 95%, 100%, and air dried. Coverslips were transferred (cells facing up) to glass slides and 80 µl of FITC-TelC 5'-$[CCCTAA]_3$-3' (Applied Biosystems) probe at 1:1000 in hybridizing solution (70% formamide, 0.5% blocking reagent [Boehringer Mannheim], 10 mM Tris-HCl pH 7.2) was added. Slides were placed on a heating block set to 70°C for 5 min. and incubated in the dark for 2 hrs. – overnight. Coverslips were washed twice for 15 min. in 70% formamide, 10 mM Tris-HCl pH 7.2 and three times for 5 min. in PBS. DAPI was added to the second PBS wash. Cover slips were sealed on glass slides with embedding media.

Microscopy and image processing

Images were captured using an Axioplan II Zeiss microscope with a Hamamatsu CCD digital camera using Improvision OpenLab software. Images were merged in OpenLab and processed with Adobe Photoshop.

Preparation of mouse genomic DNA

Cells were harvested by trypsinization and washed with PBS. 0.5 X 10^6 cells for MEFs and 1 x 10^6 cells for HeLa cells were resuspended in 50 µl PBS

and incubated at 50°C for 5 min. Using pipette tips with the ends cut off, 50 µl of 2% agarose (prewarmed to 50°C) was added to each sample, mixed, and incubated for 5 min at 50°C. The 100 µl mixture was added to the Bio-Rad plug cast, incubated at RT for 5 min. and at 4°C for 15 min. Solidified plugs were incubated in 0.5 ml Proteinase K digestion buffer (10 mM Tris-HCl pH 7.9, 250 mM EDTA pH 8.0, 0.2% sodium deoxycholate, 1% sodium lauryl sarcosine, and 1 mg/ml fresh Proteinase K) overnight at 50°C. Plugs were washed three times with TE for one hr. each at RT with nutation. Plugs were washed for 1 additional hr. at RT with TE containing 1 mM PMSF and stored at 4°C in this final wash. Prior to digestion, plugs were washed for 1 hr. in fresh TE and 20 min. in H_20. Plugs were equilibrated for 1 hr. in the appropriate restriction enzyme buffer at RT. Each plug was then digested with 60 units of MboI for MEFs and 60 units of MboI and 60 units AluI for human cells overnight at 37°C. Plugs were washed with TE for 1 hr. and equilibrated in 0.5X TBE for 30 min.

In gel hybridization to detect telomeric DNA from MEFs

DNA from MEFs was fractionated on a CHEF-DRII PFGE (Biorad) in a 1% agarose gel in 0.5X TBE for 24 hrs. at 6 V/cm at 14°C. Gels were stained with ethidium bromide and photographed. Gels were dried and then prehybridized in Church Mix (0.5M Na_2HPO_4 pH 7.2, 1 mM EDTA, 7% SDS, 1% BSA) for 1 hr. at 50°C. Hybridization was performed overnight at 50°C in Church Mix with 4 ng of a γ-32P-ATP end-labeled probe, $[CCCTAA]_4$ (See below for labeling protocol). The gel was washed at 55°C: 3 times for 30 min. each in 4X SSC and one time for 30 min. in 4X SSC, 0.1% SDS and exposed to a PhosphorImager screen. Subsequently,

the gel was denatured in 0.5 M NaOH, 1.5 M NaCl for 30 min., neutralized with two 15 minute washes in 0.5 M Tris-HCl pH 7.5, 3 M NaCl, prehybridized in Church mix for 1 hr. at 55°C, and hybridized with the same probe as above overnight at 55°C. The gel was washed and exposed as above.

Southern blot to detect telomeric DNA from human cells

DNA was separated on a 0.7% agarose gel in 0.5X TBE with ethidium bromide by running for 1 hr. at 30 V and then running at 45V until the orange G front was at the bottom of the gel (approximately overnight). At this point the gel was photographed. The gel was then run until the 1.3 kb marker was almost at the bottom of the gel. The gel was photographed again with a ruler next to the markers. Gel was gently shaken in Depurination solution (0.25 M HCl) for 30 min., twice in Denaturation solution (1.5 M NaCl; 0.5 M NaOH) for 30 min., and twice in Neutralization solution (1 M Trish pH 7.4, 1.5M NaCl) for 30 min. The DNA gel was then blotted onto a Hybond filter overnight in 20X SSC. The membrane was cross-linked, rinsed in H_20, and prehybridized and probed as in the in gel hybridization protocol above.

Chromatin Immunoprecipitation (ChIP)

Cells were trypsinized and washed with PBS, fixed in 1% formaldehyde in PBS for 60 min. at RT, washed in PBS, and lysed in 1% SDS, 50 mM Tris-HCl pH 8.0, 10 mM EDTA at a density of $1x10^7$ cells/ml. Lysates were sonicated on ice for 10 cycles of 20 seconds each (0.5 seconds on/0.5 seconds off) on power setting 5 on a Misonix Sonicator 3000. Two 50 µl

aliquots of lysates were set aside at 4°C to represent "Total" DNA. 200 µl of lysate was diluted with 1.2 ml 0.01% SDS, 1.1% Triton X-100, 1.2 mM EDTA, 16.7 mM Tris-HCl pH 8.0, and 150 mM NaCl. Antibody (20 µl crude serum or 4 µl affinity purified antibody or anti-c-myc 9E10, see antibody section below for specifics) was added and cells were nutated overnight at 4°C. 30 µl protein G sepharose beads (Amersham; blocked with 30 µg BSA and 5 µg sheared *E. coli* DNA) was added and samples were nutated for an additional 30 min. at 4°C. Beads were pelleted by centrifugation and pellets were washed with 0.1% SDS, 1% Triton X-100, 2 mM EDTA pH 8.0, 20 mM Tris-HCl pH 8.0, 150 mM NaCl. The second wash was the same except with 500 mM NaCl. Subsequent washes were with 0.25 M LiCl, 1% NP-40, 1% Na-deoxycholate, 1 mM EDTA pH 8.0, 10 mM Tris-HCl pH 8.0, 1 mM EDTA. Chromatin was eluted from beads with 500 µl 1% SDS, 0.1M Na_2CO_3. 450 µl 1% SDS, 0.1M Na_2CO_3 was added to the "Total" fractions, and these were subsequently processed along with the rest of the samples. 20 µl 5M NaCl was added and samples were incubated for 4 hr. at 65°C to reverse cross-links. At this point, 20 µl 1M Tris-HCl pH 6.5, 10 µl 0.5 M EDTA, and 20 µg DNase free RNase A was added and samples were incubated at 37°C for 30 min. 40 µg proteinase K was added and samples were digested for 60 min. at 37°C and extracted with phenol. 20 µg of glycogen was added and samples were mixed. 1 ml ethanol was added and DNA was precipitated overnight at -20°C. Precipitated DNA was dissolved in 100 µl H_20, denatured at 95°C for 5 min., and blotted onto Hybond membranes in 2X SSC (0.3M NaCl, 0.03M Sodium citrate). "Total" fractions were diluted 1/4, 1/8, and 1/16 and blotted as well. Membranes were treated with 1.5M NaCl, 0.5 N NaOH for

10 min. and then with 1 M NaCl, 0.5 M Tris-HCl pH 7.0 for 10 min. Hybridization was performed with a γ^{32}-P endlabeled $[CCCTAA]_4$ probe as described for in gel hybridization of genomic DNA. Membranes were washed 4 times in 2X SSC and exposed overnight to a PhosphorImager screen. Screens were developed using a STORM 820 Phosphorimager (Molecular Dynamics). ImageQuant software was used to quantify the percent of total telomeric DNA that was precipitated by each antibody.

C Strand STELA

Multiple ligation reactions were performed with individual C telorettes whereby 10 ng EcoRI-digested DNA was incubated in a 10 μl reaction (1× ligase buffer, 0.5 U T4 ligase, 10^{-2} to 10^{-5} μM of individual telorettes) at 35°C for 12 hr. Mutiple amplification reactions were performed (26 cycles of 95°C for 15 s, 58°C for 20 s, and 68°C for 10 min) by using 1 U of FailSafe enzyme mix (Epicenter), 12.5 μl FailSafe buffer H (2×, provided by manufacturer), and 0.1 μM primers (XpYpE2 forward primer and Teltail reverse primer) in a final volume of 25 μL containing 200 pg/μL DNA. The amplification products were resolved on a 0.5% agarose gel, denatured, transferred onto a positively charged nylon membrane (Amersham), fixed with UV, and hybridized with a subtelomeric probe (generated by PCR using XpYpE2 and XpYpB2 and labeled by random priming). The membrane was exposed to a PhosphorImager screen and scanned.

Oligonucleotides and Primers

XpYpE2 (forward primer subtelomeric), 5′-TTGTCTCAGGGTCCTAGTG-3′; XpYpB2 (reverse primer subtelomeric), 5′-TCTGAAAGTGGACC(A/T)ATCAG-3′;

C telorette 1, 5′-TGCTCCGTGCATCTGGCATCCCCTAAC-3′;

C telorette 2, 5′-TGCTCCGTGCATCTGGCATCTAACCCT-3′;

C telorette 3, 5′-TGCTCCGTGCATCTGGCATCCCTAACC-3′;

C telorette 4, 5′-TGCTCCGTGCATCTGGCATCCTAACCC-3′;

C telorette 5, 5′-TGCTCCGTGCATCTGGCATCAACCCTA-3′;

C telorette 6, 5′-TGCTCCGTGCATCTGGCATCACCCTAA-3′;

C teltail (reverse primer), 5′-TGCTCCGTGCATCTGGCATC-3′.

T Circle Amplification

1-3 μg of genomic DNA was digested with MboI and AluI and resuspended in an annealing buffer (0.2 M Tris [pH 7.5], 0.2 M KCl, and 1 mM EDTA) with 1 μM (CCCTAAA)3 primer containing thiophosphate linkages between the three 3′ terminal nucleotides. The mix was denatured at 96°C for 5 min and cooled down to 25°C for 2 hr. DNA was ethanol precipitated and resuspended in 20 μl of the TCA reaction buffer (33 mM Tris-acetate [pH 7.9], 10 mM magnesium acetate, 66 mM potassium acetate, 0.1% Tween 20, 1 mM DTT, and 0.37 mM dNTPs). Primer extension was carried out with 7.5 U of ϕ29 DNA polymerase (MBI Fermentas) at 30°C for 18 hr. The ϕ29 DNA polymerase was inactivated by incubation at 65°C for 20 min. The extension products were separated by denaturing gel electrophoresis (0.8% agarose, 50 mM NaOH, and 1 mM EDTA [pH 8]) at 2 V/cm for 18

hr, transferred onto a neutral nylon membrane, and hybridized using an [α-32P]dCTP Klenow-labeled 800-bp telomeric DNA probe from pSP73Sty11 {de Lange et al., 1990, Mol Cell Biol, 10, 518-27} {de Lange, 1992, Embo J, 11, 717-24}. Blots were exposed to PhosphorImager screens.

γ-^{32}P end labeling of oligonucleotides with T4 polynucleotide kinase (PNK)

2 µl H_20, 1 µl 10X T4 DNA PNK buffer (NEB), 1 µl 10 U/µl T4 DNA PNK (NEB), 1 µl 50 ng/µl $[CCCTAA]_4$ oligonucleotide and 5 µl 10.0 mCi/ml γ-^{32}P (NEN) were mixed and incubated for 45 min. at 37°C. 80 µl TES (10 mM Tris-HCl pH 8.0, 10 mM EDTA pH 8.0, 0.01% SDS) were added to stop the reaction. The probe was loaded onto a 3 ml G25 Sephadex column equilibrated with TNES (10 mM Tris-HCl pH 7.4, 10 mM EDTA, 100 mM NaCl, 1% SDS). The column was washed with 700 µl TNES and the probe was eluted with 600 µl TNES.

Apollo Antibodies

Antibodies to KLH-conjugated Apollo peptides

P1: (NH2-SRKIHSSHPDIHVIPYSDHSSYSC-COOH; starting at aa 258) and P2: (NH2-GDDDGGPEATGNQSAWMGHGSPLC; starting at aa 461) were generated in NZW rabbits (Covance). The resulting immune serum for Abs 1477- 1480 was affinity purified.

Antibodies used

ID	antigen	Type	Applications	Origin
765	hRap1	Rb, poly	IF 1:2000 Western 1:2000	Li/de Lange
647	hTRF2 (baculoviral-FL)	Rb poly	Western 1:1000	Zhu/de Lange lab
371	TRF1	Rb, poly	IF 1:1000 Western 1:1000	de Lange
p54	p54	Rb, poly	Western 1:2000	Konarska Lab RU
864	Tin2	Rb, poly	Western 1:2000	Ye/ de Lange
9E10	c-myc peptide	Mo mono	Western 1:1000 IF 1:1000	Calbiochem
9E10	c-myc peptide	Mo mono	IF 1:5000	Sigma

ID	antigen	Type	Applications	Origin
M2	Flag peptide	Mo mono	Western 1:10,000	Sigma
HA.11	HA peptide	Mo mono	Western 1:1000 IF 1:1000	Covance
αhTRF1	hTRF1 (baculoviral-FL)	Mo poly	IF 1:5000	Marrero/ de Lange lab
1477-1478	Apollo peptide P1	Rb, poly	Western 1:500 IF 1:500	van Overbeek/ de Lange
1479-1480	Apollo peptide P2	Rb, poly	Western 1:500 IF 1:500	van Overbeek/ de Lange
DO-1	p53	Mo, mono	Western 1:300	Santa Cruz
GNS1	Cyclin B	Mo, mono	Western 1:100	Santa Cruz
GTU88	γTubulin (peptide)	Mo mono	Western 1:5000	Sigma

ID	antigen	Type	Applications	Origin
α-γH2AX	γH2AX (phospho peptide S139)	Mo mono	IF 1:1000	Upstate
αChk1-P	Chk1-P (phospho peptide S345)	Rb mono	Western 1:1000	Cell Signaling
Chk2	Chk2	Mo, mono	Western 1:300	BD Transduction Lab
F-5	p21	mo, mono	Western 1:500	Santa Cruz
p16	human p16	mo, mono	Western 1:100	NovaCastra
α53BP1	Human 53BP1	Mo mono	IF 1:50	Halazonetis, The Wistar Institute, PA
α53BP1	53BP1 (peptide)	Rb poly	IF 1:1000	Novus
1223	mPot1b	Rb, poly	Western 1:1000	Hockemeyer/ de Lange

ID	antigen	Type	Applications	Origin
1254	mTRF2 (GST-FL)	Rb poly	Western (m) 1:5000	Celli/de Lange
979	hPot1	Rb, poly	Western 1:1000	Loayza/ de Lange
DBC-1	DBC-1	Rb, poly	Western 1:1000	Bethyl Labs
Coilin	Coilin	Mo, mono	IF 1:1000	Sigma
RuvBL2	Tip48	Rb, poly	Western 1:200	Aviva
polι	polι	Rb, poly	Western 1:1000	Novus
polη	polη	Rb, poly	1:300	Santa Cruz
PC-130	Rad51	Rb, poly	Western 1:1000	Calbiochem
Rad51C	Rad51C	Mo,	Western 1:1000	Novus

ID	antigen	Type	Applications	Origin
		mono		
ATRIP	ATRIP	Rb, poly	Western 1:400	Elledge Lab Harvard
DNA-PK (C19) 1552	DNA-PKcs	Gt, poly	Western 1:500	Santa Cruz
Ab 476	WRN	Rb, poly	Western 1:1000	Novus
Ab 200	BLM	Rb, poly	Western 1:1000	AbCam
FANCD2	FANCD2	Rb, poly	Western 1:1000	Auerbach, RU
BRCA2	BRCA2	Rb, poly	Western 1:1000	Novus
H-152	Rad54	Rb, poly	Western 1:100	Santa Cruz
BRCA1	BRCA1	Mo,	Western 1:100	Calbiochem

ID	antigen	Type	Applications	Origin
Ab-1		mono		

Rb: Rabbit; Mo: mouse; Gt: goat; poly: polyclonal; mono: monoclonal

BIBLIOGRAPHY

1. Watson, J. D. Origin of concatemeric T7 DNA. *Nat New Biol* **239**, 197-201 (1972).
2. Blackburn, E. H. & Gall, J. G. A tandemly repeated sequence at the termini of the extrachromosomal ribosomal RNA genes in Tetrahymena. *J Mol Biol* **120**, 33-53 (1978).
3. Moyzis, R. K. et al. A highly conserved repetitive DNA sequence, (TTAGGG)n, present at the telomeres of human chromosomes. *Proc Natl Acad Sci USA* **85**, 6622-6626 (1988).
4. Cross, S. H., Allshire, R. C., McKay, S. J., McGill, N. I. & Cooke, H. J. Cloning of human telomeres by complementation in yeast. *Nature* **338**, 771-774 (1989).
5. de Lange, T. et al. Structure and variability of human chromosome ends. *Mol Cell Biol* **10**, 518-527 (1990).
6. Kipling, D. & Cooke, H. J. Hypervariable ultra-long telomeres in mice. *Nature* **347**, 400-402 (1990).
7. Delany, M. E., Krupkin, A. B. & Miller, M. M. Organization of telomere sequences in birds: evidence for arrays of extreme length and for in vivo shortening. *Cytogenet Cell Genet* **90**, 139-145 (2000).
8. Sfeir, A. J., Chai, W., Shay, J. W. & Wright, W. E. Telomere-end processing the terminal nucleotides of human chromosomes. *Mol Cell* **18**, 131-138 (2005).
9. Fan, X. & Price, C. M. Coordinate regulation of G- and C strand length during new telomere synthesis. *Mol Biol Cell* **8**, 2145-2155 (1997).
10. Jacob, N. K., Skopp, R. & Price, C. M. G-overhang dynamics at Tetrahymena telomeres. *Embo J* **20**, 4299-308. (2001).
11. Griffith, J. D. et al. Mammalian telomeres end in a large duplex loop. *Cell* **97**, 503-14. (1999).

12. Murti, K. G. & Prescott, D. M. Telomeres of polytene chromosomes in a ciliated protozoan terminate in duplex DNA loops. *Proc Natl Acad Sci USA* **96**, 14436-14439 (1999).

13. Munoz-Jordan, J. L., Cross, G. A., de Lange, T. & Griffith, J. D. t-loops at trypanosome telomeres. *Embo J* **20**, 579-88. (2001).

14. Cesare, A. J., Quinney, N., Willcox, S., Subramanian, D. & Griffith, J. D. Telomere looping in P. sativum (common garden pea). *Plant J* **36**, 271-279 (2003).

15. Nikitina, T. & Woodcock, C. L. Closed chromatin loops at the ends of chromosomes. *J Cell Biol* **166**, 161-165 (2004).

16. Zhu, X. D., Kuster, B., Mann, M., Petrini, J. H. & de Lange, T. Cell-cycle-regulated association of RAD50/MRE11/NBS1 with TRF2 and human telomeres. *Nat Genet* **25**, 347-352 (2000).

17. Greider, C. W. & Blackburn, E. H. Identification of a specific telomere terminal transferase activity in Tetrahymena extracts. *Cell* **43**, 405-413 (1985).

18. Greider, C. W. & Blackburn, E. H. The telomere terminal transferase of Tetrahymena is a ribonucleoprotein enzyme with two kinds of primer specificity. *Cell* **51**, 887-898 (1987).

19. Diede, S. J. & Gottschling, D. E. Telomerase-mediated telomere addition in vivo requires DNA primase and DNA polymerases alpha and delta. *Cell* **99**, 723-733 (1999).

20. Kim, N. W. et al. Specific association of human telomerase activity with immortal cells and cancer. *Science* **266**, 2011-205. (1994).

21. Feng, J. et al. The RNA component of human telomerase. *Science* **269**, 1236-1241 (1995).

22. Cohen, S. et al. Protein Composition of Catalytically Active Human Telomerase from Immortal Cells. *Science* **315**, 1850-1853 (2007).

23. Mitchell, J. R., Wood, E. & Collins, K. A telomerase component is defective in the human disease dyskeratosis congenita. *Nature* **402**, 551-55. (1999).

24. Vulliamy, T. et al. The RNA component of telomerase is mutated in autosomal dominant dyskeratosis congenita. *Nature* **413**, 432-435 (2001).

25. Dokal, I. et al. Dyskeratosis congenita fibroblasts are abnormal and have unbalanced chromosomal rearrangements. *Blood* **80**, 3090-3096 (1992).

26. Bryan, T. M., Englezou, A., Dalla-Pozza, L., Dunham, M. A. & Reddel, R. R. Evidence for an alternative mechanism for maintaining telomere length in human tumors and tumor-derived cell lines. *Nat Med* **3**, 1271-1274 (1997).

27. Henson, J. D., Neumann, A. A., Yeager, T. R. & Reddel, R. R. Alternative lengthening of telomeres in mammalian cells. *Oncogene* **21**, 598-610 (2002).

28. Bryan, T. M., Englezou, A., Gupta, J., Bacchetti, S. & Reddel, R. R. Telomere elongation in immortal human cells without detectable telomerase activity. *Embo J* **14**, 4240-4248 (1995).

29. Murnane, J. P., Sabatier, L., Marder, B. A. & Morgan, W. F. Telomere dynamics in an immortal human cell line. *Embo J* **13**, 4953-4962 (1994).

30. Yeager, T. R. et al. Telomerase-negative immortalized human cells contain a novel type of promyelocytic leukemia (PML) body. *Cancer Res* **59**, 4175-4179 (1999).

31. Lundblad, V. & Blackburn, E. H. An alternative pathway for yeast telomere maintenance rescues est1- senescence. *Cell* **73**, 347-360 (1993).

32. Teng, S. C., Chang, J., McCowan, B. & Zakian, V. A. Telomerase-independent lengthening of yeast telomeres occurs by an abrupt Rad50p-dependent, Rif-inhibited recombinational process. *Mol Cell* **6**, 947-952 (2000).

33. Le, S., Moore, J. K., Haber, J. E. & Greider, C. W. RAD50 and RAD51 define two pathways that collaborate to maintain telomeres in the absence of telomerase. *Genetics* **152**, 143-152 (1999).

34. HAYFLICK, L. & MOORHEAD, P. S. The serial cultivation of human diploid cell strains. *Exp Cell Res* **25**, 585-621 (1961).

35. Olovnikov, A. M. A theory of marginotomy. The incomplete copying of template margin in enzymic synthesis of polynucleotides and biological significance of the phenomenon. *J Theor Biol* **41**, 181-190 (1973).

36. Hastie, N. D. et al. Telomere reduction in human colorectal carcinoma and with ageing. *Nature* **346**, 866-868 (1990).

37. Harley, C. B., Futcher, A. B. & Greider, C. W. Telomeres shorten during ageing of human fibroblasts. *Nature* **345**, 458-460 (1990).

38. Lindsey, J., McGill, N. I., Lindsey, L. A., Green, D. K. & Cooke, H. J. In vivo loss of telomeric repeats with age in humans. *Mutat Res* **256**, 45-48 (1991).

39. Bodnar, A. G. et al. Extension of life-span by introduction of telomerase into normal human cells. *Science* **279**, 349-352 (1998).

40. de Lange, T. Shelterin: the protein complex that shapes and safeguards human telomeres. *Genes Dev* **19**, 2100-2110 (2005).

41. Broccoli, D., Smogorzewska, A., Chong, L. & de Lange, T. Human telomeres contain two distinct Myb-related proteins, TRF1 and TRF2. *Nat Genet* **17**, 231-235 (1997).

42. Chong, L. et al. A human telomeric protein. *Science* **270**, 1663-1667 (1995).

43. Bianchi, A., Smith, S., Chong, L., Elias, P. & de Lange, T. TRF1 is a dimer and bends telomeric DNA. *Embo J* **16**, 1785-1794 (1997).

44. Bilaud, T. et al. Telomeric localization of TRF2, a novel human telobox protein. *Nat Genet* **17**, 236-239 (1997).

45. van Steensel, B., Smogorzewska, A. & de Lange, T. TRF2 protects human telomeres from end-to-end fusions. *Cell* **92**, 401-413 (1998).

46. Baumann, P. & Cech, T. R. Pot1, the putative telomere end-binding protein in fission yeast and humans. *Science* **292**, 1171-115. (2001).

47. Loayza, D. & de Lange, T. POT1 as a terminal transducer of TRF1 telomere length control. *Nature* **424**, 1013-1018 (2003).

48. Ye, J. Z. et al. TIN2 binds TRF1 and TRF2 simultaneously and stabilizes the TRF2 complex on telomeres. *J Biol Chem* **279**, 47264-47271 (2004).

49. Kim, S. H. et al. TIN2 mediates functions of TRF2 at human telomeres. *J Biol Chem* **279**, 43799-43804 (2004).

50. Ye, J. Z. et al. POT1-interacting protein PIP1: a telomere length regulator that recruits POT1 to the TIN2/TRF1 complex. *Genes Dev* **18**, 1649-1654 (2004).

51. Liu, D. et al. PTOP interacts with POT1 and regulates its localization to telomeres. *Nat Cell Biol* **6**, 673-680 (2004).

52. Hockemeyer, D. et al. Telomere protection by mammalian POT1 requires interaction with TPP1. *Nat Struct Mol Biol* **14**, 754-761 (2007).

53. Liu, D., O'Connor, M. S., Qin, J. & Songyang, Z. Telosome, a mammalian telomere-associated complex formed by multiple telomeric proteins. *J Biol Chem* **279**, 51338-51342 (2004).

54. Bianchi, A. et al. TRF1 binds a bipartite telomeric site with extreme spatial flexibility. *Embo J* **18**, 5735-5744 (1999).

55. van Steensel, B. & de Lange, T. Control of telomere length by the human telomeric protein TRF1. *Nature* **385**, 740-743 (1997).

56. Smogorzewska, A. et al. Control of human telomere length by TRF1 and TRF2. *Mol Cell Biol* **20**, 1659-1668 (2000).

57. Ancelin, K. et al. Targeting assay to study the cis functions of human telomeric proteins: evidence for inhibition of telomerase by TRF1 and for activation of telomere degradation by TRF2. *Mol Cell Biol* **22**, 3474-3487 (2002).

58. Karlseder, J., Smogorzewska, A. & de Lange, T. Senescence induced by altered telomere state, not telomere loss. *Science* **295**, 2446-2449 (2002).

59. Karlseder, J. et al. Targeted deletion reveals an essential function for the telomere length regulator Trf1. *Mol Cell Biol* **23**, 6533-6541 (2003).

60. Fairall, L., Chapman, L., Moss, H., de Lange, T. & Rhodes, D. Structure of the TRFH dimerization domain of the human telomeric proteins TRF1 and TRF2. *Molecular Cell* **8**, 351-361 (2001).

61. Cooper, J. P., Nimmo, E. R., Allshire, R. C. & Cech, T. R. Regulation of telomere length and function by a Myb-domain protein in fission yeast. *Nature* **385**, 744-747 (1997).

62. Li, B., Oestreich, S. & de Lange, T. Identification of human Rap1: implications for telomere evolution. *Cell* **101**, 471-483 (2000).

63. Celli, G. & de Lange, T. DNA processing not required for ATM-mediated telomere damage response after TRF2 deletion. *Nat Cell Biol* **7**, 712-718 (2005).

64. Konig, P., Giraldo, R., Chapman, L. & Rhodes, D. The crystal structure of the DNA-binding domain of yeast RAP1 in complex with telomeric DNA. *Cell* **85**, 125-136 (1996).

65. Hanaoka, S. et al. NMR structure of the hRap1 Myb motif reveals a canonical three-helix bundle lacking the positive surface charge typical of Myb DNA-binding domains. *J Mol Biol* **312**, 167-175 (2001).

66. Kanoh, J. & Ishikawa, F. spRap1 and spRif1, recruited to telomeres by Taz1, are essential for telomere function in fission yeast. *Curr Biol* **11**, 1624-1630 (2001).

67. Li, B. & de Lange, T. Rap1 affects the length and heterogeneity of human telomeres. *Mol Biol Cell* **14**, 5060-5068 (2003).

68. Gottschling, D. E. & Zakian, V. A. Telomere proteins: specific recognition and protection of the natural termini of Oxytricha macronuclear DNA. *Cell* **47**, 195-205 (1986).

69. Horvath, M. P., Schweiker, V. L., Bevilacqua, J. M., Ruggles, J. A. & Schultz, S. C. Crystal structure of the Oxytricha nova telomere end binding protein complexed with single strand DNA. *Cell* **95**, 963-974 (1998).

70. Lei, M., Zaug, A. J., Podell, E. R. & Cech, T. R. Switching human telomerase on and off with hPOT1 protein in vitro. *J Biol Chem* **280**, 20449-20456 (2005).

71. Loayza, D., Parsons, H., Donigian, J., Hoke, K. & de Lange, T. DNA binding features of human POT1: A nonamer 5'-TAGGGTTAG-3' minimal binding site, sequence specificity, and internal binding to multimeric sites. *J Biol Chem* **279**, 13241-13248 (2004).

72. Houghtaling, B. R., Cuttonaro, L., Chang, W. & Smith, S. A dynamic molecular link between the telomere length regulator TRF1 and the chromosome end protector TRF2. *Curr Biol* **14**, 1621-1631 (2004).

73. Wang, F. et al. The POT1-TPP1 telomere complex is a telomerase processivity factor. *Nature* **445**, 506-510 (2007).

74. Xin, H. et al. TPP1 is a homologue of ciliate TEBP-beta and interacts with POT1 to recruit telomerase. *Nature* **445**, 559-562 (2007).

75. Kim, S. H., Kaminker, P. & Campisi, J. TIN2, a new regulator of telomere length in human cells. *Nat Genet* **23**, 405-412 (1999).

76. Chen, Y. et al. A Shared Docking Motif in TRF1 and TRF2 Used for Differential Recruitment of Telomeric Proteins. *Science* (2008).

77. Takai, H., Smogorzewska, A. & de Lange, T. DNA damage foci at dysfunctional telomeres. *Curr Biol* **13**, 1549-1556 (2003).

78. Zhu, X. D. et al. ERCC1/XPF Removes the 3' Overhang from Uncapped Telomeres and Represses Formation of Telomeric DNA-Containing Double Minute Chromosomes. *Mol Cell* **12**, 1489-1498 (2003).

79. Smogorzewska, A., Karlseder, J., Holtgreve-Grez, H., Jauch, A. & de Lange, T. DNA Ligase IV-Dependent NHEJ of Deprotected Mammalian Telomeres in G1 and G2. *Curr Biol* **12**, 1635 (2002).

80. Celli, G. B., Lazzerini Denchi, E. & de Lange, T. Ku70 stimulates fusion of dysfunctional telomeres yet protects chromosome ends from homologous recombination. *Nat Cell Biol* **8**, 885-890 (2006).

81. Dimitrova, N. & de Lange, T. MDC1 accelerates nonhomologous end-joining of dysfunctional telomeres. *Genes Dev* **20**, 3238-3243 (2006).

82. Lazzerini Denchi, E. & de Lange, T. Protection of telomeres through independent control of ATM and ATR by TRF2 and POT1. *Nature* **448**, 1068-1071 (2007).

83. Karlseder, J., Broccoli, D., Dai, Y., Hardy, S. & de Lange, T. p53- and ATM-dependent apoptosis induced by telomeres lacking TRF2. *Science* **283**, 1321-1325 (1999).

84. Shay, J. W., Wright, W. E., Brasiskyte, D. & Van der Haegen, B. A. E6 of human papillomavirus type 16 can overcome the M1 stage of immortalization in human mammary epithelial cells but not in human fibroblasts. *Oncogene* **8**, 1407-1413 (1993).

85. Capper, R. et al. The nature of telomere fusion and a definition of the critical telomere length in human cells. *Genes Dev* **21**, 2495-2508 (2007).

86. Wang, R. C., Smogorzewska, A. & de Lange, T. Homologous recombination generates T-loop-sized deletions at human telomeres. *Cell* **119**, 355-368 (2004).

87. Liu, Y., Masson, J. Y., Shah, R., O'Regan, P. & West, S. C. RAD51C is required for Holliday junction processing in mammalian cells. *Science* **303**, 243-246 (2004).

88. Zellinger, B., Akimcheva, S., Puizina, J., Schirato, M. & Riha, K. Ku suppresses formation of telomeric circles and alternative telomere lengthening in Arabidopsis. *Mol Cell* **27**, 163-169 (2007).

89. Li, B. & Lustig, A. J. A novel mechanism for telomere size control in Saccharomyces cerevisiae. *Genes Dev* **10**, 1310-1326 (1996).

90. Lustig, A. J. Clues to catastrophic telomere loss in mammals from yeast telomere rapid deletion. *Nat Rev Genet* **4**, 916-923 (2003).

91. Tarsounas, M. et al. Telomere maintenance requires the RAD51D recombination/repair protein. *Cell* **117**, 337-347 (2004).

92. Jaco, I. et al. Role of mammalian Rad54 in telomere length maintenance. *Mol Cell Biol* **23**, 5572-5580 (2003).

93. Ranganathan, V. et al. Rescue of a telomere length defect of Nijmegen breakage syndrome cells requires NBS and telomerase catalytic subunit. *Curr Biol* **11**, 962-96. (2001).

94. Stansel, R. M., de Lange, T. & Griffith, J. D. T-loop assembly in vitro involves binding of TRF2 near the 3' telomeric overhang. *EMBO J* **20**, 5532-5540 (2001).

95. Karlseder, J. et al. The telomeric protein TRF2 binds the ATM kinase and can inhibit the ATM-dependent DNA damage response. *PLoS Biol* **2**, E240 (2004).

96. Teixeira, M. T., Arneric, M., Sperisen, P. & Lingner, J. Telomere Length Homeostasis Is Achieved via a Switch between Telomerase- Extendible and -Nonextendible States. *Cell* **117**, 323-335 (2004).

97. Pennock, E., Buckley, K. & Lundblad, V. Cdc13 delivers separate complexes to the telomere for end protection and replication. *Cell* **104**, 387-96. (2001).

98. Marcand, S., Gilson, E. & Shore, D. A protein-counting mechanism for telomere length regulation in yeast. *Science* **275**, 986-990 (1997).

99. McCarroll, R. M. & Fangman, W. L. Time of replication of yeast centromeres and telomeres. *Cell* **54**, 505-513 (1988).

100. Raghuraman, M. K. et al. Replication dynamics of the yeast genome. *Science* **294**, 115-121 (2001).

101. Wright, W. E., Tesmer, V. M., Liao, M. L. & Shay, J. W. Normal human telomeres are not late replicating. *Exp Cell Res* **251**, 492-499 (1999).

102. Zou, Y., Gryaznov, S. M., Shay, J. W., Wright, W. E. & Cornforth, M. N. Asynchronous replication timing of telomeres at opposite arms of mammalian chromosomes. *Proc Natl Acad Sci U S A* **101**, 12928-12933 (2004).

103. Henderson, E., Hardin, C. C., Walk, S. K., Tinoco, I., Jr. & Blackburn, E. H. Telomeric DNA oligonucleotides form novel intramolecular structures containing guanine-guanine base pairs. *Cell* **51**, 899-908 (1987).

104. Sundquist, W. I. & Klug, A. Telomeric DNA dimerizes by formation of guanine tetrads between hairpin loops. *Nature* **342**, 825-829 (1989).

105. Williamson, J. R., Raghuraman, M. K. & Cech, T. R. Monovalent cation-induced structure of telomeric DNA: the G-quartet model. *Cell* **59**, 871-880 (1989).

106. Crabbe, L., Verdun, R. E., Haggblom, C. I. & Karlseder, J. Defective telomere lagging strand synthesis in cells lacking WRN helicase activity. *Science* **306**, 1951-1953 (2004).

107. Opresko, P. L. et al. Telomere binding protein TRF2 binds to and stimulates the Werner and Bloom syndrome helicases. *J Biol Chem* **277**, 41110-41119 (2002).

108. Zaug, A. J., Podell, E. R. & Cech, T. R. Human POT1 disrupts telomeric G-quadruplexes allowing telomerase extension in vitro. *Proc Natl Acad Sci USA* **102**, 10864-10869 (2005).

109. Liu, Z., Frantz, J. D., Gilbert, W. & Tye, B. K. Identification and characterization of a nuclease activity specific for G4 tetrastranded DNA. *Proc Natl Acad Sci U S A* **90**, 3157-3161 (1993).

110. Liu, Z. & Gilbert, W. The yeast KEM1 gene encodes a nuclease specific for G4 tetraplex DNA: implication of in vivo functions for this novel DNA structure. *Cell* **77**, 1083-1092 (1994).

111. Sun, H., Yabuki, A. & Maizels, N. A human nuclease specific for G4 DNA. *Proc Natl Acad Sci U S A* **98**, 12444-12449 (2001).

112. Miller, K. M., Rog, O. & Cooper, J. P. Semi-conservative DNA replication through telomeres requires Taz1. *Nature* **440**, 824-828 (2006).

113. Yamaguchi-Iwai, Y. et al. Mre11 is essential for the maintenance of chromosomal DNA in vertebrate cells. *Embo J* **18**, 6619-6629 (1999).

114. Tauchi, H. et al. Nbs1 is essential for DNA repair by homologous recombination in higher vertebrate cells. *Nature* **420**, 93-98 (2002).

115. Hsu, H. L., Gilley, D., Blackburn, E. H. & Chen, D. J. Ku is associated with the telomere in mammals. *Proc Natl Acad Sci USA* **96**, 12454-12458 (1999).

116. d'Adda di Fagagna, F. et al. Effects of DNA nonhomologous end-joining factors on telomere length and chromosomal stability in mammalian cells. *Curr Biol* **11**, 1192-116. (2001).

117. O'Connor, M. S., Safari, A., Liu, D., Qin, J. & Songyang, Z. The human Rap1 protein complex and modulation of telomere length. *J Biol Chem* **279**, 28585-28591 (2004).

118. Opresko, P. L. et al. The Werner Syndrome Helicase and Exonuclease Cooperate to Resolve Telomeric D Loops in a Manner Regulated by TRF1 and TRF2. *Mol Cell* **14**, 763-774 (2004).

119. Schreiber, V., Dantzer, F., Ame, J. C. & de Murcia, G. Poly(ADP-ribose): novel functions for an old molecule. *Nat Rev Mol Cell Biol* **7**, 517-528 (2006).

120. Gomez, M. et al. PARP1 Is a TRF2-associated poly(ADP-ribose)polymerase and protects eroded telomeres. *Mol Biol Cell* **17**, 1686-1696 (2006).

121. Dantzer, F. et al. Functional interaction between poly(ADP-Ribose) polymerase 2 (PARP-2) and TRF2: PARP activity negatively regulates TRF2. *Mol Cell Biol* **24**, 1595-1607 (2004).

122. Smith, S. & de Lange, T. Tankyrase promotes telomere elongation in human cells. *Curr Biol* **10**, 1299-302. (2000).

123. Smith, S., Giriat, I., Schmitt, A. & de Lange, T. Tankyrase, a poly(ADP-ribose) polymerase at human telomeres. *Science* **282**, 1484-1487 (1998).

124. Donigian, J. R. & de Lange, T. The role of the poly(ADP-ribose) polymerase tankyrase1 in telomere length control by the TRF1 component of the shelterin complex. *J Biol Chem* **282**, 22662-22667 (2007).

125. Kaminker, P. G. et al. TANK2, a new TRF1-associated PARP, causes rapid induction of cell death upon overexpression. *J Biol Chem* **276**, 35891-35899 (2001).

126. Cook, B. D., Dynek, J. N., Chang, W., Shostak, G. & Smith, S. Role for the related poly(ADP-Ribose) polymerases tankyrase 1 and 2 at human telomeres. *Mol Cell Biol* **22**, 332-342 (2002).

127. Sbodio, J. I., Lodish, H. F. & Chi, N. W. Tankyrase-2 oligomerizes with tankyrase-1 and binds to both TRF1 (telomere-repeat-binding factor 1) and IRAP (insulin-responsive aminopeptidase). *Biochem J* **361**, 451-459 (2002).

128. Dynek, J. N. & Smith, S. Resolution of sister telomere association is required for progression through mitosis. *Science* **304**, 97-100 (2004).

129. Aravind, L. An evolutionary classification of the metallo-beta-lactamase fold proteins. *In Silico Biol* **1**, 69-91 (1999).

130. Callebaut, I., Moshous, D., Mornon, J. P. & de Villartay, J. P. Metallo-beta-lactamase fold within nucleic acids processing enzymes: the beta-CASP family. *Nucleic Acids Res* **30**, 3592-3601 (2002).

131. Ryan, K., Calvo, O. & Manley, J. L. Evidence that polyadenylation factor CPSF-73 is the mRNA 3' processing endonuclease. *RNA* **10**, 565-573 (2004).

132. Mandel, C. R. et al. Polyadenylation factor CPSF-73 is the pre-mRNA 3'-end-processing endonuclease. *Nature* **444**, 953-956 (2006).

133. Moshous, D. et al. Artemis, a novel DNA double-strand break repair/V(D)J recombination protein, is mutated in human severe combined immune deficiency. *Cell* **105**, 177-186 (2001).

134. Ma, Y., Pannicke, U., Schwarz, K. & Lieber, M. R. Hairpin opening and overhang processing by an Artemis/DNA-dependent protein kinase complex in nonhomologous end joining and V(D)J recombination. *Cell* **108**, 781-794 (2002).

135. Rooney, S. et al. Leaky Scid phenotype associated with defective V(D)J coding end processing in Artemis-deficient mice. *Mol Cell* **10**, 1379-1390 (2002).

136. Riballo, E. et al. A pathway of double-strand break rejoining dependent upon ATM, Artemis, and proteins locating to gamma-H2AX foci. *Mol Cell* **16**, 715-724 (2004).

137. Rooney, S. et al. Defective DNA repair and increased genomic instability in Artemis-deficient murine cells. *J Exp Med* **197**, 553-565 (2003).

138. Dronkert, M. L. et al. Disruption of mouse SNM1 causes increased sensitivity to the DNA interstrand cross-linking agent mitomycin C. *Mol Cell Biol* **20**, 4553-4561 (2000).

139. Demuth, I., Digweed, M. & Concannon, P. Human SNM1B is required for normal cellular response to both DNA interstrand crosslink-inducing agents and ionizing radiation. *Oncogene* **23**, 8611-8618 (2004).

140. Richie, C. T. et al. hSnm1 colocalizes and physically associates with 53BP1 before and after DNA damage. *Mol Cell Biol* **22**, 8635-8647 (2002).

141. Dignam, J. D., Lebovitz, R. M. & Roeder, R. G. Accurate transcription initiation by RNA polymerase II in a soluble extract from isolated mammalian nuclei. *Nucleic Acids Res* **11**, 1475-1489 (1983).

142. Pannicke, U. et al. Functional and biochemical dissection of the structure-specific nuclease ARTEMIS. *EMBO J* **23**, 1987-1997 (2004).

143. Kim, S. T., Lim, D. S., Canman, C. E. & Kastan, M. B. Substrate specificities and identification of putative substrates of ATM kinase family members. *J Biol Chem* **274**, 37538-37543 (1999).

144. O'Neill, T. et al. Utilization of oriented peptide libraries to identify substrate motifs selected by ATM. *J Biol Chem* **275**, 22719-22727 (2000).

145. Ma, Y. et al. The DNA-dependent protein kinase catalytic subunit phosphorylation sites in human Artemis. *J Biol Chem* **280**, 33839-33846 (2005).

146. Zhang, X. et al. Artemis is a phosphorylation target of ATM and ATR and is involved in the G2/M DNA damage checkpoint response. *Mol Cell Biol* **24**, 9207-9220 (2004).

147. Matsuoka, S. et al. ATM and ATR substrate analysis reveals extensive protein networks responsive to DNA damage. *Science* **316**, 1160-1166 (2007).

148. Lenain, C. et al. The Apollo 5' exonuclease functions together with TRF2 to protect telomeres from DNA repair. *Curr Biol* **16**, 1303-1310 (2006).

149. Hockemeyer, D., Sfeir, A. J., Shay, J. W., Wright, W. E. & de Lange, T. POT1 protects telomeres from a transient DNA damage response and determines how human chromosomes end. *EMBO J*. **24**, 2667-2678 (2005).

150. Hockemeyer, D., Daniels, J. P., Takai, H. & de Lange, T. Recent expansion of the telomeric complex in rodents: Two distinct POT1 proteins protect mouse telomeres. *Cell* **126**, 63-77 (2006).

151. d'Adda di Fagagna, F. et al. A DNA damage checkpoint response in telomere-initiated senescence. *Nature* **426**, 194-198 (2003).

152. Zou, L. & Elledge, S. J. Sensing DNA damage through ATRIP recognition of RPA-ssDNA complexes. *Science* **300**, 1542-1548 (2003).

153. Pardo, B. & Marcand, S. Rap1 prevents telomere fusions by nonhomologous end joining. *EMBO J* **24**, 3117-3127 (2005).

154. Bae, N. S. & Baumann, P. A RAP1/TRF2 complex inhibits nonhomologous end-joining at human telomeric DNA ends. *Mol Cell* **26**, 323-334 (2007).

155. Bailey, S. M., Brenneman, M. A. & Goodwin, E. H. Frequent recombination in telomeric DNA may extend the proliferative life of telomerase-negative cells. *Nucleic Acids Res* **32**, 3743-3751 (2004).

156. Bechter, O. E., Shay, J. W. & Wright, W. E. The Frequency of Homologous Recombination in Human ALT Cells. *Cell Cycle* **3**, (2004).

157. Undarmaa, B., Kodama, S., Suzuki, K., Niwa, O. & Watanabe, M. X-ray-induced telomeric instability in Atm-deficient mouse cells. *Biochem Biophys Res Commun* **315**, 51-58 (2004).

158. Philippe, C., Coullin, P. & Bernheim, A. Double telomeric signals on single chromatids revealed by FISH and PRINS. *Ann Genet* **42**, 202-209 (1999).

159. Glover, T. W., Berger, C., Coyle, J. & Echo, B. DNA polymerase alpha inhibition by aphidicolin induces gaps and breaks at common fragile sites in human chromosomes. *Hum Genet* **67**, 136-142 (1984).

160. Sheaff, R., Ilsley, D. & Kuchta, R. Mechanism of DNA polymerase alpha inhibition by aphidicolin. *Biochemistry* **30**, 8590-8597 (1991).

161. Glover, T. W. & Stein, C. K. Induction of sister chromatid exchanges at common fragile sites. *Am J Hum Genet* **41**, 882-890 (1987).

162. Glover, T. W. & Stein, C. K. Chromosome breakage and recombination at fragile sites. *Am J Hum Genet* **43**, 265-273 (1988).

163. Bailey, S. M., Goodwin, E. H., Meyne, J. & Cornforth, M. N. CO-FISH reveals inversions associated with isochromosome formation. *Mutagenesis* **11**, 139-144 (1996).

164. Canudas, S. et al. Protein requirements for sister telomere association in human cells. *EMBO J* **26**, 4867-4878 (2007).

165. Hirsch, B. Sister chromatid exchanges are preferentially induced at expressed and nonexpressed common fragile sites. *Hum Genet* **87**, 302-306 (1991).

166. Wellinger, R. J., Wolf, A. J. & Zakian, V. A. Saccharomyces telomeres acquire single-strand TG1-3 tails late in S phase. *Cell* **72**, 51-60 (1993).

167. Wellinger, R. J., Ethier, K., Labrecque, P. & Zakian, V. A. Evidence for a new step in telomere maintenance. *Cell* **85**, 423-433 (1996).

168. Dionne, I. & Wellinger, R. J. Cell cycle-regulated generation of single-stranded G-rich DNA in the absence of telomerase. *Proc Natl Acad Sci USA* **93**, 13902-13907 (1996).

169. Dionne, I. & Wellinger, R. J. Processing of telomeric DNA ends requires the passage of a replication fork. *Nucleic Acids Res* **26**, 5365-5371 (1998).

170. Boulton, S. J. & Jackson, S. P. Components of the Ku-dependent non-homologous end-joining pathway are involved in telomeric length maintenance and telomeric silencing. *Embo J* **17**, 1819-1828 (1998).

171. Ritchie, K. B. & Petes, T. D. The Mre11p/Rad50p/Xrs2p complex and the Tel1p function in a single pathway for telomere maintenance in yeast. *Genetics* **155**, 475-479 (2000).

172. Nugent, C. I. et al. Telomere maintenance is dependent on activities required for end repair of double-strand breaks. *Curr Biol* **8**, 657-660 (1998).

173. Bressan, D. A., Baxter, B. K. & Petrini, J. H. The Mre11-Rad50-Xrs2 protein complex facilitates homologous recombination-based double-strand break repair in Saccharomyces cerevisiae. *Mol Cell Biol* **19**, 7681-7687 (1999).

174. Schiestl, R. H., Zhu, J. & Petes, T. D. Effect of mutations in genes affecting homologous recombination on restriction enzyme-mediated and illegitimate recombination in Saccharomyces cerevisiae. *Mol Cell Biol* **14**, 4493-4500 (1994).

175. Moore, J. K. & Haber, J. E. Cell cycle and genetic requirements of two pathways of nonhomologous end-joining repair of double-strand breaks in Saccharomyces cerevisiae. *Mol Cell Biol* **16**, 2164-2173 (1996).

176. Moreau, S., Ferguson, J. R. & Symington, L. S. The nuclease activity of Mre11 is required for meiosis but not for mating type switching, end joining, or telomere maintenance. *Mol Cell Biol* **19**, 556-566 (1999).

177. Usui, T. et al. Complex formation and functional versatility of Mre11 of budding yeast in recombination. *Cell* **95**, 705-716 (1998).

178. Tsubouchi, H. & Ogawa, H. A novel mre11 mutation impairs processing of double-strand breaks of DNA during both mitosis and meiosis. *Mol Cell Biol* **18**, 260-268 (1998).

179. Paull, T. T. & Gellert, M. Nbs1 potentiates ATP-driven DNA unwinding and endonuclease cleavage by the Mre11/Rad50 complex. *Genes Dev* **13**, 1276-1288 (1999).

180. Diede, S. J. & Gottschling, D. E. Exonuclease activity is required for sequence addition and Cdc13p loading at a de novo telomere. *Curr Biol* **11**, 1336-140. (2001).

181. Tsukamoto, Y., Taggart, A. K. & Zakian, V. A. The role of the Mre11-Rad50-Xrs2 complex in telomerase- mediated lengthening of Saccharomyces cerevisiae telomeres. *Curr Biol* **11**, 1328-135. (2001).

182. Larrivee, M., LeBel, C. & Wellinger, R. J. The generation of proper constitutive G-tails on yeast telomeres is dependent on the MRX complex. *Genes Dev* **18**, 1391-1396 (2004).

183. Makarov, V. L., Hirose, Y. & Langmore, J. P. Long G tails at both ends of human chromosomes suggest a C strand degradation mechanism for telomere shortening. *Cell* **88**, 657-666 (1997).

184. McElligott, R. & Wellinger, R. J. The terminal DNA structure of mammalian chromosomes. *EMBO J* **16**, 3705-3714 (1997).

185. Wright, W. E., Tesmer, V. M., Huffman, K. E., Levene, S. D. & Shay, J. W. Normal human chromosomes have long G-rich telomeric overhangs at one end. *Genes Dev* **11**, 2801-2809 (1997).

186. Hemann, M. T. & Greider, C. W. G-strand overhangs on telomeres in telomerase-deficient mouse cells. *Nucleic Acids Res* **27**, 3964-3969 (1999).

187. Chai, W., Du, Q., Shay, J. W. & Wright, W. E. Human telomeres have different overhang sizes at leading versus lagging strands. *Mol Cell* **21**, 427-435 (2006).

188. Carney, J. P. et al. The hMre11/hRad50 protein complex and Nijmegen breakage syndrome: linkage of double-strand break repair to the cellular DNA damage response. *Cell* **93**, 477-486 (1998).

189. Varon, R. et al. Nibrin, a novel DNA double-strand break repair protein, is mutated in Nijmegen breakage syndrome. *Cell* **93**, 467-76. (1998).

190. Stewart, G. S. et al. The DNA double-strand break repair gene hMRE11 is mutated in individuals with an ataxia-telangiectasia-like disorder. *Cell* **99**, 577-587 (1999).

191. Chai, W., Sfeir, A. J., Hoshiyama, H., Shay, J. W. & Wright, W. E. The involvement of the Mre11/Rad50/Nbs1 complex in the generation of G-overhangs at human telomeres. *EMBO Rep* **7**, 225-230 (2006).

192. Henriques, J. A. & Moustacchi, E. Isolation and characterization of pso mutants sensitive to photo-addition of psoralen derivatives in Saccharomyces cerevisiae. *Genetics* **95**, 273-288 (1980).

193. Grossmann, K. F., Ward, A. M., Matkovic, M. E., Folias, A. E. & Moses, R. E. S. cerevisiae has three pathways for DNA interstrand crosslink repair. *Mutat Res* **487**, 73-83 (2001).

194. Li, X. & Moses, R. E. The beta-lactamase motif in Snm1 is required for repair of DNA double-strand breaks caused by interstrand crosslinks in S. cerevisiae. *DNA Repair (Amst)* **2**, 121-129 (2003).

195. Ishiai, M. et al. DNA cross-link repair protein SNM1A interacts with PIAS1 in nuclear focus formation. *Mol Cell Biol* **24**, 10733-10741 (2004).

196. Hamaguchi, M. et al. DBC2, a candidate for a tumor suppressor gene involved in breast cancer. *Proc Natl Acad Sci U S A* **99**, 13647-13652 (2002).

197. Trauernicht, A. M., Kim, S. J., Kim, N. H. & Boyer, T. G. Modulation of estrogen receptor alpha protein level and survival function by DBC-1. *Mol Endocrinol* **21**, 1526-1536 (2007).

198. Sundararajan, R., Chen, G., Mukherjee, C. & White, E. Caspase-dependent processing activates the proapoptotic activity of deleted in breast cancer-1 during tumor necrosis factor-alpha-mediated death signaling. *Oncogene* **24**, 4908-4920 (2005).

199. Beausoleil, S. A. et al. Large-scale characterization of HeLa cell nuclear phosphoproteins. *Proc Natl Acad Sci U S A* **101**, 12130-12135 (2004).

200. Linding, R. et al. Systematic discovery of in vivo phosphorylation networks. *Cell* **129**, 1415-1426 (2007).

201. Jady, B. E., Bertrand, E. & Kiss, T. Human telomerase RNA and box H/ACA scaRNAs share a common Cajal body-specific localization signal. *J Cell Biol* **164**, 647-652 (2004).

202. Zhu, Y., Tomlinson, R. L., Lukowiak, A. A., Terns, R. M. & Terns, M. P. Telomerase RNA accumulates in Cajal bodies in human cancer cells. *Mol Biol Cell* **15**, 81-90 (2004).

203. Cristofari, G. et al. Human telomerase RNA accumulation in Cajal bodies facilitates telomerase recruitment to telomeres and telomere elongation. *Mol Cell* **27**, 882-889 (2007).

204. Yang, H., Li, Q., Fan, J., Holloman, W. K. & Pavletich, N. P. The BRCA2 homologue Brh2 nucleates RAD51 filament formation at a dsDNA-ssDNA junction. *Nature* **433**, 653-657 (2005).

205. Yang, W. Damage repair DNA polymerases Y. *Curr Opin Struct Biol* **13**, 23-30 (2003).

206. Masutani, C. et al. The XPV (xeroderma pigmentosum variant) gene encodes human DNA polymerase eta. *Nature* **399**, 700-704 (1999).

207. Johnson, R. E., Kondratick, C. M., Prakash, S. & Prakash, L. hRAD30 mutations in the variant form of xeroderma pigmentosum. *Science* **285**, 263-265 (1999).

208. Johnson, R. E., Prakash, S. & Prakash, L. Efficient bypass of a thymine-thymine dimer by yeast DNA polymerase, Poleta. *Science* **283**, 1001-1004 (1999).

209. Albertella, M. R., Green, C. M., Lehmann, A. R. & O'Connor, M. J. A role for polymerase eta in the cellular tolerance to cisplatin-induced damage. *Cancer Res* **65**, 9799-9806 (2005).

210. Alt, A. et al. Bypass of DNA lesions generated during anticancer treatment with cisplatin by DNA polymerase eta. *Science* **318**, 967-970 (2007).

211. Kannouche, P. L., Wing, J. & Lehmann, A. R. Interaction of human DNA polymerase eta with monoubiquitinated PCNA: a possible mechanism for the polymerase switch in response to DNA damage. *Mol Cell* **14**, 491-500 (2004).

212. Mcllwraith, M. J. et al. Human DNA polymerase eta promotes DNA synthesis from strand invasion intermediates of homologous recombination. *Mol Cell* **20**, 783-792 (2005).

213. Andrade, L. E. et al. Human autoantibody to a novel protein of the nuclear coiled body: immunological characterization and cDNA cloning of p80-coilin. *J Exp Med* **173**, 1407-1419 (1991).

214. Andrade, L. E., Tan, E. M. & Chan, E. K. Immunocytochemical analysis of the coiled body in the cell cycle and during cell proliferation. *Proc Natl Acad Sci U S A* **90**, 1947-1951 (1993).

215. Cioce, M. & Lamond, A. I. Cajal bodies: a long history of discovery. *Annu Rev Cell Dev Biol* **21**, 105-131 (2005).

216. Sutherland, G. R., Baker, E. & Richards, R. I. Fragile sites still breaking. *Trends Genet* **14**, 501-506 (1998).

217. Yu, S. et al. Human chromosomal fragile site FRA16B is an amplified AT-rich minisatellite repeat. *Cell* **88**, 367-374 (1997).

218. Azzalin, C. M., Reichenbach, P., Khoriauli, L., Giulotto, E. & Lingner, J. Telomeric repeat containing RNA and RNA surveillance factors at mammalian chromosome ends. *Science* **318**, 798-801 (2007).

219. Verdun, R. E. & Karlseder, J. The DNA damage machinery and homologous recombination pathway act consecutively to protect human telomeres. *Cell* **127**, 709-720 (2006).